Five-layer systems analysis of *Leishmania* stage differentiation reveals an essential role for protein degradation in parasite development

Pascale Pescher[1*], Thibaut Douché[2], Quentin Giai-Gianetto[2,3], Karen Druart[2], Julie Kovarova[4], Blaise Li[3], Thomas Cokelaer[1,3], K Shanmugha Rajan[6,7], Laura Piel[1], Céline Besse[5], Anne Boland[5], Jean-François Deleuze[5], Mariette Matondo[2], Michael P. Barrett[4], Shulamit Michaeli[7] and Gerald F. Späth[1*]

[1]Institut Pasteur, Université Paris Cité, INSERM 1201, Unité de Parasitologie moléculaire et Signalisation, Paris, France, [2]Institut Pasteur, Université Paris Cité, CNRS UAR 2024, Proteomic Platform, Mass Spectrometry for Biology Unit, Paris, France , [3]Institut Pasteur, Université Paris Cité, Biostatistics and Bioinformatics Hub, Paris, France, [4]Glasgow Centre for Parasitology, University of Glasgow, Glasgow, UK, [5]Université Paris-Saclay, CEA, Centre National de Recherche en Génomique Humaine, Evry, France, [6]Weizmann Institute of Science, Department of Chemical and Structural Biology, Rehovot, Israel, [7]Bar-Ilan University, Mina and Everard Goodman Faculty of Life Sciences and Advanced and Nanotechnology Institute, Ramat-Gan, Israel.

*co-corresponding authors

Correspondence: pascale.pescher@pasteur.fr, gerald.spaeth@pasteur.fr

Keywords: *Leishmania donovani*, stage differentiation, systems analysis, protein degradation, regulatory networks

ABSTRACT

Vector-borne, protist parasites have evolved complex developmental programs to adapt to very distinct host environments. How these important pathogens transition between insect and mammalian stages is only poorly understood. Here we investigate stage differentiation in the trypanosomatid parasite *Leishmania* that shows constitutive gene transcription, thus providing a unique model system to assess how development is governed by post-transcriptional mechanisms. Using a five-layer integrative systems analysis (from genome to metabolome), we examined hamster-isolated *Leishmania donovani* amastigotes and culture-derived, insect-stage promastigotes. This approach enabled us to rule out genomic adaptation as a key driver of parasite stage differentiation, while confirming the pivotal role of differential mRNA turnover in stage-specific gene expression. Assessing transcriptomic against proteomic expression changes uncovered an unexpectedly broad dynamic range of stage-regulated changes in protein abundance that only poorly correlated with mRNA levels. This discrepancy correlated with (i) alterations in snoRNA expression and changes in rRNA modification they guide suggesting stage-specific adaptation of the protein translation apparatus that can uncouple mRNA from protein abundancies, and (ii) differential protein degradation as revealed by quantitative proteomics of parasites treated with the proteasomal inhibitor lactacystin. Lactacystin treatment stalled the transition of spleen-derived amastigotes into promastigotes in culture, further underscoring the role of proteasomal activity in stage differentiation. Integration of our five-layer systems analysis established the first link between *Leishmania* development and the expression of co-regulated genetic networks encompassing mRNA turnover, protein translation, phosphorylation, and degradation. Our findings provide a powerful new resource for research programs that aim to dissect the emergent properties of regulatory networks and feedback loops underlying *Leishmania* stage differentiation, serving as a blueprint for other vector-borne pathogens that rely on disease-associated developmental transitions.

INTRODUCTION

During their infectious cycle, many protist and fungal pathogens undergo complex developmental transitions that adapt their biology to different host environments, thus ensuring transmission, persistence or immune evasion. For example, stage differentiation of the malarial parasite *Plasmodium*

55 spp is tightly controlled at transcriptional levels by the dynamic interplay between epigenetic regulators
56 that remodel the chromatin landscape to accommodate stage-specific transcription factors, such as AP2
57 DNA-binding family members (1, 2). Likewise, the transition from fast-growing tachyzoites to slow-
58 growing bradyzoites during mammalian *Toxoplasma* infection is regulated by the single master TF
59 BFD1 (3). Unlike these apicomplexan parasites, stage-differentiation in the trypanosomatid pathogen
60 *Leishmania* spp is not regulated at the level of transcriptional control, raising the question of how these
61 parasites establish and maintain the various adaptive forms that develop inside their insect and
62 mammalian hosts.

63 *Leishmania* spp are protist parasites of humans that represent a global public health problem
64 causing a series of immunopathologies termed the leishmaniases (4-7). These parasites differentiate
65 into various developmental forms that are adapted for extracellular proliferation inside the sand fly
66 midgut (procyclic promastigotes), transmission from the vector to the mammalian host during uptake
67 of a blood meal (metacyclic promastigotes), and intracellular proliferation inside fully acidified
68 macrophage phagolysosomes (amastigotes) (8). Unlike other eukaryotes, *Leishmania* development is
69 not controlled transcriptionally as protein-coding genes in these parasites lack individual promoters and
70 are constitutively transcribed at all stages involving parasite-specific processes such as polycistronic
71 transcription and trans-splicing (9, 10). Despite the largely constitutive gene transcription, different
72 *Leishmania* stages are characterized by striking morphological, biochemical and metabolic changes
73 (11-16). These are regulated by a plethora of post-transcriptional mechanisms, including differential
74 mRNA turn over through the binding of various proteins and protein complexes to the 5' and 3'
75 untranslated regions (UTRs) (17-22), that can trigger mRNA degradation via deadenylation and
76 decapping (23, 24). Differential gene expression in *Leishmania* can further be regulated at the
77 translational level, for example through (i) selective ribosome recruitment by of one of the six isoforms
78 of the *Leishmania* cap-binding protein eIF4E that bind to the 5' UTR , (ii) stabilizing the poly(A) tail
79 via the recruitment of Poly(A) Binding Protein 1 (PABP1) to the 3' UTR promoting translation, or (iii)
80 the differential expression of ribosomal proteins that can increase the landscape of specialized
81 ribosomes (25-34). Finally, differential gene expression in *Leishmania* can also be controlled at the

82 level of protein stability, through stage-specific expression of proteasomal components, autophagy-
83 related genes (ATGs) or lysosomal proteases (35-41).
84 While each level of gene expression control has been studied individually in different
85 *Leishmania* species, how these different types of regulation are integrated during *Leishmania* stage
86 differentiation remains to be elucidated. Here, we approached this open question by applying a 5-layer,
87 systems level analysis on the two major life cycle stages of *Leishmania donovani*, i.e. hamster-isolated,
88 *bona-fide* amastigotes and derived promastigotes. Our analysis draws a complex picture of the
89 *Leishmania* differentiation process that emerges from complex, co-regulated genetic networks
90 involving mRNA turnover, protein translation, protein phosphorylation and protein degradation. Our
91 data reveal *Leishmania* as an interesting model system to analyze phenotypic adaptation in the absence
92 of transcriptional control and to dissociate the role of complex regulatory networks in the development
93 of stable, disease-causing life cycle stages in eukaryotic pathogens.
94
95
96

97 **MATERIAL & METHODS**

98 **Ethics statement.** Work on animals was performed in compliance with French and European
99 regulations on care and protection of laboratory animals (EC Directive 2010/63, French Law 2013-118,
100 February 6th, 2013). All animal experiments were approved by the Ethics Committee and the Animal
101 welfare body of Institut Pasteur and by the Ministère de l'Enseignement Supérieur, de la Recherche et
102 de l'Innovation (projects n°#19683 and #240013).

103

104 **Animals.** Twenty-five female Golden Syrian hamsters (*Mesocricetus auratus* RjHan:AURA, weighting
105 between 50 – 60 g) were purchased from Janvier Laboratories. All animals were handled under specific,
106 pathogen-free conditions in biohazard level 3 animal facilities (A3) accredited by the French Ministry
107 of Agriculture for performing experiments on live rodents (agreement A75-15-01).

108

109 **Parasites and culture.** *Leishmania donovani* strain 1S2D (MHOM/SD/62/1S-CL2D) was obtained
110 from Henry Murray, Weill Cornell Medical College, New York, USA and maintained by serial passages
111 in hamsters. Anesthetized hamsters were inoculated by intra-cardiac injection of $5x10^7$ amastigotes
112 purified from hamster infected spleens as described previously (42). The weight of the animals was
113 recorded over time, and the animals were euthanized by CO_2 asphyxiation before they reached the end-
114 point of infection represented by a 20% loss of body weight. Amastigotes were then recovered from the
115 infected hamster spleens and used for nucleic acid and protein extractions, or differentiated into
116 promastigotes at 26°C in M199 complete medium (M199, 10% FBS, 25 mM HEPES; 100 µM adenine,
117 2 mM L-glutamine, 10 µg/ml folic acid, 13.7 µM hemin, 4.2 mM $NaHCO_3$, 1xRPMI1640 vitamins, 8
118 µM 6-biopterin, 100 units penicillin and 100 µg/ml streptomycin, pH 7.4). Promastigotes, derived from
119 splenic amastigotes, were collected after 2 *in vitro* passages for nucleic acid and protein extractions.

120

121 **Experimental design.** Strains issued from independent experimental evolution assays are identified by
122 number, e.g. amastigote ama1 and promastigote pro1 are the parasites prepared from hamster H1 (see
123 Figures 1A and S1 for details). For comparative analyses, DNA, RNA, proteins and metabolites were

124 extracted from different splenic ama and their matching pro parasites, the latter being collected for
125 extraction during exponential growth phase.
126
127 **Parasite differentiation and lactacystin treatment.** Spleen-derived amastigotes were incubated at
128 $2x10^7$/ml and 26°C in presence or absence of 10 µM of lactacystin (L6785, Sigma) for 3, 6, 18 and 48h
129 in M199 complete medium. At each time point, parasites were collected to control for the presence of
130 paraflagellar rod protein 2 (PFR2) as promastigote differentiation marker. After one *in vitro* passage,
131 amastigote-derived promastigotes were incubated at a concentration of $2x10^7$ parasites per ml in
132 presence or absence of 10 µM of lactacystin for 18h. Parasite viability was assessed by FACS analysis
133 after 18h of treatment by propidium iodide (1µg/ml) or YO-PRO-1 (0.2 µM) (# Y3603, Invitrogen)
134 staining as readout using untreated and PFA-treated parasites as controls. Parasites were collected from
135 25 ml of culture after 18h of treatment for quantitative, label-free proteomics analyses.

136 **Microscopy.** Differential interference contrast (DIC) microscopy was applied on hamster-derived
137 amastigotes during *in vitro* differentiation to promastigotes using an Axioplan 2 imaging microscope
138 using a 63x oil immersion objective, the AxioVision Rel.4.8 software and an AxioCam MRm camera
139 (Carl Zeiss). Alternatively, microscopic images of amastigotes in presence or absence of the lactacystin
140 inhibitor were obtained using the EVOS FL microscope (life technologies) at a 20x magnification.

141 **Western blot analysis.** Protein extracts were obtained from parasites after 3, 6, 18 and 48h of
142 differentiation from amastigotes to promastigotes in presence or absence of lactacystin. Extracts were
143 loaded on 4-12% SDS-PAGE (NuPage 4-12% Bis-Tris gel NP0321BOX, Invitrogen), separated by
144 electrophoresis and stained with Coomassie blue or transferred onto PVDF membrane. The presence of
145 PFR2 and α-tubulin was revealed using the anti-PFR2 antibody (kindly given by Philippe Bastin), an
146 anti- α-tubulin antibody (clone B-5-1-2, Sigma), the corresponding HRP-conjugated secondary
147 antibodies (Invitrogen) and the SuperSignal West Pico PLUS kit (Thermoscientific). Protein extracts
148 from lactacystin-treated or untreated amastigotes and promastigotes were labelled with Cy5, loaded on
149 4-12% SDS-PAGE (NuPage 4-12% Bis-Tris gel NP0321BOX, Invitrogen), separated by

150 electrophoresis and transferred onto PVDF membrane. The presence of ubiquitinated proteins was
151 revealed using the mouse anti-ubiquitin monoclonal antibody P4D1 (Abcam), the HRP-conjugated anti-
152 mouse secondary antibody (Invitrogen) and the ECL Prime western blotting detection reagent (Cytiva).
153 Images were acquired using the ImageQuant 800 (Cytiva).

154 **Genome sequencing and data analysis.** DNA was prepared from splenic amastigotes and
155 promastigotes at exponential culture phase (three biological replicates). Parasites were centrifuged at
156 1,600 x *g* (pro) or 2,000 x *g* (ama) for 10 min at room temperature. Approximately $1x10^8$ promastigotes
157 from logarithmic growth phase were re-suspended in 200 µl PBS and genomic DNA was purified using
158 DNeasy Blood and Tissue kit from Qiagen and RNase A, according to the manufacturer's instructions.
159 DNA concentrations were measured in duplicate by fluorescence using a Molecular Device
160 fluorescence plate reader (Quant-IT kits, Thermo Fischer Scientific). The quality of DNA was
161 controlled by determining the DNA Integrity Number (DIN) analyzing 20 ng of DNA on a TapeStation
162 4200 (Agilent). One µg of genomic DNA was used to prepare a library for whole genome sequencing
163 on an automated platform, using the Illumina "TruSeq DNA PCR-Free Library Preparation Kit",
164 according to the manufacturer's instructions. After normalization and quality control, qualified libraries
165 were sequenced on a HiSeqX5 platform from Illumina (Illumina Inc., CA, USA) at the Centre National
166 de Recherche en Génétique Humaine (CEA, Evry, France), generating paired-ended, 150-bp reads.
167 Sequence quality parameters were assessed throughout the sequencing run. Standard bioinformatics
168 analysis of sequencing data was based on the Illumina pipeline to generate a FASTQ file for each
169 sample.

170 Genomic DNA reads were aligned to the *L. donovani* Ld1S reference genome
171 (https://www.ncbi.nlm.nih.gov/bioproject/PRJNA396645, GCA_002243465.1) with BWA mem
172 (version 0.7.12) with the flag -M to mark shorter split hits as secondary. Samtools fixmate, sort, and
173 index (version 1.3) were used to process the alignment files and turn them into bam format (43).
174 RealignerTargetCreator and IndelRealigner from the GATK suite were run to homogenize indels (44).
175 Eventually, PCR and optical duplicates were labeled with Picard MarkDuplicates (version 1.94(1484))
176 (https://broadinstitute.github.io/picard/) using the option

177 “VALIDATION_STRINGENCY=LENIENT”. For each read alignment file, Samtools view (version
178 1.3) and BEDTools genomecov (version 2.25.0) were used to measure the sequencing depth of each
179 nucleotide (45). Samtools was run with options “-q 50 -F 1028” to discard reads with a low map quality
180 score or potential duplicates, while BEDTools genomecov was run with options “-d -split” to compute
181 the coverage of each nucleotide. The coverage of each nucleotide was divided by the median genomic
182 coverage. This normalization is done to account for library size differences. The chromosome
183 sequencing coverage was used to evaluate aneuploidy between EP.1 and LP.1 samples. Then for each
184 sample and for each chromosome, the median sequencing coverage was computed for contiguous
185 windows of 2,500 bases. As previously published (46), the stably disomic chromosome 36 was used to
186 normalize chromosome read depth and to estimate chromosome polysomy levels in each sample. Gene
187 counts were produced using featureCounts (version 1.4.6-p3 (47)) with these parameters: -s 0 -t gene -
188 g gene_id and were normalized according to the median-ratio method.

189 For the generation of the chromosome median somy score heatmap, mean coverage in 300 bp bins as
190 generated by the GIP pipeline (48) were used to compute somy scores per chromosome by first
191 normalizing bin scores for a sample by their median across all genome (to obtain comparable values
192 between samples), multiplying by two (to scale somy values to the default diploid state assumed for
193 most of the genome), and then taking the median across bins belonging to a given chromosome (see
194 also https://gip.readthedocs.io/en/latest/giptools/karyotype.html). These chromosome scores were then
195 displayed on a sample x chromosome heatmap, excluding the “maxi” chromosome. This was done using
196 the Pandas 1.4.2 (49, 50) Pandas-dev/pandas: Pandas 1.2.4, https://zenodo.org/records/4681666 (50)),
197 Matplotlib 3.5.1 (51) and Seaborn 0.11.2 (52) Python libraries.

198 For the assessment of gene coverage ratios, normalized mean coverages per gene are reported
199 by GIP (version 1.1.0 (48)), as the mean coverage of the gene divided by the median coverage of the
200 chromosome containing the gene. For a given gene, and a given amastigote - promastigote pair, a gene
201 coverage ratio was computed adding 0.1 to the gene coverages of the individual samples, in order to
202 avoid zero division errors. The genes were sorted by genomic coordinate and assigned successive

203 integers to create a "genomic index". Gene coverage ratios were then plotted along this genomic index,
204 using the same Python libraries as above.
205 For the SNP analysis, alternative (Alt) allele frequencies for SNPs were retrieved from the
206 output of the SNV giptools module (provided along with the GIP pipeline). Euclidean distances between
207 samples in the SNP allele frequencies space were computed and used to build a dendrogram using the
208 scipy.cluster.hierarchy Python module (SciPy version: 1.8.0). The clustering was obtained using the
209 UPGMA method.
210
211 **RNA-seq analysis.** Total RNA was extracted from splenic amastigotes and promastigotes in
212 exponential culture phase (4 biological replicates). Amastigotes and promastigotes were centrifuged
213 respectively at 2,000 x *g* or 1,600 x *g* for 10 min at 4°C, and re-suspended in the lysis buffer supplied
214 with the Qiagen RNeasy Plus kit. The samples were stored at -80°C and RNA extractions were
215 performed according to the manufacturer's instructions, including a DNase treatment. RNA integrity
216 was validated using the Agilent Bioanalyzer. DNase-treated RNA extracts were used for library
217 preparation. Libraries were constructed using an Illumina Stranded mRNA Prep (Illumina, USA)
218 following the supplier's recommendations. RNA sequencing was performed at the Biomics Center
219 (Institut Pasteur, Paris, France) on the Illumina NextSeq 2000 platform for a target of 40M paired-end
220 reads per sample.
221 The RNA-seq analysis was performed using the Sequana RNA-seq pipeline (version 0.20.1,
222 https://github.com/sequana/sequana_rnaseq) from the Seauqnq project (53). The pipeline workflow
223 manager is Snakemake 7.3.2 (54). The pipeline was executed with default parameters and
224 bioinformatics software are available as reproducible containers from the Damona project
225 (https://github.com/cokelaer/damona). Reads were mapped to the *Leishmania donovani* reference
226 using bowtie2 2.4.5 (55). Gene-level quantification was conducted using FeatureCounts 2.0.1 (47)
227 assigning reads to genomic features based on the gene annotation and gene_id attribute, while
228 accounting for strand-specificity information. Differential expression analysis was performed using
229 DESeq2 v1.24.0 (56) scripts available in the Sequana library. Statistical testing identified differentially

230 expressed genes by comparing amastigote and promastigote sample groups, with significance
231 determined using Benjamini-Hochberg adjusted p-values (false discovery rate FDR < 0.05).
232 To specifically assess the differential expression of snoRNA, RNA-seq libraries from
233 promastigote and amastigote stages were mapped to the Ld1S genome, and snoRNA read counts were
234 obtained using bedtools multiBamCov. For snoRNAs with multiple copies, read counts were summed
235 per sample to generate a single expression value per snoRNA family. DESeq2 was then used to perform
236 differential expression analysis between amastigote and promastigote stages based on the summed
237 snoRNA counts.
238
239 **Label-free, quantitative total proteome analyses.** Untreated amastigotes (ama and ama-18h) and
240 promastigotes (pro), and lactacystin-treated parasites (ama lacta and pro lacta) were recovered from
241 four replicates (Figure 1A and S1) and washed three times with cold PBS at 2,000 x *g* or 1,600 x *g* for
242 10 min at 4°C. Parasite lysates were prepared in eFASP lysis buffer (4% SDS / 0.2 % DCA / 50mM
243 TCEP / 50 mM ammonium bicarbonate buffer pH 8) (61). For detailed protocol see supplementary data
244 file. MS scans were acquired at a resolution of 70,000 and MS/MS scans (fixed first mass 100 m/z) at
245 a resolution of 17,500. The AGC target and maximum injection time for the survey scans and the
246 MS/MS scans were set to 3 x 10^6 for 20 ms and 10^6 for 60 ms, respectively. An automatic selection of
247 the 10 most intense precursor ions was activated (Top 10) with a 40 s dynamic exclusion. The isolation
248 window was set to 1.6 m/z and normalized collision energy fixed to 28 for HCD fragmentation. We
249 used a minimum AGC target of 10^4 corresponding to an intensity threshold of 1.7 x 10^5. Unassigned
250 precursor ion charge states as well as 1, 7, 8 and >8 charged states were rejected and match was disabled.
251
252 **Label-free quantitative phosphoproteome analyses.** Amastigote (ama) and promastigote (pro)
253 parasites from four biological replicates were recovered and washed three times by centrifugation in
254 cold M199 at respectively 2,000 x *g* or 1,600 x *g* for 10 min at 4°C. Samples were incubated for 10 min
255 at 4°C in lysis buffer (1ml per 1.5x10^9 parasites) consisting of 8 M urea, 50 mM Tris, supplemented
256 with a protease inhibitor cocktail (cOmplete from Roche) and a phosphatase inhibitor cocktail
257 (PhosStop from Roche). Following sonication for 5 min using a sequence of 10 s pulse and 20 s pause,

258 the lysates were centrifuged 15 min at 14,000 x *g* and 4°C, and the supernatant was collected and stored
259 at -80°C until use. Proteins were quantified by RC DC protein assay (Bio-Rad) and adjusted to 1.3
260 $\mu g.\mu l^{-1}$ in lysis buffer. For detailed protocol see supplementary data file. Phosphopeptide enrichment
261 was carried out as described in (62) and detailed in supplementary data. All analyses were performed
262 on a Q Exactive HF Mass Spectrometer (Thermo Fisher Scientific) coupled with a Proxeon EASY-nLC
263 1000 (Thermo Fisher Scientific) as detailed in supplementary data. Details for the proteomics and
264 phosphoproteomics analyses following the data acquisition are available in supplementary data. Results
265 are presented in table 6 and 10.

266 Phosphopeptides were selected for Gene Ontology enrichment analyses if (i) they were
267 exclusively identified in one of the two stages, (ii) they showed significant, stage-specific changes in
268 phosphopeptide abundance (fold change ≥ 2, adj. p-value < 0.01) even if the corresponding protein was
269 not detected in the total proteome analysis, and (iii) they showed a significant increase in relative
270 phosphorylation normalized to protein abundance (p-value < 0.05) as calculated by the ratio 'change in
271 phosphopeptide abundance' vs 'change in protein abundance' using a cut off of fold changes ≥ 2 and
272 adj. p-value < 0.01 for both analyses (see table 11).

273

274 **Metabolomic analysis.** The sample extraction was performed as described previously (63). Briefly, 10^8
275 cells were used per each 200 µL sample (4 replicates/stage). Firstly, cells were rapidly quenched in a
276 dry ice/ethanol bath to 4°C, then centrifuged, washed with 1 x PBS, and resuspended in the extraction
277 solvent (chloroform:methanol:water, 1:3:1). After vigorous shaking at 4°C for 1 h, extracts were
278 centrifuged (16,000 x g, 4°C, 10 min) and the supernatants collected and stored at -80°C until the
279 analysis. LC-MS analyses were performed using separation on 150 x 4.6 mm, 5 mm ZIC-pHILIC
280 (Merck) on UltiMate 3000 RSLC (Thermo Scientific) followed by mass detection on an Orbitrap
281 Exactive mass spectrometer (Thermo Fisher) at Glasgow Polyomics. Analyses were performed in
282 positive and negative polarity switching mode, using 10 µl injection volume and a flow rate of 300
283 µl/min over 26 min on the column maintained at 30ºC, as follows: 0 to 20 min 20%-to 80% solution A,
284 15 to 17 min 95% solution A, 17 to 26 min 20% solution A where solution A is 20 mM ammonium
285 carbonate in water and solution B is acetonitrile). The samples were run alongside 249 authentic

286 standards at 10 μM each. Mass spectrometry data was processed using Mzmatch (64) and Ideom (63)
287 software. Unique signals were extracted using the centwave algorithm and matched across biological
288 replicates based on mass-to-charge ratio and retention time. These grouped peaks were then filtered
289 based on relative standard deviation and combined into a single file. The combined sets were then
290 filtered on signal-to-noise score, minimum intensity and minimum detections. The final peak set was
291 then gap-filled and converted to text for use Putative metabolite identification corresponds for the most
292 part to Metabolite Standards Initiative (MSI) level 2 (mass only, and thus only considered a tentative
293 annotation), whereas metabolites matching in retention time to an included standard correspond to level
294 1 (considered likely an accurate annotation). Peaks having an area with root squared deviation across
295 pooled samples > 50% were excluded, as were those with a retention time < 4 min (due to poor
296 resolution).
297
298 **Localizing rRNA modification on *Leishmania* cryo-EM ribosome structure**. The cryo-EM atomic
299 model of *Leishmania major* 80S ribosomes bound to mRNA and all three tRNAs (PDB: 8RXH) was
300 used to project rRNA modifications of the ribosome. Figures were generated using UCSF Chimera-X
301 software (65).
302
303 **Systems-level analyses.** A lists of *L. donovani* GO terms (66) was built in house. The Biological
304 Networks Gene Ontology tool (BiNGO) plugin of the Cytoscape software package (version 3.8.2) was
305 used to map and visualize functional enrichments in each data set based on the GO hierarchy. A
306 Benjamini & Hochberg false discovery rate with a significance level of 0.05 was applied. Cluster
307 efficiency represents the percentage of genes for a given GO term compared to the total number of
308 genes with any GO annotation in the considered set of genes. Enrichment score corresponds to the
309 percentage of genes for a given GO term compared to all the genes sharing the same GO term in the
310 genome. Word Cloud of GO enrichment analysis limited to GO Slim terms and a threshold of p-value
311 < 0.05 for the category Biological Process was performed on TriTrypdb (https://tritrypdb.org) using the
312 *L. donovani* LdBPK orthologs for all genes that showed statistically significant expression changes (p-
313 value < 0.01) at both RNA or protein levels.

314 For the phosphoproteomic work, phosphopeptides were selected for Gene Ontology enrichment
315 analyses if (i) they were exclusively identified in one of the two stages, (ii) they showed significant,
316 stage-specific changes in phosphopeptide abundance (fold change ≥ 2, adj. p-value < 0.01) even if the
317 corresponding protein was not detected in the total proteome analysis, and (iii) they showed a significant
318 increase in relative phosphorylation normalized to protein abundance (p-value < 0.05) as calculated by
319 the ratio 'change in phosphopeptide abundance' vs 'change in protein abundance' using a cut off of fold
320 changes ≥ 2 and adj. p-value < 0.01 for both analyses (see table 11).
321 Functional enrichment networks were built with the STRING plugin of the Cytoscape software
322 package (version 3.8.2) using the *L. infantum* orthologs, and the full STRING network with a confidence
323 score cutoff of 0.4. A false discovery rate with a significance level of 0.05 was applied. The
324 "ClusterProfiler" package (version 4.2.2) of R was used for KEGG (Kyoto encyclopedia of genes and
325 genomes) gene set enrichment analysis (GSEA) and for data mapping on metabolic pathways available
326 in the KEGG database. Results were visualized using the "pathview" packages (version 1.34.0).
327
328 **Data availability.** The mass spectrometry proteomics data were deposited to the ProteomeXchange
329 Consortium via the PRIDE partner repository with the dataset identifiers PXD035697
330 (phosphoproteome data) and PXD035698 (proteome upon lactacystin treatment) (67). The DNAseq
331 data have been deposited in NCBI's Gene Expression Omnibus (68) and are accessible in the BioProject
332 PRJNA1231373 (https://www.ncbi.nlm.nih.gov/bioproject/PRJNA1231373). The RNAseq data have
333 been deposited in ArrayExpress (EMBL-EBI) (69) under the accession number E-MTAB-16528. The
334 mass spectrometry metabolomic data are available on Figshare at
335 https://doi.org/10.6084/m9.figshare.31027849. The scripts for GIP and giptools are available at
336 https://github.com/susefranssen/Global_genome_diversity_Ldonovani_complex.
337
338
339

340 **RESULTS**

341 ***Leishmania* stage differentiation occurs independently from changes in gene dosage.** We carried
342 out an in-depth, systems analysis of independent *L. donovani* amastigote preparations isolated from
343 infected hamster spleens and their culture-derived promastigotes at *in vitro* passage 2, with the aim of
344 revealing mechanisms controlling stage-specific differential expression across five quantifiable
345 information levels, by comparing the genome, transcriptome, proteome, metabolome and phospho-
346 proteome of the two life-cycle stages (Figure 1A and Figure S1). We first investigated the possible role
347 of genome instability in stage-differentiation, given the very well documented propensity of *L. donovani*
348 to establish and tolerate chromosome and gene copy number variations in culture and during sand fly
349 or hamster infection (46, 66, 70).

350 Applying our computational pipeline termed 'GIP' (48) to the genome sequences of three
351 independent pairs of amastigotes and promastigotes confirmed the largely disomic state of the
352 *Leishmania* genome at both stages, except for the known constitutive tetrasomy of chr 31 (Figure 1B
353 and Figure S2A, Table 1). We did not detect any major changes at karyotypic levels following
354 promastigote differentiation, confirming our previous observations that stage differentiation occurs
355 independent of karyotypic adaptation (46, 70). Nevertheless, a clear pattern emerged for promastigotes
356 that showed a slight but reproducible increase in median coverage for chr 1, 2, 3, 4, 6 and 20, suggesting
357 the emergence of mosaic aneuploidy for these chromosomes early during culture adaptation. However,
358 these minor signals are not predictive for the karyotypic changes characteristic of culture-adapted Ld1S
359 parasites (i.e. chr 5, 26, 33, (46, 70)). Likewise, differentiation of promastigotes was not associated with
360 any major gene copy number variation at early passage 2 (Figure 1C, Table 2). Even though a number
361 of genes showed increased (e.g. Ld1S_300477100 encoding an intraflagellar transport (IFT) protein) or
362 decreased (e.g. Ld1S_220235700 encoding a hypothetical protein) read depth in individual pro strains,
363 none of these changes converged across all pro samples. In the absence of convergent selection, it is
364 impossible to distinguish if these gene CNVs provide some strain-specific advantage or are merely the
365 result of random genetic drift. Plotting the normalized read depth ratios between amastigotes and
366 promastigotes revealed an intriguing, undulating pattern that was highly reproducible across the three
367 independent experiments and has been previously associated with nascent DNA produced during the

368 replicative S-phase of the cell cycle (71-73). Finally, differentiation did not affect the SNP frequency
369 distribution (Figure S2B, Table 3), which resulted in a largely diagonal pattern when plotting amastigote
370 against promastigote SNP frequencies (Figure 1D).

371 In conclusion, unlike long-term culture adaptation, which drives important karyotypic changes
372 (46, 74) that can affect transcript- and protein abundance levels as demonstrated by a recent 4-layer
373 systems analysis (75) *in vitro* differentiation of splenic amastigotes into promastigotes was not
374 associated with significant changes in chromosome or gene copy number, ruling out gene dosage effects
375 as the source of stage-specific expression differences. Thus, *L. donovani* promastigote differentiation
376 *in vitro* is independent of genomic adaptation, confirming our previous results obtained with sand fly-
377 derived, promastigote parasites (66, 76).

378

379 **Comparative RNA-seq analysis reveals stage-specific, co-regulated gene clusters that are**
380 **controlled at post-transcriptional levels.** We next analyzed stage-specific expression changes
381 applying RNA-seq analyses on four amastigote and derived promastigote strains. In contrast to the
382 relatively stable genome infrastructure maintained between stages, we observed substantial, stage-
383 specific differences in transcript abundance. From 10402 detected transcripts in both stages, 6478
384 showed statistically significant differences (adj. p-value < 0.01, base mean reads ≥ 10 reads), including
385 1234 and 1027 transcripts with a 2-fold or higher increase in abundance in amastigotes and
386 promastigotes, respectively (Table 4). Considering the lack of promoter-driven expression control of
387 individual, protein coding genes in *Leishmania* and the absence of stage-specific gene dosage effects
388 (see Figure 1), the observed differences in amastigote and promastigote transcript abundances are most
389 likely attributable to stage-specific mRNA turnover. Interestingly, non-coding (nc) RNAs account for
390 64.7% of the differentially expressed transcripts at the amastigote stage (Figures 2A).

391 Analyzing the stage-specific RNA-seq data sets identified clusters of co-regulated transcripts
392 that share a common annotation (Figure 2B, Table 4). In promastigotes, we observed increased
393 abundance for 66 transcripts annotated for the interconnected GO terms 'microtubule based process',
394 'cytoskeleton organization' and 'ciliary cell motility', confirming the post-transcriptional co-regulation
395 of flagellar biosynthesis as previously shown in *L. mexicana* (77) (Figure 2B left panel, Table 4, sheet

396 G). Other co-regulated, functional gene sets are defined by the GO terms 'oxidation reduction' (46
397 transcripts), 'glycolysis' (15 transcripts), 'post-transcriptional regulation of gene expression' (46
398 transcripts) and 'translational elongation' (28 transcripts), further supporting translational control as a
399 regulatory step in stage differentiation.

400 In amastigotes, a major co-regulated gene cluster is represented by 77 amastin transcripts
401 encoded on 5 different chromosomes that show increased abundance in amastigotes, confirming the
402 stage-specific, post-transcriptional regulation of this gene family as previously described (19, 78, 79)
403 (Table 4, sheet C, E and F). Another functional gene cluster showing increased abundance in
404 amastigotes was associated with protein translation, with GO enrichment observed for the terms
405 'ribosome biogenesis' (26 transcripts), 'ncRNA processing' (22 transcripts), including 17 transcripts
406 annotated for the GO term 'rRNA processing', and 6 transcripts for 'tRNA processing' (Figure 2B,
407 middle and right panel, Table 4, sheet E and F).

408 These data suggest ribosome and epi-transcriptomic regulation as possible central components
409 in *Leishmania* stage differentiation. Indeed, analyzing poly-A transcriptome libraries of amastigotes
410 and promastigotes we observed significant differences in stage-specific expression of 110 pre-snoRNAs
411 (Table 5, Figure 2C). These data fit with the expression of a series of methyl- and pseudouridyl-
412 transferases at this stage (see Table 6, sheets A and E). Stage-specific expression of some of these
413 snoRNAs correlated with stage-specific changes previously observed in Pseudouridine and 2'-O-
414 Methylation rRNA modifications (34). The positions of these modifications and the corresponding
415 snoRNAs known to affect ribosome translational activity are indicated on the high resolution cryo-EM
416 structure of the *Leishmania* ribosome (Figure 2D).

417 In conclusion, our RNAseq data reveal a series of functionally related, stage-specific gene
418 clusters whose mRNA abundance is regulated in a coordinated manner at post-transcriptional level.
419 Whether this co-regulation is governed by stage-specific mRNA decay mechanisms acting on 5' and 3'
420 UTRs or by stage-specific mRNA stabilization via RNA-binding proteins or mRNA modification
421 remains to be established.

422

423 **Quantitative proteome analysis reveals co-regulated gene clusters that are independent of stage-**
424 **specific mRNA turnover.** We next employed quantitative proteomic analysis to assess how the
425 different co-regulated gene clusters observed in our RNAseq analyses translate into stage-specific
426 proteomes. Label-free quantitative proteomic analysis of 4 replicates of amastigotes and derived
427 promastigotes identified over 4000 proteins, including 1987 differentially expressed proteins (adjusted
428 p-value < 0.01), and 1534 that were exclusively detected in either ama or pro (Figure 3A left panel,
429 Table 6). Considering the 822 proteins that are specific or more abundant in amastigotes (fold change
430 ≥ 2), functional enrichment was mainly observed for the GO terms 'oxidation reduction' (61 proteins),
431 'vesicle mediated transport' (23 proteins) and 'phosphorylation' (41 proteins) (Figure 3A, middle panel,
432 Table 6, sheets B and D). Considering the 1637 proteins that are specific or more abundant in
433 promastigotes (fold change ≥ 2), functional enrichment was observed for the GO terms 'post-
434 transcriptional regulation of gene expression' (71), 'translation' (69 proteins), 'ribosome biogenesis'
435 (21 proteins) and 'ciliary cell motility' (42 proteins) (Figure 3A, right panel, Table 6, sheet C and E).
436 The metabolomic analysis of four independent amastigote and promastigote samples (Figure
437 S4A) supported our proteomic data. Promastigotes showed increased amino acid biosynthetic activity
438 that matched the changes in protein abundance observed for this pathway, while the amastigote
439 metabolome indicates a shift from glycolytic to TCA cycle-dependent energy production that was
440 previously described (12, 14, 80) (Figures S4B-D), with a notable increase in metabolites involved in
441 butanoate metabolism indicative of a shift between carbohydrate use as a primary energy source to
442 utilization of fatty acid oxidation. The amastigote expression profile and metabolome further indicate
443 the stage-specific production of the storage-carbohydrate mannogen, thus corroborating previous
444 observations (81) (Figure S4E).
445 Surprisingly, only few enriched GO terms matched between transcriptomics and proteomics
446 datasets, suggesting additional layers of regulation between the transcriptional and translational levels
447 of gene expression. To investigate this aspect on a genome-wide level, we next plotted the simple
448 numerical values we obtained when calculating the ratios of expression changes between ama and pro
449 observed in the transcriptomics and proteomics datasets (Figure 3B, Table 7). Only expression changes
450 were considered that either showed statistically significant differential abundance at both RNA and

451 protein levels ($p < 0.01$), or showed significant RNA changes ($p < 0.01$) with the corresponding protein
452 being detected in only one of the two stages. These latter proteins are identified by signals that were
453 arbitrarily placed at the upper (detected in ama) or the lower (detected in pro) parts of the graph.
454 Whether these proteins just escape detection due to low expression or are truly not expressed remains
455 to be established. The double ratio analysis of the resulting 2349 gene products defined four quadrants:
456 Quadrants 2 (Q2) and 4 (Q4) correspond to 430 and 1042 genes (Table 7, sheet E and I), respectively,
457 for which stage-specific expression changes correlate between protein and RNA levels, suggesting that
458 the abundance of these proteins may be mainly regulated by mRNA turn-over. Q2 (mRNA and protein
459 up in ama) includes the GO terms 'vesicle mediated transport' (17 genes) and 'lipid metabolic process'
460 (21 genes) (Table 7, sheet F), while Q4 (mRNA and protein up in pro) includes the GO term 'cell
461 motility' (41 genes) (Table 7, sheet J).

462 Counter-correlations between RNA and protein abundances (p-value < 0.01) were observed for
463 463 and 414 genes, respectively falling into quadrants Q1 (RNA down and protein up in ama) and Q3
464 (RNA down and protein up in pro) (Figure 3B, Table 7, sheets C and G). The most important difference
465 was observed for 35 genes annotated for the GO term 'ribosome biogenesis' (Figure 3C, Table 7, sheet
466 H). While this GO term defined a positively regulated gene cluster at mRNA level in amastigotes (see
467 Figure 2B), the same genes show reduced expression at this stage at protein level (Figure 3C). This lack
468 of correlation may be explained by stage-specific changes in mRNA translation efficiency.

469 In conclusion, while many stage-specific changes of protein abundance are strictly regulated
470 by similar changes at mRNA level, others show discrepancies in stage-specific abundances between
471 transcript and protein levels, revealing regulatory mechanisms that act independent of mRNA stability,
472 for example at the level of translational control or differential protein stability.

473

474 **Stage-specific protein turn-over is required for parasite differentiation.** The discrepancies we
475 observed in a sub-set of genes between changes in mRNA and protein abundance during the amastigote-
476 to-promastigote transition (see Figure 3B) primed us to investigate the role of proteasomal protein
477 degradation in *Leishmania* differentiation. We chose the highly specific and irreversible proteasome
478 inhibitor lactacystin (82, 83) over the typanosomatid-specific, reversible drug candidate LXE408 (84)

479 as the latter's potent cytotoxicity can confound direct effects on protein turnover with secondary
480 consequences of cell death, limiting its utility for dissecting proteasome function in living parasites.
481 Comparative, quantitative proteomics analyses were performed with (i) spleen-derived amastigotes
482 (ama), (ii) amastigotes after the first 18h of differentiation in the absence (control, ama-18h) and the
483 presence of latacystin (ama-lacta), and (iii) promastigotes in culture without (pro) and after 18h of
484 treatment with lactacystin (pro-lacta) (Table 8, Figure 4A and S5).

485 This data set allowed us important insight into processes of early differentiation, revealing
486 increased abundance in ama-18h compared to ama for 694 proteins (fold change ≥ 2, adjusted p-value
487 < 0.01) (Table 8b, sheet B) with GO enrichment observed for the terms 'ribosome biogenesis', 'RNA
488 methylation', 'rRNA processing', 'gene expression', and 'post-transcriptional regulation of gene
489 expression', the latter including 6 genes encoding for pseudouridine transferases known to modify
490 ribosomal (r) RNA (Figures S5A and S6) (Table 8b, sheets D to H). These data further sustain a role of
491 epitranscriptomic regulation and stage-adapted ribosomes as key processes that may initiate *Leishmania*
492 promastigote differentiation, at least in culture (31, 34, 66).

493 Lactacystin treatment further uncovered an essential regulatory role of proteasomal protein
494 degradation in *L. donovani* development, which builds on previous published observations (85). While
495 the presence of the inhibitor neither affected parasite viability (Figure S7A) nor morphology (data not
496 shown and Figure S7B) or promastigote growth (as previously shown by Silva-Jardim et al (85)),
497 lactacystin treatment abrogated the amastigote-to-promastigote developmental transition as judged by
498 the persistence of an amastigote-like morphology (i.e. oval cell shape, retracted flagellum), and the
499 absence of PFR2 expression characteristic of promastigotes (Figures 4B and C). In contrast, untreated
500 amastigotes spontaneously converted to flagellate promastigotes after 48h in culture (Figure S7D).
501 Proteasome inhibition by lactacystin blocked amastigote-to-promastigote differentiation without
502 inducing rapid global accumulation of ubiquitinated proteins (Figure S7C), which are observed only at
503 later time points and correlated with differentiation-associated remodeling rather than acute proteasome
504 inhibition.

505 Comparing the proteomics signatures of lactacystin-treated samples and untreated controls
506 (Figure S5) allowed us to reveal the proteasomal targets, whose rescue correlated with the observed

507 abrogation of differentiation. This analysis is complicated by the fact that amastigotes will not only
508 respond to the 18h treatment but also initiate their differentiation into promastigotes during this period,
509 at least in the untreated control sample. To distinguish between changes caused by lactacysin treatment
510 and changes due to the differentiation process, we plotted the ratio of ama/ama-lacta against the ratio
511 ama-18h/ama-lacta (Figure 4D), which defined one quadrant (Q3) representing 129 proteins whose
512 increased abundance in ama-lacta was exclusively due to rescue from degradation (Table 9, sheet A).
513 Applying STRING and GO analyses on these proteins, some of the most significantly enrichment terms
514 included 'protein kinase', 'cellular response to stimulus', and 'cell cycle' (Figure S8 lower panel, Table
515 9, sheet B and G).

516 Proteomics analysis of lactacystin-treated promastigotes (pro-lacta) revealed the rescue of 289
517 proteins from degradation when compared to untreated control (pro) (Table 9, sheet C). Comparison of
518 rescued proteins across both ama and pro stages revealed a series of intriguing findings: First, most of
519 these proteins were rescued in a stage-specific manner, confirming differential protein degradation as
520 an important regulatory component in the development and maintenance of *Leishmania* life cycle stages
521 as suggested by previous reports (37, 86-92). Second, just like the proteins rescued from proteasomal
522 degradation in ama-lacta, the pro-lacta data set too showed GO enrichment for the terms 'protein kinase'
523 and 'cellular response to stimulus', involving distinct sets of proteins (Figure S8, upper panel) (Table
524 9, sheets D, E and G). Thus, *Leishmania* differentiation correlates with the expression of complex
525 signaling networks that are established in a stage-specific manner. Third, when projecting the
526 lactacystin-rescued proteins to the established, stage-specific proteomes (see Figure 3), an intriguing
527 pattern emerged: the majority of proteins that were rescued in ama-lacta turned out to be part of the
528 promastigote proteome data set (Figure 4E). *Vice versa,* many proteins rescued in pro-lacta were part
529 of the amastigote-specific proteome data set (Table 9, sheets H and I), a pattern that affected 14 protein
530 kinases (Figure 4F). Thus, these proteins seem to be expressed constitutively across both stages, while
531 their steady-state stage-specific abundance is regulated by proteasomal degradation. Surprisingly, 12
532 proteins (including the protein kinase Ld1S_220237000) were rescued from degradation in both ama-
533 lacta and pro-lacta but were never identified in the proteomes of the corresponding untreated controls,

534 suggesting that they are constitutively degraded in both stages under our experimental conditions
535 (Figure 4G, Table 9, sheet F).
536 In conclusion, our results confirm the important role of protein degradation in regulating the *L.*
537 *donovani* amastigote and promastigote proteomes and identify protein kinases as key targets of stage-
538 specific proteasomal activities.
539
540 **Quantitative phosphoproteome analysis reveals *Leishmania* biological networks associated with**
541 **stage differentiation.** The investigations above associated the expression of protein kinases (and their
542 degradation) to *Leishmania* stage differentiation (Figure 4F, S8 and S9), thus confirming previous
543 reports on the importance of phosphotransferase activities in trypanosomatid development (93-103).
544 Differential turnover of these important signaling proteins by stage-specific proteasomal activities
545 likely represents a regulatory switch controlling parasite development. To further investigate how this
546 putative regulatory switch operates, we screened for stage-specific protein kinase substrates applying
547 label-free, quantitative phospho-proteomic analyses on three independent amastigote and promastigote
548 samples. We identified a total of 2079 phospho-peptides in amastigotes and 7095 phospho-peptides in
549 promastigotes, suggesting a three-fold increase in global protein phosphorylation in insect-stage
550 parasites (Table 10). However, increased TiO_2 phosphopeptide enrichment in a given sample may be
551 due either to increased substrate expression or increased *de novo* phosphorylation (Figure 5A and S10).
552 To distinguish between these two possibilities we assessed stage-specific relative phosphorylation
553 changes normalized to protein abundance (Figure 5B).

554 We identified 877 phosphoproteins in amastigote samples carrying 2079 phosphosites of which
555 55.8% (1160) were uniquely identified at this stage, while 12.6% (565) showed a significant change in
556 normalized phosphorylation levels compared to promastigotes (Figure S10, Table 11 sheets A to D).
557 Conversely, 2054 phosphoproteins with 7095 phosphorylation sites were identified in promastigote
558 samples, of which 70% (4967) were exclusively detected at this stage, while 1% (73) presented a
559 significant change in normalized phosphorylation levels compared to amastigotes (Figure S10, Table
560 11 sheets F to I). These data reveal a surprising level of stage-specific phosphorylation in promastigotes,

561 which may reflect their increased biosynthetic and proliferative activities compared to amastigotes, or
562 may be a consequence of culture adaptation.

563 We next investigated the pathways regulated by phosphotransferase activities analyzing the
564 phosphoproteomes of amastigote and promastigote for enriched biological processes (Figure 5C) (Table
565 11, sheets E and J). Stage-specific enrichment was observed in the pro dataset for 'ciliary cell motility',
566 indicating that flagellar biogenesis and activity are not only regulated by increased protein abundance,
567 but also by increased phosphorylation of flagellar proteins. Surprisingly, in both the ama and pro
568 datasets, similar functions were enriched, including cell division (e.g. 'cytokinesis', 'cell cycle'),
569 signaling (e.g. 'protein aa phosphorylation', 'signal transduction'), or post-transcriptional regulation of
570 gene expression. Thus, aside stage-specific protein turnover (see above, Figure 4), differential
571 phosphorylation represents yet another layer of regulation that contributes to the establishment of
572 biological networks in *Leishmania* that share similar function in both ama and pro, but whose
573 components are stage-specifically regulated at post-translational levels.

574 Analyzing stage-enriched, functional networks in further detail using the STRING applications
575 of the Cytoscape software package revealed a series of potential regulatory interactions (Figure S11,
576 Table 12): A first group of protein kinase substrates is represented by protein kinases themselves with
577 more than 30 and 100 members of this large protein family identified in the ama and pro
578 phosphoproteomes, respectively (Table 11, sheets D and H, see Figure 5D for phosphorylation pattern
579 of some members of the MAP kinase pathway). An additional group of protein kinase substrates in both
580 amastigote and promastigote phosphoproteomes include stage-specific phosphatases (18 in ama and 55
581 in pro) that can counteract protein kinase activities and even deactivate signaling cascades by
582 dephosphorylation of protein kinase substrates (Figure S11, Table 11, sheets D and H). Furthermore,
583 the stage-specific phosphoproteomes showed enrichment in functional networks linked to ribosomal
584 biogenesis and RNA processing suggesting that protein kinases may control the establishment of stage-
585 specific ribosomes. Finally, the identification of networks linked to proteasomal protein degradation in
586 both ama and pro datasets not only further sustains the role of protein turnover in *Leishmania* stage
587 differentiation, but uncovers a possible feedback loop between proteasomal activities controlling stage-
588 specific degradation of protein kinases (see Figure 4), which in turn may control stage-specific ubiquitin

589 ligases and deubiquitinating enzymes via differential phosphorylation (see Figure 5D for
590 phosphorylation pattern of selected members of the Ubiquitin proteasomal system).

591 **Discussion**

592 By applying a 5-layer systems analysis to spleen-derived bona fide amastigotes and culture-derived
593 promastigotes, we identified a series of functionally related gene clusters that are co-regulated during
594 *Leishmania donovani* stage differentiation. This co-regulation occurs at multiple levels, including
595 transcript stability, proteasomal protein turnover, and protein phosphorylation. Our study underscores
596 the complex molecular architecture of the *Leishmania* developmental process and provides novel
597 insights into possible regulatory feedback loops that may coordinate stage-specific transitions. These
598 results raise important questions regarding the integration of these regulatory networks during
599 differentiation, and their contributions to environmental sensing and adaptive evolution. In the
600 following we discuss these putative networks in the context of the current literature and propose
601 experimental strategies for their downstream, mechanistic analyses.

602 A first series of possible regulatory networks proposed by our results could rely on recursive or
603 self-controlling interactions, where components of a given pathway are regulated by the pathway itself
604 (Figure 6A). In promastigotes for example, a co-regulated, functional gene cluster showing stage-
605 specific increase in transcript abundance was defined by the GO term 'post-transcriptional regulation
606 of gene expression'. In the absence of stage-specific gene dosage changes (Figure 1) and the lack of
607 transcriptional regulation of gene expression in *Leishmania* (104) the stage-specific expression changes
608 of these transcripts thus is likely regulated itself at the post-transcriptional level. Such auto-regulatory
609 feedback is common for RNA-binding proteins (RBPs), which play a central role in controlling mRNA
610 stability, often targeting their own transcript (105). This helps keep protein levels stable (negative
611 feedback) or create on/off switches for developmental processes (positive feedback) (106). In *T. brucei*
612 <u>for example</u>, the stage-specific expression of RBPs, such as ZC3H22 or RBP9, is regulated at post-
613 transcriptional levels (107), while other RBPs, such as TbZFP3 or RBP10, can control developmental
614 transitions by stabilizing cohorts of mRNAs, thus defining developmental regulons (108, 109). In
615 *Leishmania*, RBPs are likely to participate in comparable regulatory networks. These can be
616 investigated through methods such as crosslinking and immunoprecipitation (CLIP) to map RBP

617 binding to 3' untranslated regions (3'UTRs), computational approaches to identify conserved regulatory
618 sequence motifs, and loss-of-function analyses targeting either trans-acting factors (RBPs and their
619 interaction partners) or cis-acting elements (e.g., RBP binding sites within 3'UTRs).

620 Our data propose a similar recursive feedback loop that seems to act on the level of protein
621 translation, which was revealed by a paradox: while amastigotes showed increased abundance for 38
622 transcripts annotated for the GO term 'ribosome biogenesis' (Table 4, sheet E), the corresponding
623 proteins showed reduced abundance in amastigotes compared with promastigotes (Figure 3C). This
624 dissociation between RNA and protein abundances indicates that ribosomal components themselves
625 may be regulated at translational levels. Increased ribosomal protein abundance in promastigotes could
626 satisfy the requirement of increased translation capacity at this fast-growing stage (31, 110). In contrast,
627 increased mRNA abundance of ribosomal components in amastigotes may indicate stage-specific
628 mechanisms of mRNA storage (111) that may allow to jump start promastigote differentiation and
629 accelerated growth following exposure to low temperature and neutral pH. This possibility is supported
630 by our proteomics investigations of the early differentiation process, revealing ribosomal biogenesis as
631 one of the first pathways induced over the initial 18h during the amastigote-to-promastigote
632 developmental transition (Figure S6).

633 Differentiation to promastigotes was associated not only with quantitative changes of ribosomal
634 components as indicated by co-regulated expression of ribosomal proteins and translation factors (see
635 Table 8), but also seems to affect ribosome structure itself as indicated by stage-specific expression
636 changes of gene sets enriched in the GO terms 'RNA methylation' (8 methyltransferases, including the
637 rRNA methyltransferases Ld1S_350672300 and Ld1S_350694000) and 'pseudouridine synthesis' (6
638 pseudouridine synthases and the H/ACA snoRNP Nop10 (Ld1S_360722900) (Table 8, sheets D to H).
639 The differential expression of snoRNAs (see Figure 2C and Table 5) and the developmentally regulated
640 changes in rRNA modification that can affect ribosome activity (34) (Figure 2D) indeed support the
641 existence of such stage-specific ribosomes. These results are in line with our recent reports providing
642 indication for specialized ribosomes in *Leishmania* adaptation, in which we correlated changes in rRNA
643 pseudouridylation to *L. donovani* fitness gain in culture (31, 66). Cryo-EM analysis of purified

644 ribosomes from amastigotes and derived promastigotes, combined with targeted deletion of individual
645 snoRNA genes, will be critical to uncover stage-specific structural and functional adaptations of such
646 stage-specific ribosomes.

647 Finally, a third possible recursive feedback loop seems to act at the post-translational level
648 involving members of various protein kinase (PK) families, which not only showed stage-specific
649 expression, but also represented a main class of phosphorylation substrates themselves. This interaction
650 may reflect stage-specific signaling cascades, where downstream kinases are activated through
651 phosphorylation by upstream kinases, such as exemplified by the MAP kinase pathway (103, 112).
652 Indeed, 11 members of the MAP kinase family showed stage-specific changes in their phosphorylation
653 pattern (Figure 5D), 9 of which were only detected in the promastigote phospho-proteome and were
654 previously associated with this stage, being implicated in flagellar biogenesis (MPK9 and MPK3) or
655 metacyclogenesis (MPK4) (98, 102, 113). In contrast, the two MAP kinases MPK2 and MPK10 -
656 previously linked to amastigote differentiation and virulence (99, 102) - showed an amastigote-specific
657 increase in protein abundance and relative phosphorylation change for defined phosphorylation sites.
658 In *L. mexicana*, such a recursive PK feedback loop has been identified between the interacting protein
659 kinases LmxMKK and LmxMPK3, which cross-phosphorylate each other to regulate flagellar length
660 (113). To further dissociate the complex regulatory relationships between parasite PKs, protein-protein
661 interaction maps should be established (e.g. co-IP, proximity labelling), combined with in vitro kinase
662 assays to reveal direct kinase-substrate relationships.

663 Most PKs have pleiotropic effects across biological systems, due to their ability to
664 phosphorylate a wide range of functionally unrelated substrates (114). Our analysis of relative
665 phosphorylation changes normalized to protein abundance confirms such pleotropic function in
666 *Leishmania* and suggests parasite PKs at the center of a second form of possible feedback loop defined
667 by reciprocal interactions, where components of two or more regulatory pathways may cross-control
668 each other (Figure 6A). For example, as judged by changes in phosphorylation abundance, it seems that
669 stage-specific PK activities act on a series of phosphatases, which in return may modify kinase activities
670 by dephosphorylation (Table 11, sheets D and G). Such reciprocal regulation between both enzyme

671 families is well-established across many eukaryotic systems, for example between mammalian ERK1/2
672 and the MAPK phosphatase DUSP6/MKP-3 (115), or yeast CDK1 and the phosphatase Cdc25,
673 controlling mitotic entry (116). In addition, 47 differentially phosphorylated proteins were associated
674 with 'Translation', some of which have been linked in *Leishmania* to translational control, cell cycle
675 regulation or infectivity (29, 117-121). This opens the possibility of yet another reciprocal feedback
676 loop, where phosphorylation of ribosomal components could fine tune translational control, which in
677 turn may affect the expression of protein kinases themselves (122-130).

678 Finally, our results suggest the possibility of a third reciprocal feedback loop between protein
679 kinases and proteins of the proteasomal system that may govern *Leishmania* stage transitions. Previous
680 genetic analyses demonstrated an essential role for various components of this system in promastigote-
681 to-amastigote transition and intracellular survival, including *L. mexicana* ubiquitin conjugating (E2)
682 enzymes (UBC1/CDC34, UBC2 and UEV1), the E3 ubiquitin ligase HECT2 or various deubiquitinases
683 (e.g. DUBs 4, 7, 13) (91, 92). By applying the irreversible proteasome inhibitor lactacystin, we extended
684 this role to the reverse process - amastigote-to-promastigote differentiation - demonstrating that
685 proteasomal activities are critical for both directions of the developmental cycle (Figure 4). The
686 constitutive expression of many proteasomal components across both amastigote and promastigote
687 stages supports a role of phosphorylation in regulating stage-specific proteasomal activities, considering
688 that phosphorylation of DUBs has been linked to changes in their stability, localization, specificity or
689 catabolic activity (131, 132). We indeed identified 11 DUBs and 10 ubiquitin ligases/transferases
690 showing stage-specific phosphorylation at specific residues (Table 11, sheets D and I). This correlated
691 with the stage-specific proteasomal degradation of 14 PKs (Figure 4F, Table 9, sheet G), including two
692 previously implicated in *Leishmania in vivo* fitness (Repressor of differentiation kinase 1,
693 Ld1S_320540600; differentiation inhibitory kinase, Ld1S_280397500) (102). These findings support
694 the existence of a possible kinase/proteasome reciprocal feedback loop in early parasite development.
695 The experimental validation of such regulatory interactions will require in-depth biochemical,
696 molecular, and systems biology approaches involving global kinase-substrate mapping (114), in vitro
697 reconstitution assays using recombinant proteins to demonstrate reciprocal kinase and proteolytic
698 activities, and genetic perturbation test to reveal the biological impact of the regulatory interaction.

699

700

701 The complexity of regulatory interactions between protein kinases and the proteasomal
702 pathway is further increased by observations showing that substrate phosphorylation can mediate
703 subsequent ubiquitination and degradation, while ubiquitination of MAP kinase family members can
704 regulate kinase activity and localization rather than promote degradation (139-141). Future experiments
705 simultaneously analyzing changes in both phosphoproteome and ubiquitome during *Leishmania* stage-
706 differentiation and making precision mutants that lack the ubiquitination or phosphorylation sites may
707 help elucidate this complex regulatory interaction and identify individual proteins and their PTMs that
708 drive parasite development

709 In conclusion, our data represent an important novel resource to experimentally assess the
710 regulatory landscape of *Leishmania* stage development. We propose genetic feedback control as a
711 central mechanism in parasite differentiation, with stage-specific interactions between genes and their
712 products likely adapting the parasite phenotype to the environmental changes encountered inside its
713 vertebrate and invertebrate hosts. In contrast to the major phenotypic shift observed between
714 mammalian-stage amastigotes and insect-stage promastigotes, each developmental stage is stably
715 maintained within its respective host even in the wake of environmental fluctuations. Such phenotypic
716 robustness is known to rely on highly inter-connected, stage-specific regulatory networks (142), which
717 in the case of *Leishmania* could implicate recursive and reciprocal genetic interactions between protein
718 translation, protein degradation and protein phosphorylation (Figure 6B and C). Our results define
719 *Leishmania* differentiation as an excellent model system to study how alternations between phenotypic
720 plasticity (i.e. developmental transitions) and robustness (stable maintenance of stages) shape microbial
721 fitness, and provides a powerful experimental framework for future studies on the emergence of stable,
722 adaptive biological traits through feedback regulation.

723

724

725 **Figure legends**

726

727 **Figure 1: Comparative genomic analysis of *L. donovani* lesion-isolated amastigotes and derived**
728 **promastigotes.** (A) Schematic overview of the parasite samples used for the various systems level
729 analyses presented in this study. A more detailed overview is shown in Figure S1. (B - D) Genomic
730 analyses. (B) Heatmap showing the somy score of three individual differentiation experiments using
731 hamster-isolated amastigotes (ama1, ama2 and ama3) and their corresponding, culture-derived
732 promastigotes analysed at passage 2 (pro1, pro2 and pro3). Samples and chromosomes are indicated on
733 the x- and y-axis, respectively. The somy scores were calculated as described in Material and Methods
734 and correlate to the grey level according to the shown legend. (C) Ratio plot showing the gene coverage
735 ratio ama versus pro (y-axis) for all genes across the 36 chromosomes (x-axis) as calculated based on
736 median read depth normalized by the somy score. Each color represents one individual differentiation
737 experiment using ama isolates from individual hamsters. The red dotted lines indicate the ratio values
738 corresponding to 1.5 (upper line) and 0.5 (lower line), indicating respectively gain or loss of one gene
739 copy in the ama samples. Fluctuations between 0.5 and 1.5 were not considered significant. (D)
740 Correlation plots representing the individual (histograms on the diagonal) and pairwise (off-diagonal
741 scatterplots) distributions of SNP frequencies for the indicated samples. Of note, only SNPs with a
742 frequency above 10% were plotted. Due to bottle neck events, some low frequency SNPs appear to be
743 unique in one or the other stage as they are either 'lost' (filtered out) or 'gained' (passing the 10%
744 cutoff) between the ama and pro samples. The absence of SNPs at 100% is explained by the
745 heterozygous nature of the Ld1S genome.

746

747 **Figure 2: Stage-specific transcript profiling.** (A) Volcano plots (left panels) showing differential
748 transcripts abundance between ama and pro samples as assessed by RNA-seq analysis. The dotted lines
749 indicate fold change (FC) = 2 (vertical line) and p-value = 0.01 (horizontal line). Transcripts with FC <
750 2 or adjusted p-value > 0.01 are represented by black dots. Transcripts with significant increased
751 abundance FC ≥ 2 and adjusted p-value < 0.01 in ama and pro are indicated respectively in dark cyan
752 and dark grey for all transcripts (left panel) or transcripts of only coding genes (middle panel).

753 Transcripts for non-coding genes with significant increased abundance FC ≥ 2 and adjusted p-value <
754 0.01 in ama and pro are indicated in the right volcano plot (orange dots). The pie chart (right panel)
755 depicts the percentage of transcripts for each of the categories. (B) GO term enrichment analysis of
756 these transcripts for the category 'biological process' was performed, and 'cluster efficiency' (blue) and
757 'enrichment score' (orange) were plotted for pro (left panel) and ama datasets (all transcripts, middle
758 panel; transcripts for coding genes, right panel). The graphs show some of the most significantly
759 enriched GO terms associated with a Benjamini and Hochberg (BH) p-value < 0.05 that were identified
760 using the BiNGO plug-in in Cytoscape. (C) Volcano plot corresponding to the differential expression
761 of snoRNA between pro and ama stages. Cyan dots (ama) and grey dots (pro) represent signals with FC
762 ≥ 2 and adj. p-value < 0.05. Black dots represent non-significant changes. (D) Localization of
763 differentially modified rRNA sites on the *Leishmania* ribosome. The RNA modifications are indicated
764 as space filling in the *Leishmania* cryo-EM structure (PDB: 8RXH). The identity of the RNA
765 modification is defined by the label (Ψ, pseudouridine; Gm and Cm refer to guanine and cytosine
766 methylation, respectively; numbers indicate residues). Upregulated and downregulated RNA
767 modifications in amastigotes according to Rajan et al (34) are indicated in red and blue, respectively.
768
769
770 **Figure 3: Systems analysis of the stage-specific transcriptome and proteome.** (A) Volcano plot
771 showing differential protein abundance between four ama and pro samples as assessed by label-free,
772 quantitative proteomics analysis. The dotted lines indicate fold change (FC) = 2 (vertical line) and false
773 discovery rate (FDR) = 0.01 (horizontal line). Proteins with FC < 2 or FDR > 0.01 are represented by
774 light grey dots. Proteins that were reproducibly detected in only one of the two stages (considered
775 unique) are represented by the lateral histograms plotting their relative abundance according the iBAQ
776 value. These proteins together with proteins showing differential abundance of FC ≥ 2 and adjusted p-
777 value < 0.01 are indicated for ama in dark cyan and for pro in dark grey (see Table 6). GO term
778 enrichment analysis for the category 'biological process' was performed, and the resulting values for
779 'cluster efficiency' (blue) and 'enrichment score' (orange) were plotted for ama (middle panel) and pro
780 (right panel). The graphs show the main GO terms identified using the BiNGO plug-in in Cytoscape

781 and associated with a BH p-value < 0.05. (B) Double ratio plot showing the log2 fold change between
782 ama and pro in transcript (x-axis) and protein (y-axis) abundances. Red dots correspond to changes in
783 both transcript and protein abundance defined either by significant differential abundance at both levels
784 (p-value < 0.01), or by significant RNA changes (p-value < 0.01) corresponding to proteins detected in
785 only one of the two stages. The dotted lines indicate fold changes (FC) = 2. The infinite symbol (∞)
786 represents proteins that are unique in the ama (upper signals) or pro (lower signals) datasets. Word
787 cloud enrichment performed with the *L. donovani* LdBPK orthologs is presented for each of the 4
788 quadrants, Q1 to Q4 and a detailed GO enrichment analysis is given in Table 7. The font size is
789 proportional to the number of genes per GO term and the grey scale refers to the p-value calculated for
790 each GO term. (C) KEGG map for ribosome biogenesis. Each gene associated with expression changes
791 indicated in Q1 to Q4 (see Figure 2C) and annotated with the GO term 'ribosome biogenesis' has been
792 projected on the ribosome biogenesis KEGG map. Each gene is represented by a square with the left
793 segment showing fold changes between ama and pro at transcript and the right segment showing fold
794 changes at the protein level, with the differential abundance indicated by the color and its intensity (red,
795 increase; green, decrease). Only genes quantified in both transcriptome and proteome analyses and
796 associated with an adjusted p-value < 0.01 were considered.
797
798 **Figure 4: Analysis of stage-specific proteasomal protein turn-over.** (A) Overview of experimental
799 workflow. To assess early and late steps of differentiation (left part of the graph in black), comparative,
800 quantitative proteomics analyses were performed on tissue-isolated amastigotes (ama), amastigotes at
801 18h into the transition to promastigotes in culture (ama-18h) and fully differentiated promastigotes after
802 1 passage *in vitro* (pro). To gain insight into stage-specific and constitutive protein degradation (right
803 part of the graph in red), amastigotes and promastigotes were treated with the irreversible inhibitor
804 lactacystin (ama-lacta and pro-lacta). (B) Microscopic images of amastigotes at 18h in absence of
805 lactacystin treatment (amastigotes, left), after 48h in absence (-, middle) or presence of the inhibitor (+,
806 right). (C) Western blot analysis. Protein extracts were obtained from $2x10^6$ parasites after 3, 6, 18 and
807 48h of differentiation from amastigotes to promastigotes in presence (+) or absence (-) of lactacystin.
808 Extracts were separated by electrophoresis, transferred onto PVDF membrane and the presence of PFR2

809 was revealed using an anti-PFR2 antibody (upper panel). A Coomassie blue stain of the same gel is
810 shown as loading control (lower panel). (D) Double ratio plot comparing the log2 fold changes in
811 protein abundance between ama-18h/ama-lacta (x-axis) and ama/ama-lacta (y-axis). Dashed lines
812 indicate FC = 2 and the infinite symbol (∞) represent proteins that are unique to one or the other
813 comparison. (E) Projection of the proteins stabilized in presence of the inhibitor in ama (ama-lacta,
814 orange) and pro (pro-lacta, pink) onto the double ratio plot shown in Figure 3B. Note that ama-specific
815 proteins are rescued from degradation in pro-lacta, while pro-specific proteins are rescued from
816 degradation in ama-lacta. (F) List of the protein kinases stabilized after lactacystin treatment in pro or
817 ama (columns lacta rescued) and either not detected in the total proteome (column ama vs pro, grey
818 cell) or specifically quantified at the ama (red cell) or the pro (green cell) stage. (G) Venn diagram
819 showing the number of proteins specifically stabilized in ama or pro or stabilized in both stages after
820 lactacystin treatment.
821
822 **Figure 5: Stage-specific phospho-proteomic profiling.** (A) Volcano plots corresponding to the total
823 proteome (right panel) and phosphoproteome (left panel) analyses. Proteins and phosphosites (P-sites)
824 only identified in one stage are presented at each side of the volcano plots. Cyan dots (ama) and grey
825 dots (pro) represent signals with FC ≥ 2 and FDR < 1%. Light grey dots represent non-significant
826 changes. (B) Relative phosphorylation change normalized to protein abundance. Ratio plot comparing
827 the log2 fold changes in total protein abundance between ama and pro (x-axis) and phosphosite
828 abundance in ama versus pro (y-axis). Dashed lines indicate a FC = 2. The color intensity of each dot
829 reflects the p-value calculated for the relative phosphorylation change normalized to protein abundance
830 as indicated in the graph. Confidence values were derived as described in Supplementary Methods. (C)
831 GO term enrichment analysis for the category 'biological process. Only stage-specific phosphosites
832 were considered (i.e. sites that showed a significant increase in relative phosphorylation normalized to
833 protein abundance, and sites that were only detected in one or the other stage, whether the protein was
834 identified or not in the total proteome analysis). The histogram plots show 'cluster efficiency' in blue
835 and 'enrichment score' in orange for the GO term enrichment analysis performed with the ama (middle
836 panel) and pro (right panel) datasets. The main GO terms identified using the BiNGO plug-in in

837 Cytoscape and associated with a BH p-value < 0.05 are shown. (D) Phosphorylation pattern of MAPK
838 and MAPKK proteins (left panel) or Ubiquitin hydrolases and transferases (right panel) identified in
839 the relative phosphorylation change normalized to protein abundance. The positions of the
840 phosphorylated amino acid specific to ama (red) and pro (green) are indicated. Only phosphopeptides
841 identified in the relative phosphorylation change normalized to phosphorylation level (see Table 11)
842 and detected either in one stage or the other or quantified with a FC ≥ 2 were considered for the
843 identification of the phosphosites.
844
845 **Figure 6: Network analyses.** (A) Model of *Leishmania* gene expression regulation during stage
846 differentiation. (B-C) Network analysis. Networks, restricted to the protein kinases (blue nodes),
847 proteins implicated in ribosome biogenesis and ribosomal proteins (violet nodes) and proteins linked to
848 ubiquitination/deubiquitination (orange nodes) identified based on normalized phosphorylation levels
849 conducted in ama (B) or pro (C), were generated with the STRING plug-in of the Cytoscape software
850 package using *L. infantum* orthologs and full STRING network with a confidence score cutoff of 0.4.
851 Each node represents a phosphoprotein with the respective gene identifier indicated. GO terms
852 associated to the proteins are represented by the colored segments around the nodes according to the
853 legend shown in the graph. Only GO terms associated with a p-value < 0.05 were considered.
854
855 **Sup figure legends**
856 **Figure S1:** Overview of the samples used in this study. Each *L. donovani* infected hamster is identified
857 by the cage number, as are the hamster-derived amastigotes (ama) and corresponding promastigotes
858 (pro).
859
860 **Figure S2:** (A) Box plots representing the median somy score for all the chromosomes. Each box
861 corresponds to one of three biological replicates for ama and pro as indicated in the graph. Sample
862 identifiers are detailed in the legend of Figure 1A and Figure S1. (B) Frequency distribution plots
863 representing, for each biological replicate and each chromosome, a kernel density estimate of the
864 distribution of SNP frequencies in the amastigote and promastigote sample.

865

866 **Figure S3:** (A) Hierarchical clustering of the samples. The dendogram is built using the Ward method.
867 The normed data was log-transformed first and at max 5,000 most variable features were selected. (B)
868 Principal component analysis. The two main components are represented. Ama and pro samples
869 correspond to blue and orange dots respectively.

870

871 **Figure S4:** (A) Cluster analysis of metabolites showing differential abundance in ama and pro samples.
872 (B) Quantification of amino-acids or metabolites involved in glycolysis, TCA cycle and mannogen
873 cycle. The y-axis represents the intensity for each metabolite as detected by MS. (C-D) Correlation
874 between metabolomic and proteomic analyses for TCA cycle (C) and Glycolysis/Gluconeogenesis (D).
875 Fold changes in proteins abundance (squares) and metabolite abundance (circles) with adjusted p-values
876 of respectively < 0.01 and < 0.05 were projected on the respective KEGG maps. The color intensity
877 reflects the fold change value as indicated by the legends in the graphs. (E) Representation of the
878 mannogen pathway. Metabolites are represented by a square, with red-lined squares corresponding to
879 the metabolites that accumulate at the ama stage. Proteins are represented by a circle, with fold changes
880 in protein abundance between ama and pro datasets indicated by color and intensity (red, increase;
881 green, decrease).

882

883 **Figure S5:** Label free quantitative proteomic analyses in presence or absence of lactacystin. (A) to (E)
884 Volcano plots representing changes in protein abundance for the different comparisons (left panels) and
885 GO term enrichment analyses for the indicated sample (right panels). Proteins identified by at least two
886 peptides in at least three out of four biological replicates were considered. For volcano plots, colored
887 dots indicate values with FDR < 0.01 and FC ≥ 2 (see Table 8). The light grey dots indicate non-
888 significant expression changes. The colored bars indicate unique protein identifications in one (green)
889 or the other (orange) condition with relative abundance indicated by the iBAQ value (left panels).
890 Proteins quantified in only one condition or showing a significant increase in abundance (FC ≥ 2 and
891 adjusted p-value < 0.01) were used to perform the GO analysis for the category 'biological process'.
892 The histogram plots show 'cluster efficiency' in blue and 'enrichment score' in orange (right panels)

893 for a selection of GO terms identified using the BiNGO plug-in in Cytoscape and associated with a BH
894 p-value < 0.05. (A) ama vs ama-18h; (B) ama-18h vs pro; (C) ama vs ama lacta; (D) ama-18h vs ama
895 lacta; (E) pro vs pro lacta.
896
897 **Figure S6:** (A) Functional network enrichment analysis for proteins showing increased abundance in
898 ama-18h compared to ama. The network was generated with the *L. infantum* orthologs using the
899 STRING plug-in of the Cytoscape software package and considering the full STRING network with a
900 confidence score cutoff of 0.4. The GO terms associated with each protein are represented by the
901 colored segments according to the legend. Only GO terms associated with a p-value < 0.05 were
902 considered. (B) KEGG map for ribosome biogenesis showing changes in abundance protein between
903 ama and ama-18h. Only proteins with an adjusted p-value < 0.01 were considered. Differential
904 abundance is indicated by the color and its intensity (red, increase; green, decrease).
905
906 **Figure S7:** (A) Viability assessment of the indicated amastigote (upper panel) and promastigote (lower
907 panel) samples after lactacystin treatment by FACS analysis using propidium iodide or YoPro staining.
908 (B) Microscopic images of promastigotes at 18h in absence (upper image) or presence of 10 µM of
909 lactacystin (lower image). (C) Western blot analysis of protein extracts obtained from ama (upper
910 image) and pro (lower image) in presence or absence of lactacystin treatment. 10 µg of proteins were
911 labelled with Cy5, separated on NuPAGE 4-12%, and transferred onto PVDF membrane. Membranes
912 were subsequently incubated with a monoclonal antibody against ubiquitin and revealed with HRP-
913 conjugated secondary antibodies. Images of Cy5-labelled proteins (left images), ubiquitinated proteins
914 (middle images) and an overlay of both images (right images, Cy5-labelled proteins in green,
915 ubiquitinated proteins in red) are presented. The table shows the relative quantification after
916 normalization using the Cy5-labelled proteins of untreated samples as a loading control. (D) Western
917 blot analysis of protein extracts obtained at the indicated time points after *in vitro* differentiation from
918 hamster-derived amastigotes to promastigotes. 10 µg of protein were separated on NuPAGE 4-12%,
919 transferred onto PVDF membrane subsequently incubated with antibodies against paraflagellar rod
920 proteins 1 and 2 and alpha-tubulin, and revealed with HRP-conjugated secondary antibodies (left

921 image). Micrographs showing hamster-derived amastigotes during *in vitro* differentiation to
922 promastigotes (right image). Parasites were collected at the time points indicated, fixed in 4% PFA, and
923 seeded on poly-L-lysine-treated coverslips. Parasites were observed with a 63x oil immersion objective
924 and images were processed with AxioVision Rel.4.8 software. Differential interference contrast (DIC)
925 microscopy was performed with Axioplan 2 imaging microscope using a 63x oil immersion objective,
926 Axiovision software and AxioCam MRm camera (Carl Zeiss). The scale bars correspond to 1 µm.
927
928 **Figure S8:** Functional network enrichment analysis for the proteins stabilized in presence of lactacystin
929 in promastigote (pro) and amastigote (ama) datasets. The network was generated with the *L. infantum*
930 orthologs using the STRING plug-in of the Cytoscape software package and considering the full
931 STRING network with a confidence score cutoff of 0.4. The GO terms associated with each protein are
932 represented by the coloured segments according to the legend. Only GO terms associated with a p-value
933 < 0.05 were considered.
934
935 **Figure S9:** List of protein kinases stabilized in presence of lactacystin. Their corresponding orthologs
936 in *L. donovani* strain LdBPK and *L. mexicana* are indicated, as well as the knock-out phenotype as
937 published by Baker et al (2021) (102).
938
939 **Figure S10:** Upset plot representing the number of phosphopeptides (y-axis, blue histograms, numbers
940 are indicated) and the samples in which they were quantified (x-axis). Pie chart of the phosphopeptide
941 analysis showing the distribution of the phosphorylation sites according to the condition in which they
942 were quantified as indicated in the legend of the graph.
943
944 **Figure S11:** Functional Network analysis. Networks for proteins that show unique or increased
945 phosphorylation in ama (upper panel) and in pro (lower panel) datasets were generated with the
946 STRING plug-in of the Cytoscape software package using *L. infantum* orthologs and considering the
947 full STRING network with a confidence score cutoff of 0.4. The nodes represent phosphoproteins
948 associated with one or more GO terms (listed in the graph), with the respective gene identifier indicated.

949 The GO terms associated to the proteins are represented by the colored segments around the nodes
950 according to the legend shown in the graph. Only GO terms associated with a FDR < 0.05 were
951 considered.
952
953
954
955

Acknowledgments

We thank the CEA-CNRGH for its contribution to the sequencing costs and all the CEA-CNRGH staff who performed sample preparation and sequencing for their excellent technical assistance. We acknowledge the help of the HPC Core Facility of the Institut Pasteur for this work. We thank Georges Haustant and Caroline Proux from the Biomics Platform, C2RT, Institut Pasteur, Paris, France for the library preparation and the sequencing, Hugo Varet and Rachel Legendre from Institut Pasteur, Université Paris Cité, Biostatistics and Bioinformatics Hub, Paris, France for their contribution to the RNA seq data analysis. We thank Karim Sébastien from the animal facility of the Institut Pasteur for his commitment in the care of our animals.

This work was supported by the Agence Nationale pour la Recherche Labex 'Integrative Biology of Emerging Infectious Diseases' contract ANR-10-LABX-62-IBEID and Labex 'French Alliance for Parasitology and Health Care' contract ANR-11-LABX-0024 (GFS, PP), the France Génomique National infrastructure, funded as part of the « Investissements d'Avenir » program managed by the Agence Nationale pour la Recherche contract ANR-10-INBS-09 (GH, HV, RL, CP), and the ERC SYNERGY project DecoLeishRN, Grant agreement ID: 101071613.

984 **REFERENCES**

985

986

987 1. Hollin T, Le Roch KG. From Genes to Transcripts, a Tightly Regulated Journey in
988 Plasmodium. Frontiers in cellular and infection microbiology. 2020;10:618454. doi:
989 10.3389/fcimb.2020.618454. PubMed PMID: 33425787; PubMed Central PMCID:
990 PMC7793691.
991 2. Modrzynska K, Pfander C, Chappell L, Yu L, Suarez C, Dundas K, Gomes AR,
992 Goulding D, Rayner JC, Choudhary J, Billker O. A Knockout Screen of ApiAP2 Genes Reveals
993 Networks of Interacting Transcriptional Regulators Controlling the Plasmodium Life Cycle.
994 Cell host & microbe. 2017;21(1):11-22. doi: 10.1016/j.chom.2016.12.003. PubMed PMID:
995 28081440; PubMed Central PMCID: PMC5241200.
996 3. Waldman BS, Schwarz D, Wadsworth MH, 2nd, Saeij JP, Shalek AK, Lourido S.
997 Identification of a Master Regulator of Differentiation in Toxoplasma. Cell. 2020;180(2):359-
998 72 e16. doi: 10.1016/j.cell.2019.12.013. PubMed PMID: 31955846; PubMed Central PMCID:
999 PMC6978799.
1000 4. Alvar J, Velez ID, Bern C, Herrero M, Desjeux P, Cano J, Jannin J, den Boer M, Team
1001 WHOLC. Leishmaniasis worldwide and global estimates of its incidence. PloS one.
1002 2012;7(5):e35671. doi: 10.1371/journal.pone.0035671. PubMed PMID: 22693548; PubMed
1003 Central PMCID: PMC3365071.
1004 5. WHO. Leishmaniasis 2023. Available from: https://www.who.int/news-room/fact-
1005 sheets/detail/leishmaniasis.
1006 6. Maia C, Conceicao C, Pereira A, Rocha R, Ortuno M, Munoz C, Jumakanova Z, Perez-
1007 Cutillas P, Ozbel Y, Toz S, Baneth G, Monge-Maillo B, Gasimov E, Van der Stede Y, Torres
1008 G, Gossner CM, Berriatua E. The estimated distribution of autochthonous leishmaniasis by
1009 Leishmania infantum in Europe in 2005-2020. PLoS neglected tropical diseases.
1010 2023;17(7):e0011497. doi: 10.1371/journal.pntd.0011497. PubMed PMID: 37467280;
1011 PubMed Central PMCID: PMC10389729.
1012 7. Barbiero A, Spinicci M, Aiello A, Maruotto M, Antonello RM, Formica G, Piccica M,
1013 Isola P, Parisio EM, Nardone M, Valentini S, Mangano V, Brunelli T, Bianchi L, Bartalesi F,
1014 Costa C, Sambo M, Tumbarello M, Sani S, Fabiani S, Rossetti B, Nencioni C, Lanari A,
1015 Aquilini D, Montorzi G, Venturini E, Galli L, Rinninella G, Falcone M, Ceriegi F, Amadori F,
1016 Vincenti A, Blanc P, Vellere I, Tacconi D, Luchi S, Moneta S, Massi D, Brogi M, Voller F,
1017 Gemmi F, Rossolini GM, Cusi MG, Bruschi F, Bartoloni A, Zammarchi L. The Uprise of
1018 Human Leishmaniasis in Tuscany, Central Italy: Clinical and Epidemiological Data from a
1019 Multicenter Study. Microorganisms. 2024;12(10). doi: 10.3390/microorganisms12101963.
1020 PubMed PMID: 39458272; PubMed Central PMCID: PMC11509187.
1021 8. Handman E. Cell biology of Leishmania. Advances in parasitology. 1999;44:1-39. doi:
1022 10.1016/s0065-308x(08)60229-8. PubMed PMID: 10563394.
1023 9. Clayton CE. Life without transcriptional control? From fly to man and back again. The
1024 EMBO journal. 2002;21(8):1881-8. doi: 10.1093/emboj/21.8.1881. PubMed PMID:
1025 11953307; PubMed Central PMCID: PMC125970.
1026 10. Liang XH, Haritan A, Uliel S, Michaeli S. trans and cis splicing in trypanosomatids:
1027 mechanism, factors, and regulation. Eukaryotic cell. 2003;2(5):830-40. doi:
1028 10.1128/EC.2.5.830-840.2003. PubMed PMID: 14555465; PubMed Central PMCID:
1029 PMC219355.

1030 11. McConville MJ, Ralton JE. Developmentally regulated changes in the cell surface
1031 architecture of Leishmania parasites. Behring Institute Mitteilungen. 1997(99):34-43. PubMed
1032 PMID: 9303200.
1033 12. McConville MJ, de Souza D, Saunders E, Likic VA, Naderer T. Living in a
1034 phagolysosome; metabolism of Leishmania amastigotes. Trends in parasitology.
1035 2007;23(8):368-75. doi: 10.1016/j.pt.2007.06.009. PubMed PMID: 17606406.
1036 13. Rosenzweig D, Smith D, Opperdoes F, Stern S, Olafson RW, Zilberstein D. Retooling
1037 Leishmania metabolism: from sand fly gut to human macrophage. FASEB journal : official
1038 publication of the Federation of American Societies for Experimental Biology.
1039 2008;22(2):590-602. doi: 10.1096/fj.07-9254com. PubMed PMID: 17884972.
1040 14. McConville MJ, Naderer T. Metabolic pathways required for the intracellular survival
1041 of Leishmania. Annual review of microbiology. 2011;65:543-61. doi: 10.1146/annurev-micro-
1042 090110-102913. PubMed PMID: 21721937.
1043 15. Sunter J, Gull K. Shape, form, function and Leishmania pathogenicity: from textbook
1044 descriptions to biological understanding. Open biology. 2017;7(9). doi: 10.1098/rsob.170165.
1045 PubMed PMID: 28903998; PubMed Central PMCID: PMC5627057.
1046 16. Dandugudumula R, Fischer-Weinberger R, Zilberstein D. Morphogenesis Dynamics in
1047 Leishmania Differentiation. Pathogens. 2022;11(9). doi: 10.3390/pathogens11090952.
1048 PubMed PMID: 36145385; PubMed Central PMCID: PMC9505065.
1049 17. Trenaman A, Glover L, Hutchinson S, Horn D. A post-transcriptional respiratome
1050 regulon in trypanosomes. Nucleic acids research. 2019;47(13):7063-77. doi:
1051 10.1093/nar/gkz455. PubMed PMID: 31127277; PubMed Central PMCID: PMC6648352.
1052 18. Boucher N, Wu Y, Dumas C, Dube M, Sereno D, Breton M, Papadopoulou B. A
1053 common mechanism of stage-regulated gene expression in Leishmania mediated by a
1054 conserved 3'-untranslated region element. The Journal of biological chemistry.
1055 2002;277(22):19511-20. doi: 10.1074/jbc.M200500200. PubMed PMID: 11912202.
1056 19. McNicoll F, Muller M, Cloutier S, Boilard N, Rochette A, Dube M, Papadopoulou B.
1057 Distinct 3'-untranslated region elements regulate stage-specific mRNA accumulation and
1058 translation in Leishmania. The Journal of biological chemistry. 2005;280(42):35238-46. doi:
1059 10.1074/jbc.M507511200. PubMed PMID: 16115874.
1060 20. Bringaud F, Muller M, Cerqueira GC, Smith M, Rochette A, El-Sayed NM,
1061 Papadopoulou B, Ghedin E. Members of a large retroposon family are determinants of post-
1062 transcriptional gene expression in Leishmania. PLoS pathogens. 2007;3(9):1291-307. doi:
1063 10.1371/journal.ppat.0030136. PubMed PMID: 17907803; PubMed Central PMCID:
1064 PMC2323293.
1065 21. Azizi H, Dumas C, Papadopoulou B. The Pumilio-domain protein PUF6 contributes to
1066 SIDER2 retroposon-mediated mRNA decay in Leishmania. Rna. 2017;23(12):1874-85. doi:
1067 10.1261/rna.062950.117. PubMed PMID: 28877997; PubMed Central PMCID: PMC5689007.
1068 22. Clayton C, Estevez A. The exosomes of trypanosomes and other protists. Advances in
1069 experimental medicine and biology. 2011;702:39-49. doi: 10.1007/978-1-4419-7841-7_4.
1070 PubMed PMID: 21713676.
1071 23. Schwede A, Manful T, Jha BA, Helbig C, Bercovich N, Stewart M, Clayton C. The role
1072 of deadenylation in the degradation of unstable mRNAs in trypanosomes. Nucleic acids
1073 research. 2009;37(16):5511-28. doi: 10.1093/nar/gkp571. PubMed PMID: 19596809; PubMed
1074 Central PMCID: PMC2760810.
1075 24. Kramer S. The ApaH-like phosphatase TbALPH1 is the major mRNA decapping
1076 enzyme of trypanosomes. PLoS pathogens. 2017;13(6):e1006456. doi:
1077 10.1371/journal.ppat.1006456. PubMed PMID: 28628654; PubMed Central PMCID:
1078 PMC5491325.

1079 25. Yoffe Y, Zuberek J, Lewdorowicz M, Zeira Z, Keasar C, Orr-Dahan I, Jankowska-
1080 Anyszka M, Stepinski J, Darzynkiewicz E, Shapira M. Cap-binding activity of an eIF4E
1081 homolog from Leishmania. Rna. 2004;10(11):1764-75. doi: 10.1261/rna.7520404. PubMed
1082 PMID: 15388875; PubMed Central PMCID: PMC1370664.
1083 26. Yoffe Y, Zuberek J, Lerer A, Lewdorowicz M, Stepinski J, Altmann M, Darzynkiewicz
1084 E, Shapira M. Binding specificities and potential roles of isoforms of eukaryotic initiation
1085 factor 4E in Leishmania. Eukaryotic cell. 2006;5(12):1969-79. doi: 10.1128/EC.00230-06.
1086 PubMed PMID: 17041189; PubMed Central PMCID: PMC1694823.
1087 27. David M, Gabdank I, Ben-David M, Zilka A, Orr I, Barash D, Shapira M. Preferential
1088 translation of Hsp83 in Leishmania requires a thermosensitive polypyrimidine-rich element in
1089 the 3' UTR and involves scanning of the 5' UTR. Rna. 2010;16(2):364-74. doi:
1090 10.1261/rna.1874710. PubMed PMID: 20040590; PubMed Central PMCID: PMC2811665.
1091 28. Freire ER, Sturm NR, Campbell DA, de Melo Neto OP. The Role of Cytoplasmic
1092 mRNA Cap-Binding Protein Complexes in Trypanosoma brucei and Other Trypanosomatids.
1093 Pathogens. 2017;6(4). doi: 10.3390/pathogens6040055. PubMed PMID: 29077018; PubMed
1094 Central PMCID: PMC5750579.
1095 29. Shrivastava R, Tupperwar N, Schwartz B, Baron N, Shapira M. LeishIF4E-5 Is a
1096 Promastigote-Specific Cap-Binding Protein in Leishmania. International journal of molecular
1097 sciences. 2021;22(8). doi: 10.3390/ijms22083979. PubMed PMID: 33921489; PubMed
1098 Central PMCID: PMC8069130.
1099 30. Assis LA, Santos Filho MVC, da Cruz Silva JR, Bezerra MJR, de Aquino I, Merlo KC,
1100 Holetz FB, Probst CM, Rezende AM, Papadopoulou B, da Costa Lima TDC, de Melo Neto
1101 OP. Identification of novel proteins and mRNAs differentially bound to the Leishmania
1102 Poly(A) Binding Proteins reveals a direct association between PABP1, the RNA-binding
1103 protein RBP23 and mRNAs encoding ribosomal proteins. PLoS neglected tropical diseases.
1104 2021;15(10):e0009899. doi: 10.1371/journal.pntd.0009899. PubMed PMID: 34705820;
1105 PubMed Central PMCID: PMC8575317 competing interests.
1106 31. Piel L, Rajan KS, Bussotti G, Varet H, Legendre R, Proux C, Douche T, Giai-Gianetto
1107 Q, Chaze T, Cokelaer T, Vojtkova B, Gordon-Bar N, Doniger T, Cohen-Chalamish S, Rengaraj
1108 P, Besse C, Boland A, Sadlova J, Deleuze JF, Matondo M, Unger R, Volf P, Michaeli S,
1109 Pescher P, Spath GF. Experimental evolution links post-transcriptional regulation to
1110 Leishmania fitness gain. PLoS pathogens. 2022;18(3):e1010375. doi:
1111 10.1371/journal.ppat.1010375. PubMed PMID: 35294501; PubMed Central PMCID:
1112 PMC8959184.
1113 32. Rodriguez-Almonacid CC, Kellogg MK, Karamyshev AL, Karamysheva ZN.
1114 Ribosome Specialization in Protozoa Parasites. International journal of molecular sciences.
1115 2023;24(8). doi: 10.3390/ijms24087484. PubMed PMID: 37108644; PubMed Central PMCID:
1116 PMC10138883.
1117 33. Gutierrez Guarnizo SA, Tikhonova EB, Karamyshev AL, Muskus CE, Karamysheva
1118 ZN. Translational reprogramming as a driver of antimony-drug resistance in Leishmania.
1119 Nature communications. 2023;14(1):2605. doi: 10.1038/s41467-023-38221-1. PubMed PMID:
1120 37147291; PubMed Central PMCID: PMC10163012.
1121 34. Rajan KS, Aryal S, Hiregange DG, Bashan A, Madmoni H, Olami M, Doniger T,
1122 Cohen-Chalamish S, Pescher P, Taoka M, Nobe Y, Fedorenko A, Bose T, Zimermann E, Prina
1123 E, Aharon-Hefetz N, Pilpel Y, Isobe T, Unger R, Spath GF, Yonath A, Michaeli S. Structural
1124 and mechanistic insights into the function of Leishmania ribosome lacking a single
1125 pseudouridine modification. Cell reports. 2024;43(5):114203. doi:
1126 10.1016/j.celrep.2024.114203. PubMed PMID: 38722744.
1127 35. Besteiro S, Williams RA, Morrison LS, Coombs GH, Mottram JC. Endosome sorting
1128 and autophagy are essential for differentiation and virulence of Leishmania major. The Journal

1129 of biological chemistry. 2006;281(16):11384-96. doi: 10.1074/jbc.M512307200. PubMed
1130 PMID: 16497676.
1131 36. Williams RA, Tetley L, Mottram JC, Coombs GH. Cysteine peptidases CPA and CPB
1132 are vital for autophagy and differentiation in Leishmania mexicana. Molecular microbiology.
1133 2006;61(3):655-74. doi: 10.1111/j.1365-2958.2006.05274.x. PubMed PMID: 16803590.
1134 37. Besteiro S, Williams RA, Coombs GH, Mottram JC. Protein turnover and
1135 differentiation in Leishmania. International journal for parasitology. 2007;37(10):1063-75. doi:
1136 10.1016/j.ijpara.2007.03.008. PubMed PMID: 17493624; PubMed Central PMCID:
1137 PMC2244715.
1138 38. Williams RA, Smith TK, Cull B, Mottram JC, Coombs GH. ATG5 is essential for
1139 ATG8-dependent autophagy and mitochondrial homeostasis in Leishmania major. PLoS
1140 pathogens. 2012;8(5):e1002695. doi: 10.1371/journal.ppat.1002695. PubMed PMID:
1141 22615560; PubMed Central PMCID: PMC3355087.
1142 39. Williams RA, Mottram JC, Coombs GH. Distinct roles in autophagy and importance in
1143 infectivity of the two ATG4 cysteine peptidases of Leishmania major. The Journal of biological
1144 chemistry. 2013;288(5):3678-90. doi: 10.1074/jbc.M112.415372. PubMed PMID: 23166325;
1145 PubMed Central PMCID: PMC3561585.
1146 40. Sakamoto H, Nakada-Tsukui K, Besteiro S. The Autophagy Machinery in Human-
1147 Parasitic Protists; Diverse Functions for Universally Conserved Proteins. Cells. 2021;10(5).
1148 doi: 10.3390/cells10051258. PubMed PMID: 34069694; PubMed Central PMCID:
1149 PMC8161075.
1150 41. Casgrain PA, Martel C, McMaster WR, Mottram JC, Olivier M, Descoteaux A.
1151 Cysteine Peptidase B Regulates Leishmania mexicana Virulence through the Modulation of
1152 GP63 Expression. PLoS pathogens. 2016;12(5):e1005658. doi: 10.1371/journal.ppat.1005658.
1153 PubMed PMID: 27191844; PubMed Central PMCID: PMC4871588.
1154 42. Pescher P, Blisnick T, Bastin P, Spath GF. Quantitative proteome profiling informs on
1155 phenotypic traits that adapt Leishmania donovani for axenic and intracellular proliferation.
1156 Cellular microbiology. 2011;13(7):978-91. doi: 10.1111/j.1462-5822.2011.01593.x. PubMed
1157 PMID: 21501362.
1158 43. Li H, Handsaker B, Wysoker A, Fennell T, Ruan J, Homer N, Marth G, Abecasis G,
1159 Durbin R, Genome Project Data Processing S. The Sequence Alignment/Map format and
1160 SAMtools. Bioinformatics. 2009;25(16):2078-9. doi: 10.1093/bioinformatics/btp352. PubMed
1161 PMID: 19505943; PubMed Central PMCID: PMC2723002.
1162 44. DePristo MA, Banks E, Poplin R, Garimella KV, Maguire JR, Hartl C, Philippakis AA,
1163 del Angel G, Rivas MA, Hanna M, McKenna A, Fennell TJ, Kernytsky AM, Sivachenko AY,
1164 Cibulskis K, Gabriel SB, Altshuler D, Daly MJ. A framework for variation discovery and
1165 genotyping using next-generation DNA sequencing data. Nature genetics. 2011;43(5):491-8.
1166 doi: 10.1038/ng.806. PubMed PMID: 21478889; PubMed Central PMCID: PMC3083463.
1167 45. Quinlan AR, Hall IM. BEDTools: a flexible suite of utilities for comparing genomic
1168 features. Bioinformatics. 2010;26(6):841-2. doi: 10.1093/bioinformatics/btq033. PubMed
1169 PMID: 20110278; PubMed Central PMCID: PMC2832824.
1170 46. Prieto Barja P, Pescher P, Bussotti G, Dumetz F, Imamura H, Kedra D, Domagalska
1171 M, Chaumeau V, Himmelbauer H, Pages M, Sterkers Y, Dujardin JC, Notredame C, Spath GF.
1172 Haplotype selection as an adaptive mechanism in the protozoan pathogen Leishmania
1173 donovani. Nature ecology & evolution. 2017;1(12):1961-9. doi: 10.1038/s41559-017-0361-x.
1174 PubMed PMID: 29109466.
1175 47. Liao Y, Smyth GK, Shi W. featureCounts: an efficient general purpose program for
1176 assigning sequence reads to genomic features. Bioinformatics. 2014;30(7):923-30. doi:
1177 10.1093/bioinformatics/btt656. PubMed PMID: 24227677.

48. Spath GF, Bussotti G. GIP: an open-source computational pipeline for mapping genomic instability from protists to cancer cells. Nucleic acids research. 2022;50(6):e36. doi: 10.1093/nar/gkab1237. PubMed PMID: 34928370; PubMed Central PMCID: PMC8989552.
49. McKinney W. Data Structures for Statistical Computing in Python2010. doi: doi.org/10.25080/Majora-92bf1922-00a.
50. Reback J, jbrockmendel, McKinney W, Van Den Bossche J, Augspurger T, Cloud P, Hawkins S, gfyoung, Sinhrks, Roeschke M, Klein A, Petersen T, Tratner J, She C, Ayd W. pandas-dev/pandas: Pandas 1.3.1.
51. Hunter JD. Matplotlib: A 2D Graphics Environment. Computing in Science & Engineering. 2007;9(3):90-5. doi: 10.1109/MCSE.2007.55.
52. Waskom ML. Seaborn: statistical data visualization. . Journal of Open Source Software. 2021;6(60). doi: 10.21105/joss.03021.
53. Cokelaer T. Sequana': a Set of Snakemake NGS pipelines. Journal of Open Source Software. 2017;2(16). doi: 10.21105/joss.00352.
54. Koster J, Rahmann S. Snakemake--a scalable bioinformatics workflow engine. Bioinformatics. 2012;28(19):2520-2. doi: 10.1093/bioinformatics/bts480. PubMed PMID: 22908215.
55. Langmead B, Salzberg SL. Fast gapped-read alignment with Bowtie 2. Nature methods. 2012;9(4):357-9. doi: 10.1038/nmeth.1923. PubMed PMID: 22388286; PubMed Central PMCID: PMC3322381.
56. Love MI, Huber W, Anders S. Moderated estimation of fold change and dispersion for RNA-seq data with DESeq2. Genome biology. 2014;15(12):550. doi: 10.1186/s13059-014-0550-8. PubMed PMID: 25516281; PubMed Central PMCID: PMC4302049.
57. Martin M. Cutadapt removes adapter sequences from high-throughput sequencing reads. EMBnetjournal. 2011;17(1). doi: 10.14806/ej.17.1.200.
58. Dobin A, Davis CA, Schlesinger F, Drenkow J, Zaleski C, Jha S, Batut P, Chaisson M, Gingeras TR. STAR: ultrafast universal RNA-seq aligner. Bioinformatics. 2013;29(1):15-21. doi: 10.1093/bioinformatics/bts635. PubMed PMID: 23104886; PubMed Central PMCID: PMC3530905.
59. Team RC. R: A Language and Environment for Statistical Computing. R Foundation for Statistical Computing2016.
60. Benjamini YHY. Controlling the False Discovery Rate: A Practical and Powerful Approach to Multiple Testing. Journal of the Royal Statistical Society: Series B (Methodological). 1995;57(1):289-300. doi: 10.1111/j.2517-6161.1995.tb02031.x.
61. Erde J, Loo RR, Loo JA. Enhanced FASP (eFASP) to increase proteome coverage and sample recovery for quantitative proteomic experiments. Journal of proteome research. 2014;13(4):1885-95. doi: 10.1021/pr4010019. PubMed PMID: 24552128; PubMed Central PMCID: PMC3993969.
62. Matheron L, van den Toorn H, Heck AJ, Mohammed S. Characterization of biases in phosphopeptide enrichment by Ti(4+)-immobilized metal affinity chromatography and TiO2 using a massive synthetic library and human cell digests. Analytical chemistry. 2014;86(16):8312-20. doi: 10.1021/ac501803z. PubMed PMID: 25068997.
63. Creek DJ, Jankevics A, Burgess KE, Breitling R, Barrett MP. IDEOM: an Excel interface for analysis of LC-MS-based metabolomics data. Bioinformatics. 2012;28(7):1048-9. doi: 10.1093/bioinformatics/bts069. PubMed PMID: 22308147.
64. Scheltema RA, Jankevics A, Jansen RC, Swertz MA, Breitling R. PeakML/mzMatch: a file format, Java library, R library, and tool-chain for mass spectrometry data analysis. Analytical chemistry. 2011;83(7):2786-93. doi: 10.1021/ac2000994. PubMed PMID: 21401061.

1227 65. Pettersen EF, Goddard TD, Huang CC, Meng EC, Couch GS, Croll TI, Morris JH,
1228 Ferrin TE. UCSF ChimeraX: Structure visualization for researchers, educators, and developers.
1229 Protein science : a publication of the Protein Society. 2021;30(1):70-82. doi: 10.1002/pro.3943.
1230 PubMed PMID: 32881101; PubMed Central PMCID: PMC7737788.
1231 66. Bussotti G, Piel L, Pescher P, Domagalska MA, Rajan KS, Cohen-Chalamish S,
1232 Doniger T, Hiregange DG, Myler PJ, Unger R, Michaeli S, Spath GF. Genome instability
1233 drives epistatic adaptation in the human pathogen Leishmania. Proceedings of the National
1234 Academy of Sciences of the United States of America. 2021;118(51). doi:
1235 10.1073/pnas.2113744118. PubMed PMID: 34903666; PubMed Central PMCID:
1236 PMC8713814.
1237 67. Perez-Riverol Y, Csordas A, Bai J, Bernal-Llinares M, Hewapathirana S, Kundu DJ,
1238 Inuganti A, Griss J, Mayer G, Eisenacher M, Perez E, Uszkoreit J, Pfeuffer J, Sachsenberg T,
1239 Yilmaz S, Tiwary S, Cox J, Audain E, Walzer M, Jarnuczak AF, Ternent T, Brazma A,
1240 Vizcaino JA. The PRIDE database and related tools and resources in 2019: improving support
1241 for quantification data. Nucleic acids research. 2019;47(D1):D442-D50. doi:
1242 10.1093/nar/gky1106. PubMed PMID: 30395289; PubMed Central PMCID: PMC6323896.
1243 68. Edgar R, Domrachev M, Lash AE. Gene Expression Omnibus: NCBI gene expression
1244 and hybridization array data repository. Nucleic acids research. 2002;30(1):207-10. doi:
1245 10.1093/nar/30.1.207. PubMed PMID: 11752295; PubMed Central PMCID: PMC99122.
1246 69. Athar A, Fullgrabe A, George N, Iqbal H, Huerta L, Ali A, Snow C, Fonseca NA,
1247 Petryszak R, Papatheodorou I, Sarkans U, Brazma A. ArrayExpress update - from bulk to
1248 single-cell expression data. Nucleic acids research. 2019;47(D1):D711-D5. doi:
1249 10.1093/nar/gky964. PubMed PMID: 30357387; PubMed Central PMCID: PMC6323929.
1250 70. Bussotti G, Li B, Pescher P, Vojtkova B, Louradour I, Pruzinova K, Sadlova J, Volf P,
1251 Spath GF. Leishmania allelic selection during experimental sand fly infection correlates with
1252 mutational signatures of oxidative DNA damage. Proceedings of the National Academy of
1253 Sciences of the United States of America. 2023;120(10):e2220828120. doi:
1254 10.1073/pnas.2220828120. PubMed PMID: 36848551; PubMed Central PMCID:
1255 PMC10013807.
1256 71. Marques CA, Dickens NJ, Paape D, Campbell SJ, McCulloch R. Genome-wide
1257 mapping reveals single-origin chromosome replication in Leishmania, a eukaryotic microbe.
1258 Genome biology. 2015;16:230. doi: 10.1186/s13059-015-0788-9. PubMed PMID: 26481451;
1259 PubMed Central PMCID: PMC4612428.
1260 72. Bussotti G, Gouzelou E, Cortes Boite M, Kherachi I, Harrat Z, Eddaikra N, Mottram
1261 JC, Antoniou M, Christodoulou V, Bali A, Guerfali FZ, Laouini D, Mukhtar M, Dumetz F,
1262 Dujardin JC, Smirlis D, Lechat P, Pescher P, El Hamouchi A, Lemrani M, Chicharro C, Llanes-
1263 Acevedo IP, Botana L, Cruz I, Moreno J, Jeddi F, Aoun K, Bouratbine A, Cupolillo E, Spath
1264 GF. Leishmania Genome Dynamics during Environmental Adaptation Reveal Strain-Specific
1265 Differences in Gene Copy Number Variation, Karyotype Instability, and Telomeric
1266 Amplification. mBio. 2018;9(6). doi: 10.1128/mBio.01399-18. PubMed PMID: 30401775;
1267 PubMed Central PMCID: PMC6222132.
1268 73. Kloehn J, Saunders EC, O'Callaghan S, Dagley MJ, McConville MJ. Characterization
1269 of metabolically quiescent Leishmania parasites in murine lesions using heavy water labeling.
1270 PLoS pathogens. 2015;11(2):e1004683. doi: 10.1371/journal.ppat.1004683. PubMed PMID:
1271 25714830; PubMed Central PMCID: PMC4340956.
1272 74. Bussotti G, Benkahla A, Jeddi F, Souiai O, Aoun K, Spath GF, Bouratbine A. Nuclear
1273 and mitochondrial genome sequencing of North-African Leishmania infantum isolates from
1274 cured and relapsed visceral leishmaniasis patients reveals variations correlating with geography
1275 and phenotype. Microbial genomics. 2020;6(10). doi: 10.1099/mgen.0.000444. PubMed
1276 PMID: 32975503; PubMed Central PMCID: PMC7660250.

1277 75. Cuypers B, Meysman P, Erb I, Bittremieux W, Valkenborg D, Baggerman G, Mertens
1278 I, Sundar S, Khanal B, Notredame C, Dujardin JC, Domagalska MA, Laukens K. Four layer
1279 multi-omics reveals molecular responses to aneuploidy in Leishmania. PLoS pathogens.
1280 2022;18(9):e1010848. doi: 10.1371/journal.ppat.1010848. PubMed PMID: 36149920;
1281 PubMed Central PMCID: PMC9534393.
1282 76. Dumetz F, Imamura H, Sanders M, Seblova V, Myskova J, Pescher P, Vanaerschot M,
1283 Meehan CJ, Cuypers B, De Muylder G, Spath GF, Bussotti G, Vermeesch JR, Berriman M,
1284 Cotton JA, Volf P, Dujardin JC, Domagalska MA. Modulation of Aneuploidy in Leishmania
1285 donovani during Adaptation to Different In Vitro and In Vivo Environments and Its Impact on
1286 Gene Expression. mBio. 2017;8(3). doi: 10.1128/mBio.00599-17. PubMed PMID: 28536289;
1287 PubMed Central PMCID: PMC5442457.
1288 77. Fiebig M, Kelly S, Gluenz E. Comparative Life Cycle Transcriptomics Revises
1289 Leishmania mexicana Genome Annotation and Links a Chromosome Duplication with
1290 Parasitism of Vertebrates. PLoS pathogens. 2015;11(10):e1005186. doi:
1291 10.1371/journal.ppat.1005186. PubMed PMID: 26452044; PubMed Central PMCID:
1292 PMC4599935.
1293 78. Wu Y, El Fakhry Y, Sereno D, Tamar S, Papadopoulou B. A new developmentally
1294 regulated gene family in Leishmania amastigotes encoding a homolog of amastin surface
1295 proteins. Molecular and biochemical parasitology. 2000;110(2):345-57. doi: 10.1016/s0166-
1296 6851(00)00290-5. PubMed PMID: 11071288.
1297 79. Haile S, Dupe A, Papadopoulou B. Deadenylation-independent stage-specific mRNA
1298 degradation in Leishmania. Nucleic acids research. 2008;36(5):1634-44. doi:
1299 10.1093/nar/gkn019. PubMed PMID: 18250085; PubMed Central PMCID: PMC2275140.
1300 80. Saunders EC, Sernee MF, Ralton JE, McConville MJ. Metabolic stringent response in
1301 intracellular stages of Leishmania. Current opinion in microbiology. 2021;63:126-32. doi:
1302 10.1016/j.mib.2021.07.007. PubMed PMID: 34340099.
1303 81. Sernee MF, Ralton JE, Nero TL, Sobala LF, Kloehn J, Vieira-Lara MA, Cobbold SA,
1304 Stanton L, Pires DEV, Hanssen E, Males A, Ward T, Bastidas LM, van der Peet PL, Parker
1305 MW, Ascher DB, Williams SJ, Davies GJ, McConville MJ. A Family of Dual-Activity
1306 Glycosyltransferase-Phosphorylases Mediates Mannogen Turnover and Virulence in
1307 Leishmania Parasites. Cell host & microbe. 2019;26(3):385-99 e9. doi:
1308 10.1016/j.chom.2019.08.009. PubMed PMID: 31513773.
1309 82. Zhang H, Lin G. Microbial proteasomes as drug targets. PLoS pathogens.
1310 2021;17(12):e1010058. doi: 10.1371/journal.ppat.1010058. PubMed PMID: 34882737;
1311 PubMed Central PMCID: PMC8659679.
1312 83. Omura S, Crump A. Lactacystin: first-in-class proteasome inhibitor still excelling and
1313 an exemplar for future antibiotic research. The Journal of antibiotics. 2019;72(4):189-201. doi:
1314 10.1038/s41429-019-0141-8. PubMed PMID: 30755736; PubMed Central PMCID:
1315 PMC6760633.
1316 84. Nagle A, Biggart A, Be C, Srinivas H, Hein A, Caridha D, Sciotti RJ, Pybus B,
1317 Kreishman-Deitrick M, Bursulaya B, Lai YH, Gao MY, Liang F, Mathison CJN, Liu X, Yeh
1318 V, Smith J, Lerario I, Xie Y, Chianelli D, Gibney M, Berman A, Chen YL, Jiricek J, Davis LC,
1319 Liu X, Ballard J, Khare S, Eggimann FK, Luneau A, Groessl T, Shapiro M, Richmond W,
1320 Johnson K, Rudewicz PJ, Rao SPS, Thompson C, Tuntland T, Spraggon G, Glynne RJ, Supek
1321 F, Wiesmann C, Molteni V. Discovery and Characterization of Clinical Candidate LXE408 as
1322 a Kinetoplastid-Selective Proteasome Inhibitor for the Treatment of Leishmaniases. Journal of
1323 medicinal chemistry. 2020;63(19):10773-81. doi: 10.1021/acs.jmedchem.0c00499. PubMed
1324 PMID: 32667203; PubMed Central PMCID: PMC7549094 authors are employees or former
1325 employees of GNF or NITD or NIBR: A.S.N., A.B., C.B., S.H., A.H., B.B., Y.H.L., M.-Y.G.,
1326 F.L., C.J.N.M., X.L., V.Y., J.S., I.L., Y.X., D.C., M.G., A.B., Y.-L.C., J.J., L.C.D., X.L., J.B.,

1327 S.K., F.K.E., A.L., T.G., M.S., W.R., K.J., P.J.R., S.P.S.R., T.T., G.S., R.J.G., F.S., C.W., and
1328 V.M.
1329 85. Silva-Jardim I, Horta MF, Ramalho-Pinto FJ. The Leishmania chagasi proteasome: role
1330 in promastigotes growth and amastigotes survival within murine macrophages. Acta tropica.
1331 2004;91(2):121-30. doi: 10.1016/j.actatropica.2004.03.007. PubMed PMID: 15234661.
1332 86. Kumar P, Sundar S, Singh N. Degradation of pteridine reductase 1 (PTR1) enzyme
1333 during growth phase in the protozoan parasite Leishmania donovani. Experimental
1334 parasitology. 2007;116(2):182-9. doi: 10.1016/j.exppara.2006.12.008. PubMed PMID:
1335 17275814.
1336 87. Perez-Pertejo Y, Alvarez-Velilla R, Estrada CG, Balana-Fouce R, Reguera RM.
1337 Leishmania donovani: proteasome-mediated down-regulation of methionine
1338 adenosyltransferase. Parasitology. 2011;138(9):1082-92. doi: 10.1017/S0031182011000862.
1339 PubMed PMID: 21813028.
1340 88. Vince JE, Tull D, Landfear S, McConville MJ. Lysosomal degradation of Leishmania
1341 hexose and inositol transporters is regulated in a stage-, nutrient- and ubiquitin-dependent
1342 manner. International journal for parasitology. 2011;41(7):791-800. doi:
1343 10.1016/j.ijpara.2011.02.003. PubMed PMID: 21447343; PubMed Central PMCID:
1344 PMC3592973.
1345 89. Khare S, Nagle AS, Biggart A, Lai YH, Liang F, Davis LC, Barnes SW, Mathison CJ,
1346 Myburgh E, Gao MY, Gillespie JR, Liu X, Tan JL, Stinson M, Rivera IC, Ballard J, Yeh V,
1347 Groessl T, Federe G, Koh HX, Venable JD, Bursulaya B, Shapiro M, Mishra PK, Spraggon G,
1348 Brock A, Mottram JC, Buckner FS, Rao SP, Wen BG, Walker JR, Tuntland T, Molteni V,
1349 Glynne RJ, Supek F. Proteasome inhibition for treatment of leishmaniasis, Chagas disease and
1350 sleeping sickness. Nature. 2016;537(7619):229-33. doi: 10.1038/nature19339. PubMed PMID:
1351 27501246; PubMed Central PMCID: PMC5161665.
1352 90. Wyllie S, Brand S, Thomas M, De Rycker M, Chung CW, Pena I, Bingham RP, Bueren-
1353 Calabuig JA, Cantizani J, Cebrian D, Craggs PD, Ferguson L, Goswami P, Hobrath J, Howe J,
1354 Jeacock L, Ko EJ, Korczynska J, MacLean L, Manthri S, Martinez MS, Mata-Cantero L, Moniz
1355 S, Nuhs A, Osuna-Cabello M, Pinto E, Riley J, Robinson S, Rowland P, Simeons FRC,
1356 Shishikura Y, Spinks D, Stojanovski L, Thomas J, Thompson S, Viayna Gaza E, Wall RJ,
1357 Zuccotto F, Horn D, Ferguson MAJ, Fairlamb AH, Fiandor JM, Martin J, Gray DW, Miles TJ,
1358 Gilbert IH, Read KD, Marco M, Wyatt PG. Preclinical candidate for the treatment of visceral
1359 leishmaniasis that acts through proteasome inhibition. Proceedings of the National Academy
1360 of Sciences of the United States of America. 2019;116(19):9318-23. doi:
1361 10.1073/pnas.1820175116. PubMed PMID: 30962368; PubMed Central PMCID:
1362 PMC6511062.
1363 91. Burge RJ, Damianou A, Wilkinson AJ, Rodenko B, Mottram JC. Leishmania
1364 differentiation requires ubiquitin conjugation mediated by a UBC2-UEV1 E2 complex. PLoS
1365 pathogens. 2020;16(10):e1008784. doi: 10.1371/journal.ppat.1008784. PubMed PMID:
1366 33108402; PubMed Central PMCID: PMC7647121.
1367 92. Damianou A, Burge RJ, Catta-Preta CMC, Geoghegan V, Nievas YR, Newling K,
1368 Brown E, Burchmore R, Rodenko B, Mottram JC. Essential roles for deubiquitination in
1369 Leishmania life cycle progression. PLoS pathogens. 2020;16(6):e1008455. doi:
1370 10.1371/journal.ppat.1008455. PubMed PMID: 32544189; PubMed Central PMCID:
1371 PMC7319358.
1372 93. Parsons M, Worthey EA, Ward PN, Mottram JC. Comparative analysis of the kinomes
1373 of three pathogenic trypanosomatids: Leishmania major, Trypanosoma brucei and
1374 Trypanosoma cruzi. BMC genomics. 2005;6:127. doi: 10.1186/1471-2164-6-127. PubMed
1375 PMID: 16164760; PubMed Central PMCID: PMC1266030.

1376 94. Morales MA, Renaud O, Faigle W, Shorte SL, Spath GF. Over-expression of
1377 Leishmania major MAP kinases reveals stage-specific induction of phosphotransferase
1378 activity. International journal for parasitology. 2007;37(11):1187-99. doi:
1379 10.1016/j.ijpara.2007.03.006. PubMed PMID: 17481635.
1380 95. Rotureau B, Morales MA, Bastin P, Spath GF. The flagellum-mitogen-activated protein
1381 kinase connection in Trypanosomatids: a key sensory role in parasite signalling and
1382 development? Cellular microbiology. 2009;11(5):710-8. doi: 10.1111/j.1462-
1383 5822.2009.01295.x. PubMed PMID: 19207727.
1384 96. Morales MA, Pescher P, Spath GF. Leishmania major MPK7 protein kinase activity
1385 inhibits intracellular growth of the pathogenic amastigote stage. Eukaryotic cell. 2010;9(1):22-
1386 30. doi: 10.1128/EC.00196-09. PubMed PMID: 19801421; PubMed Central PMCID:
1387 PMC2805286.
1388 97. Potenza M, Schenkman S, Laverriere M, Tellez-Inon MT. Functional characterization
1389 of TcCYC2 cyclin from Trypanosoma cruzi. Experimental parasitology. 2012;132(4):537-45.
1390 doi: 10.1016/j.exppara.2012.09.002. PubMed PMID: 22982808.
1391 98. Dacher M, Morales MA, Pescher P, Leclercq O, Rachidi N, Prina E, Cayla M,
1392 Descoteaux A, Spath GF. Probing druggability and biological function of essential proteins in
1393 Leishmania combining facilitated null mutant and plasmid shuffle analyses. Molecular
1394 microbiology. 2014;93(1):146-66. doi: 10.1111/mmi.12648. PubMed PMID: 24823804.
1395 99. Cayla M, Rachidi N, Leclercq O, Schmidt-Arras D, Rosenqvist H, Wiese M, Spath GF.
1396 Transgenic analysis of the Leishmania MAP kinase MPK10 reveals an auto-inhibitory
1397 mechanism crucial for stage-regulated activity and parasite viability. PLoS pathogens.
1398 2014;10(9):e1004347. doi: 10.1371/journal.ppat.1004347. PubMed PMID: 25232945;
1399 PubMed Central PMCID: PMC4169501.
1400 100. Jones NG, Thomas EB, Brown E, Dickens NJ, Hammarton TC, Mottram JC. Regulators
1401 of Trypanosoma brucei cell cycle progression and differentiation identified using a kinome-
1402 wide RNAi screen. PLoS pathogens. 2014;10(1):e1003886. doi:
1403 10.1371/journal.ppat.1003886. PubMed PMID: 24453978; PubMed Central PMCID:
1404 PMC3894213.
1405 101. Rachidi N, Taly JF, Durieu E, Leclercq O, Aulner N, Prina E, Pescher P, Notredame C,
1406 Meijer L, Spath GF. Pharmacological assessment defines Leishmania donovani casein kinase
1407 1 as a drug target and reveals important functions in parasite viability and intracellular
1408 infection. Antimicrobial agents and chemotherapy. 2014;58(3):1501-15. doi:
1409 10.1128/AAC.02022-13. PubMed PMID: 24366737; PubMed Central PMCID: PMC3957854.
1410 102. Baker N, Catta-Preta CMC, Neish R, Sadlova J, Powell B, Alves-Ferreira EVC,
1411 Geoghegan V, Carnielli JBT, Newling K, Hughes C, Vojtkova B, Anand J, Mihut A, Walrad
1412 PB, Wilson LG, Pitchford JW, Volf P, Mottram JC. Systematic functional analysis of
1413 Leishmania protein kinases identifies regulators of differentiation or survival. Nature
1414 communications. 2021;12(1):1244. doi: 10.1038/s41467-021-21360-8. PubMed PMID:
1415 33623024; PubMed Central PMCID: PMC7902614.
1416 103. Cayla M, Nievas YR, Matthews KR, Mottram JC. Distinguishing functions of
1417 trypanosomatid protein kinases. Trends in parasitology. 2022;38(11):950-61. doi:
1418 10.1016/j.pt.2022.08.009. PubMed PMID: 36075845.
1419 104. Grunebast J, Lorenzen S, Clos J. Genome-wide quantification of polycistronic
1420 transcription in Leishmania major. mBio. 2025;16(1):e0224124. doi: 10.1128/mbio.02241-24.
1421 PubMed PMID: 39584812; PubMed Central PMCID: PMC11708010.
1422 105. Muller-McNicoll M, Rossbach O, Hui J, Medenbach J. Auto-regulatory feedback by
1423 RNA-binding proteins. Journal of molecular cell biology. 2019;11(10):930-9. doi:
1424 10.1093/jmcb/mjz043. PubMed PMID: 31152582; PubMed Central PMCID: PMC6884704.

1425 106. Perrimon N, Pitsouli C, Shilo BZ. Signaling mechanisms controlling cell fate and
1426 embryonic patterning. Cold Spring Harbor perspectives in biology. 2012;4(8):a005975. doi:
1427 10.1101/cshperspect.a005975. PubMed PMID: 22855721; PubMed Central PMCID:
1428 PMC3405863.
1429 107. Erben E, Leiss K, Liu B, Gil DI, Helbig C, Clayton C. Insights into the functions and
1430 RNA binding of Trypanosoma brucei ZC3H22, RBP9 and DRBD7. Parasitology.
1431 2021;148(10):1186-95. doi: 10.1017/S0031182021000123. PubMed PMID: 33536101;
1432 PubMed Central PMCID: PMC8312216.
1433 108. Walrad PB, Capewell P, Fenn K, Matthews KR. The post-transcriptional trans-acting
1434 regulator, TbZFP3, co-ordinates transmission-stage enriched mRNAs in Trypanosoma brucei.
1435 Nucleic acids research. 2012;40(7):2869-83. doi: 10.1093/nar/gkr1106. PubMed PMID:
1436 22140102; PubMed Central PMCID: PMC3326296.
1437 109. Mugo E, Clayton C. Expression of the RNA-binding protein RBP10 promotes the
1438 bloodstream-form differentiation state in Trypanosoma brucei. PLoS pathogens.
1439 2017;13(8):e1006560. doi: 10.1371/journal.ppat.1006560. PubMed PMID: 28800584;
1440 PubMed Central PMCID: PMC5568443.
1441 110. Avila CC, Mule SN, Rosa-Fernandes L, Viner R, Barison MJ, Costa-Martins AG,
1442 Oliveira GS, Teixeira MMG, Marinho CRF, Silber AM, Palmisano G. Proteome-Wide
1443 Analysis of Trypanosoma cruzi Exponential and Stationary Growth Phases Reveals a
1444 Subcellular Compartment-Specific Regulation. Genes. 2018;9(8). doi: 10.3390/genes9080413.
1445 PubMed PMID: 30111733; PubMed Central PMCID: PMC6115888.
1446 111. Fritz M, Vanselow J, Sauer N, Lamer S, Goos C, Siegel TN, Subota I, Schlosser A,
1447 Carrington M, Kramer S. Novel insights into RNP granules by employing the trypanosome's
1448 microtubule skeleton as a molecular sieve. Nucleic acids research. 2015;43(16):8013-32. doi:
1449 10.1093/nar/gkv731. PubMed PMID: 26187993; PubMed Central PMCID: PMC4652759.
1450 112. Cargnello M, Roux PP. Activation and function of the MAPKs and their substrates, the
1451 MAPK-activated protein kinases. Microbiology and molecular biology reviews : MMBR.
1452 2011;75(1):50-83. doi: 10.1128/MMBR.00031-10. PubMed PMID: 21372320; PubMed
1453 Central PMCID: PMC3063353.
1454 113. Erdmann M, Scholz A, Melzer IM, Schmetz C, Wiese M. Interacting protein kinases
1455 involved in the regulation of flagellar length. Molecular biology of the cell. 2006;17(4):2035-
1456 45. doi: 10.1091/mbc.e05-10-0976. PubMed PMID: 16467378; PubMed Central PMCID:
1457 PMC1415332.
1458 114. Johnson JL, Yaron TM, Huntsman EM, Kerelsky A, Song J, Regev A, Lin TY,
1459 Liberatore K, Cizin DM, Cohen BM, Vasan N, Ma Y, Krismer K, Robles JT, van de Kooij B,
1460 van Vlimmeren AE, Andree-Busch N, Kaufer NF, Dorovkov MV, Ryazanov AG, Takagi Y,
1461 Kastenhuber ER, Goncalves MD, Hopkins BD, Elemento O, Taatjes DJ, Maucuer A,
1462 Yamashita A, Degterev A, Uduman M, Lu J, Landry SD, Zhang B, Cossentino I, Linding R,
1463 Blenis J, Hornbeck PV, Turk BE, Yaffe MB, Cantley LC. An atlas of substrate specificities for
1464 the human serine/threonine kinome. Nature. 2023;613(7945):759-66. doi: 10.1038/s41586-
1465 022-05575-3. PubMed PMID: 36631611; PubMed Central PMCID: PMC9876800 and is a
1466 founder and receives research support from Petra Pharmaceuticals; is listed as an inventor on
1467 a patent (WO2019232403A1, Weill Cornell Medicine) for combination therapy for PI3K-
1468 associated disease or disorder, and the identification of therapeutic interventions to improve
1469 response to PI3K inhibitors for cancer treatment; is a co-founder and shareholder in Faeth
1470 Therapeutics; has equity in and consults for Cell Signaling Technologies, Volastra, Larkspur
1471 and 1 Base Pharmaceuticals; and consults for Loxo-Lilly. M.B.Y receives research support
1472 from Cardiff Oncology. T.M.Y. is a co-founder and stockholder and is on the board of directors
1473 of DESTROKE, an early-stage start-up developing mobile technology for automated clinical
1474 stroke detection. J.L.J has received consulting fees from Scorpion Therapeutics and Volastra

Therapeutics. O.E. is a founder and equity holder of Volastra Therapeutics and OneThree Biotech; is a member of the scientific advisory board of Owkin, Freenome, Genetic Intelligence, Acuamark and Champions Oncology; and receives research support from Eli Lilly, Janssen and Sanofi. D.J.T. is a member of the scientific advisory board at Dewpoint Therapeutics. A.D. is an equity holder of Denali Therapeutics; and receives research support from Interline Therapeutics. N.V. reports consulting activities for Novartis and is on the scientific advisory board of Heligenics. M.D.G. is a co-founder and shareholder of Faeth Therapeutics, which is developing dietary and pharmacological therapies for cancer; and has received speaking and/or consulting fees from Pfizer, Novartis, Scorpion Therapeutics and Faeth Therapeutics.

115. Ekerot M, Stavridis MP, Delavaine L, Mitchell MP, Staples C, Owens DM, Keenan ID, Dickinson RJ, Storey KG, Keyse SM. Negative-feedback regulation of FGF signalling by DUSP6/MKP-3 is driven by ERK1/2 and mediated by Ets factor binding to a conserved site within the DUSP6/MKP-3 gene promoter. The Biochemical journal. 2008;412(2):287-98. doi: 10.1042/BJ20071512. PubMed PMID: 18321244; PubMed Central PMCID: PMC2474557.

116. Hoffmann I, Clarke PR, Marcote MJ, Karsenti E, Draetta G. Phosphorylation and activation of human cdc25-C by cdc2--cyclin B and its involvement in the self-amplification of MPF at mitosis. The EMBO journal. 1993;12(1):53-63. doi: 10.1002/j.1460-2075.1993.tb05631.x. PubMed PMID: 8428594; PubMed Central PMCID: PMC413175.

117. Zinoviev A, Leger M, Wagner G, Shapira M. A novel 4E-interacting protein in Leishmania is involved in stage-specific translation pathways. Nucleic acids research. 2011;39(19):8404-15. doi: 10.1093/nar/gkr555. PubMed PMID: 21764780; PubMed Central PMCID: PMC3201875.

118. Shrivastava R, Tupperwar N, Drory-Retwitzer M, Shapira M. Deletion of a Single LeishIF4E-3 Allele by the CRISPR-Cas9 System Alters Cell Morphology and Infectivity of Leishmania. mSphere. 2019;4(5). doi: 10.1128/mSphere.00450-19. PubMed PMID: 31484740; PubMed Central PMCID: PMC6731530.

119. Tupperwar N, Shrivastava R, Shapira M. LeishIF4E1 Deletion Affects the Promastigote Proteome, Morphology, and Infectivity. mSphere. 2019;4(6). doi: 10.1128/mSphere.00625-19. PubMed PMID: 31722993; PubMed Central PMCID: PMC6854042.

120. Tupperwar N, Shrivastava R, Baron N, Korchev O, Dahan I, Shapira M. Characterization of an Atypical eIF4E Ortholog in Leishmania, LeishIF4E-6. International journal of molecular sciences. 2021;22(23). doi: 10.3390/ijms222312720. PubMed PMID: 34884522; PubMed Central PMCID: PMC8657474.

121. Baron N, Purushotham R, Pullaiahgari D, Bose P, Zarivach R, Shapira M. LeishIF4E2 is a cap-binding protein that plays a role in Leishmania cell cycle progression. FASEB journal : official publication of the Federation of American Societies for Experimental Biology. 2024;38(1):e23367. doi: 10.1096/fj.202301665R. PubMed PMID: 38095329.

122. Baird TD, Wek RC. Eukaryotic initiation factor 2 phosphorylation and translational control in metabolism. Advances in nutrition. 2012;3(3):307-21. doi: 10.3945/an.112.002113. PubMed PMID: 22585904; PubMed Central PMCID: PMC3649462.

123. Sloan KE, Warda AS, Sharma S, Entian KD, Lafontaine DLJ, Bohnsack MT. Tuning the ribosome: The influence of rRNA modification on eukaryotic ribosome biogenesis and function. RNA biology. 2017;14(9):1138-52. doi: 10.1080/15476286.2016.1259781. PubMed PMID: 27911188; PubMed Central PMCID: PMC5699541.

124. Imami K, Milek M, Bogdanow B, Yasuda T, Kastelic N, Zauber H, Ishihama Y, Landthaler M, Selbach M. Phosphorylation of the Ribosomal Protein RPL12/uL11 Affects Translation during Mitosis. Molecular cell. 2018;72(1):84-98 e9. doi: 10.1016/j.molcel.2018.08.019. PubMed PMID: 30220558.

125. Merrick WC, Pavitt GD. Protein Synthesis Initiation in Eukaryotic Cells. Cold Spring Harbor perspectives in biology. 2018;10(12). doi: 10.1101/cshperspect.a033092. PubMed PMID: 29735639; PubMed Central PMCID: PMC6280705.
126. Piazzi M, Bavelloni A, Gallo A, Faenza I, Blalock WL. Signal Transduction in Ribosome Biogenesis: A Recipe to Avoid Disaster. International journal of molecular sciences. 2019;20(11). doi: 10.3390/ijms20112718. PubMed PMID: 31163577; PubMed Central PMCID: PMC6600399.
127. Jungers CF, Elliff JM, Masson-Meyers DS, Phiel CJ, Origanti S. Regulation of eukaryotic translation initiation factor 6 dynamics through multisite phosphorylation by GSK3. The Journal of biological chemistry. 2020;295(36):12796-813. doi: 10.1074/jbc.RA120.013324. PubMed PMID: 32703900; PubMed Central PMCID: PMC7476728.
128. Janin M, Coll-SanMartin L, Esteller M. Disruption of the RNA modifications that target the ribosome translation machinery in human cancer. Molecular cancer. 2020;19(1):70. doi: 10.1186/s12943-020-01192-8. PubMed PMID: 32241281; PubMed Central PMCID: PMC7114786.
129. Bohlen J, Roiuk M, Teleman AA. Phosphorylation of ribosomal protein S6 differentially affects mRNA translation based on ORF length. Nucleic acids research. 2021;49(22):13062-74. doi: 10.1093/nar/gkab1157. PubMed PMID: 34871442; PubMed Central PMCID: PMC8682771.
130. Khoshnevis S, Dreggors-Walker RE, Marchand V, Motorin Y, Ghalei H. Ribosomal RNA 2'-O-methylations regulate translation by impacting ribosome dynamics. Proceedings of the National Academy of Sciences of the United States of America. 2022;119(12):e2117334119. doi: 10.1073/pnas.2117334119. PubMed PMID: 35294285; PubMed Central PMCID: PMC8944910.
131. Das T, Shin SC, Song EJ, Kim EE. Regulation of Deubiquitinating Enzymes by Post-Translational Modifications. International journal of molecular sciences. 2020;21(11). doi: 10.3390/ijms21114028. PubMed PMID: 32512887; PubMed Central PMCID: PMC7312083.
132. Wang F, Ning S, Yu B, Wang Y. USP14: Structure, Function, and Target Inhibition. Frontiers in pharmacology. 2021;12:801328. doi: 10.3389/fphar.2021.801328. PubMed PMID: 35069211; PubMed Central PMCID: PMC8766727.
133. Gonzalez J, Ramalho-Pinto FJ, Frevert U, Ghiso J, Tomlinson S, Scharfstein J, Corey EJ, Nussenzweig V. Proteasome activity is required for the stage-specific transformation of a protozoan parasite. The Journal of experimental medicine. 1996;184(5):1909-18. doi: 10.1084/jem.184.5.1909. PubMed PMID: 8920878; PubMed Central PMCID: PMC2192890.
134. Cardoso J, Soares MJ, Menna-Barreto RF, Le Bloas R, Sotomaior V, Goldenberg S, Krieger MA. Inhibition of proteasome activity blocks Trypanosoma cruzi growth and metacyclogenesis. Parasitology research. 2008;103(4):941-51. doi: 10.1007/s00436-008-1081-6. PubMed PMID: 18581141.
135. Cardoso J, Lima Cde P, Leal T, Gradia DF, Fragoso SP, Goldenberg S, De Sa RG, Krieger MA. Analysis of proteasomal proteolysis during the in vitro metacyclogenesis of Trypanosoma cruzi. PloS one. 2011;6(6):e21027. doi: 10.1371/journal.pone.0021027. PubMed PMID: 21698116; PubMed Central PMCID: PMC3117861.
136. Munoz C, San Francisco J, Gutierrez B, Gonzalez J. Role of the Ubiquitin-Proteasome Systems in the Biology and Virulence of Protozoan Parasites. BioMed research international. 2015;2015:141526. doi: 10.1155/2015/141526. PubMed PMID: 26090380; PubMed Central PMCID: PMC4452248.
137. Bijlmakers MJ. Ubiquitination and the Proteasome as Drug Targets in Trypanosomatid Diseases. Frontiers in chemistry. 2020;8:630888. doi: 10.3389/fchem.2020.630888. PubMed PMID: 33732684; PubMed Central PMCID: PMC7958763.

138. Wiese M. Leishmania MAP kinases--familiar proteins in an unusual context. International journal for parasitology. 2007;37(10):1053-62. doi: 10.1016/j.ijpara.2007.04.008. PubMed PMID: 17548090.
139. Hunter T. The age of crosstalk: phosphorylation, ubiquitination, and beyond. Molecular cell. 2007;28(5):730-8. doi: 10.1016/j.molcel.2007.11.019. PubMed PMID: 18082598.
140. Nguyen LK, Kolch W, Kholodenko BN. When ubiquitination meets phosphorylation: a systems biology perspective of EGFR/MAPK signalling. Cell communication and signaling : CCS. 2013;11:52. doi: 10.1186/1478-811X-11-52. PubMed PMID: 23902637; PubMed Central PMCID: PMC3734146.
141. Barbour H, Nkwe NS, Estavoyer B, Messmer C, Gushul-Leclaire M, Villot R, Uriarte M, Boulay K, Hlayhel S, Farhat B, Milot E, Mallette FA, Daou S, Affar EB. An inventory of crosstalk between ubiquitination and other post-translational modifications in orchestrating cellular processes. iScience. 2023;26(5):106276. doi: 10.1016/j.isci.2023.106276. PubMed PMID: 37168555; PubMed Central PMCID: PMC10165199.
142. Waddington CH. Canalization of development and genetic assimilation of acquired characters. Nature. 1959;183(4676):1654-5. doi: 10.1038/1831654a0. PubMed PMID: 13666847.
143. Cox J, Mann M. MaxQuant enables high peptide identification rates, individualized p.p.b.-range mass accuracies and proteome-wide protein quantification. Nature biotechnology. 2008;26(12):1367-72. doi: 10.1038/nbt.1511. PubMed PMID: 19029910.
144. Cox J, Neuhauser N, Michalski A, Scheltema RA, Olsen JV, Mann M. Andromeda: a peptide search engine integrated into the MaxQuant environment. Journal of proteome research. 2011;10(4):1794-805. doi: 10.1021/pr101065j. PubMed PMID: 21254760.
145. Cox J, Hein MY, Luber CA, Paron I, Nagaraj N, Mann M. Accurate proteome-wide label-free quantification by delayed normalization and maximal peptide ratio extraction, termed MaxLFQ. Molecular & cellular proteomics : MCP. 2014;13(9):2513-26. doi: 10.1074/mcp.M113.031591. PubMed PMID: 24942700; PubMed Central PMCID: PMC4159666.
146. Garcia-Garcia T, Douche T, Giai Gianetto Q, Poncet S, El Omrani N, Smits WK, Cuenot E, Matondo M, Martin-Verstraete I. In-Depth Characterization of the Clostridioides difficile Phosphoproteome to Identify Ser/Thr Kinase Substrates. Molecular & cellular proteomics : MCP. 2022;21(11):100428. doi: 10.1016/j.mcpro.2022.100428. PubMed PMID: 36252736; PubMed Central PMCID: PMC9674922.
147. Wieczorek S, Combes F, Lazar C, Giai Gianetto Q, Gatto L, Dorffer A, Hesse AM, Coute Y, Ferro M, Bruley C, Burger T. DAPAR & ProStaR: software to perform statistical analyses in quantitative discovery proteomics. Bioinformatics. 2017;33(1):135-6. doi: 10.1093/bioinformatics/btw580. PubMed PMID: 27605098; PubMed Central PMCID: PMC5408771.
148. Ritchie ME, Phipson B, Wu D, Hu Y, Law CW, Shi W, Smyth GK. limma powers differential expression analyses for RNA-sequencing and microarray studies. Nucleic acids research. 2015;43(7):e47. doi: 10.1093/nar/gkv007. PubMed PMID: 25605792; PubMed Central PMCID: PMC4402510.
149. Smyth GK. Limma: linear models for microarray data. Gentleman RC, Carey VJ, Dudoit S, Irizarry RA, Huber W, editors. New York: Springer; 2005. 397-420 p.
150. Giai Gianetto Q, Combes F, Ramus C, Bruley C, Coute Y, Burger T. Calibration plot for proteomics: A graphical tool to visually check the assumptions underlying FDR control in quantitative experiments. Proteomics. 2016;16(1):29-32. doi: 10.1002/pmic.201500189. PubMed PMID: 26572953.
151. Pounds S, Cheng C. Robust estimation of the false discovery rate. Bioinformatics. 2006;22(16):1979-87. doi: 10.1093/bioinformatics/btl328. PubMed PMID: 16777905.

152. Schwanhausser B, Busse D, Li N, Dittmar G, Schuchhardt J, Wolf J, Chen W, Selbach M. Global quantification of mammalian gene expression control. Nature. 2011;473(7347):337-42. doi: 10.1038/nature10098. PubMed PMID: 21593866.
153. Giai Gianetto Q. Statistical Analysis of Post-Translational Modifications Quantified by Label-Free Proteomics Across Multiple Biological Conditions with R: Illustration from SARS-CoV-2 Infected Cells. Methods in molecular biology. 2023;2426:267-302. doi: 10.1007/978-1-0716-1967-4_12. PubMed PMID: 36308693.
154. Gianetto QG, Wieczorek S, Couté Y, Burger T. A peptide-level multiple imputation strategy accounting for the different natures of missing values in proteomics data. bioRxiv. 2020:2020.05.29.122770. doi: 10.1101/2020.05.29.122770.

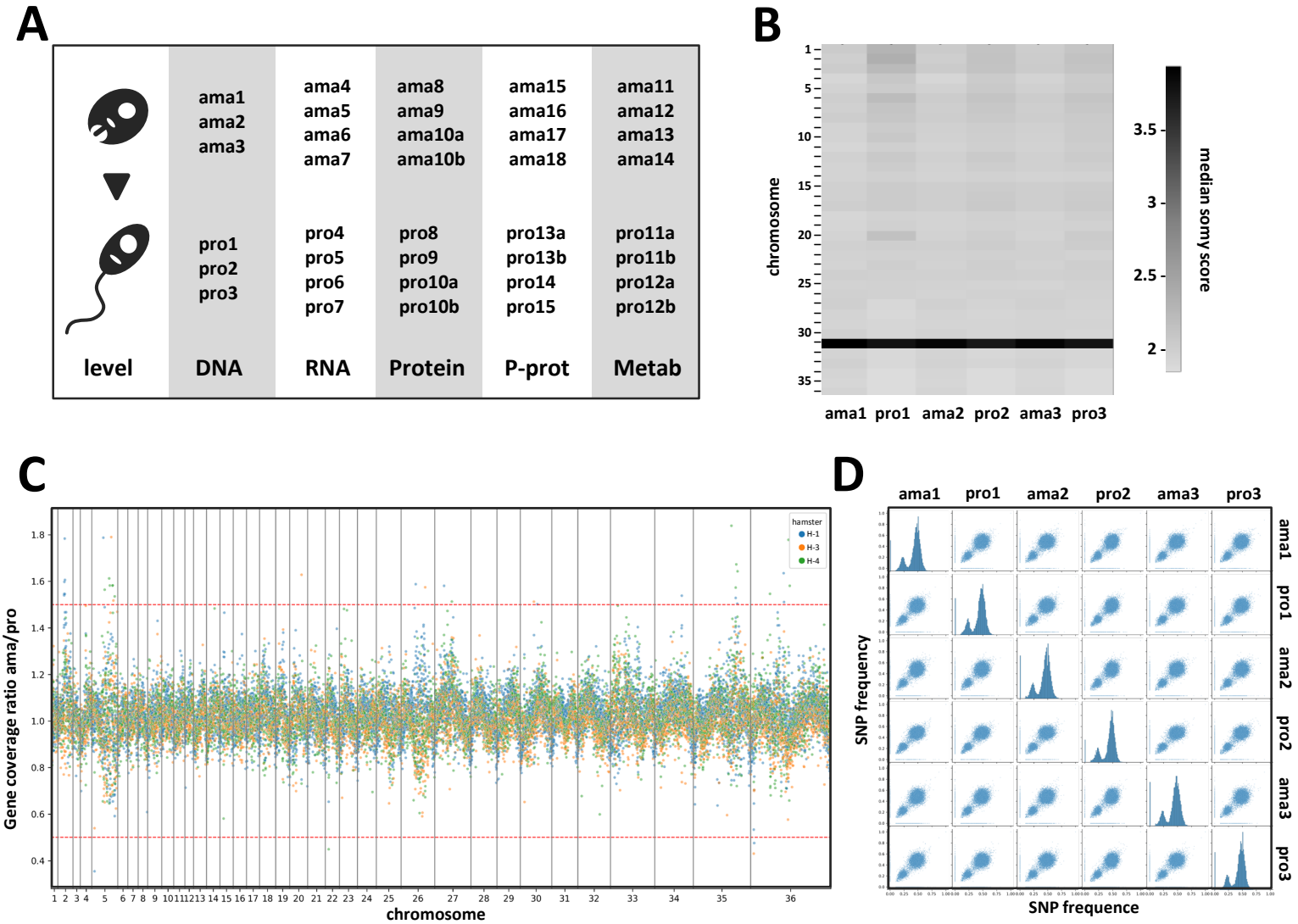
A
ama1
ama2
ama3
ama4
ama5
ama6
ama7
ama8
ama9
ama10a
ama10b
ama15
ama16
ama17
ama18
ama11
ama12
ama13
ama14
pro1
pro2
pro3
pro4
pro5
pro6
pro7
pro8
pro9
pro10a
pro10b
pro13a
pro13b
pro14
pro15
pro11a
pro11b
pro12a
pro12b
level
DNA
RNA
Protein
P-prot
Metab
B
chromosome
median somy score
ama1 pro1 ama2 pro2 ama3 pro3
C
Gene coverage ratio ama/pro
chromosome
hamster
H-1
H-3
H-4
D
SNP frequency
SNP frequence
ama1 pro1 ama2 pro2 ama3 pro3

Figure 1

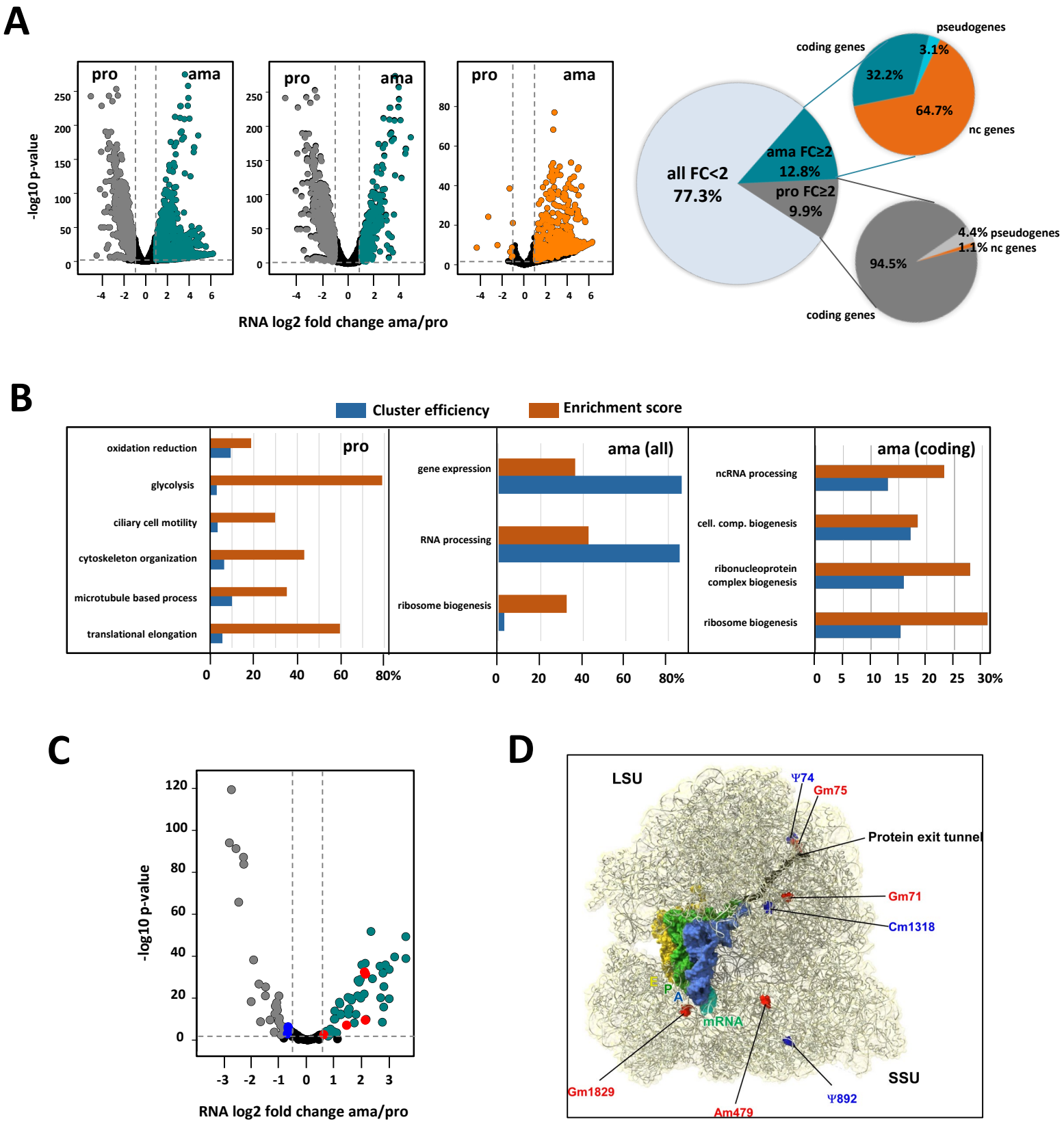
A
pro
ama
-log10 p-value
RNA log2 fold change ama/pro
pseudogenes
coding genes
3.1%
32.2%
64.7%
nc genes
all FC<2
77.3%
ama FC≥2
12.8%
pro FC≥2
9.9%
4.4% pseudogenes
1.1% nc genes
94.5%
coding genes
B
Cluster efficiency
Enrichment score
oxidation reduction
glycolysis
ciliary cell motility
cytoskeleton organization
microtubule based process
translational elongation
gene expression
RNA processing
ribosome biogenesis
ncRNA processing
cell. comp. biogenesis
ribonucleoprotein complex biogenesis
ribosome biogenesis
C
-log10 p-value
RNA log2 fold change ama/pro
D
LSU
Ψ74
Gm75
Protein exit tunnel
Gm71
Cm1318
E
P
A
mRNA
SSU
Gm1829
Am479
Ψ892

Figure 2

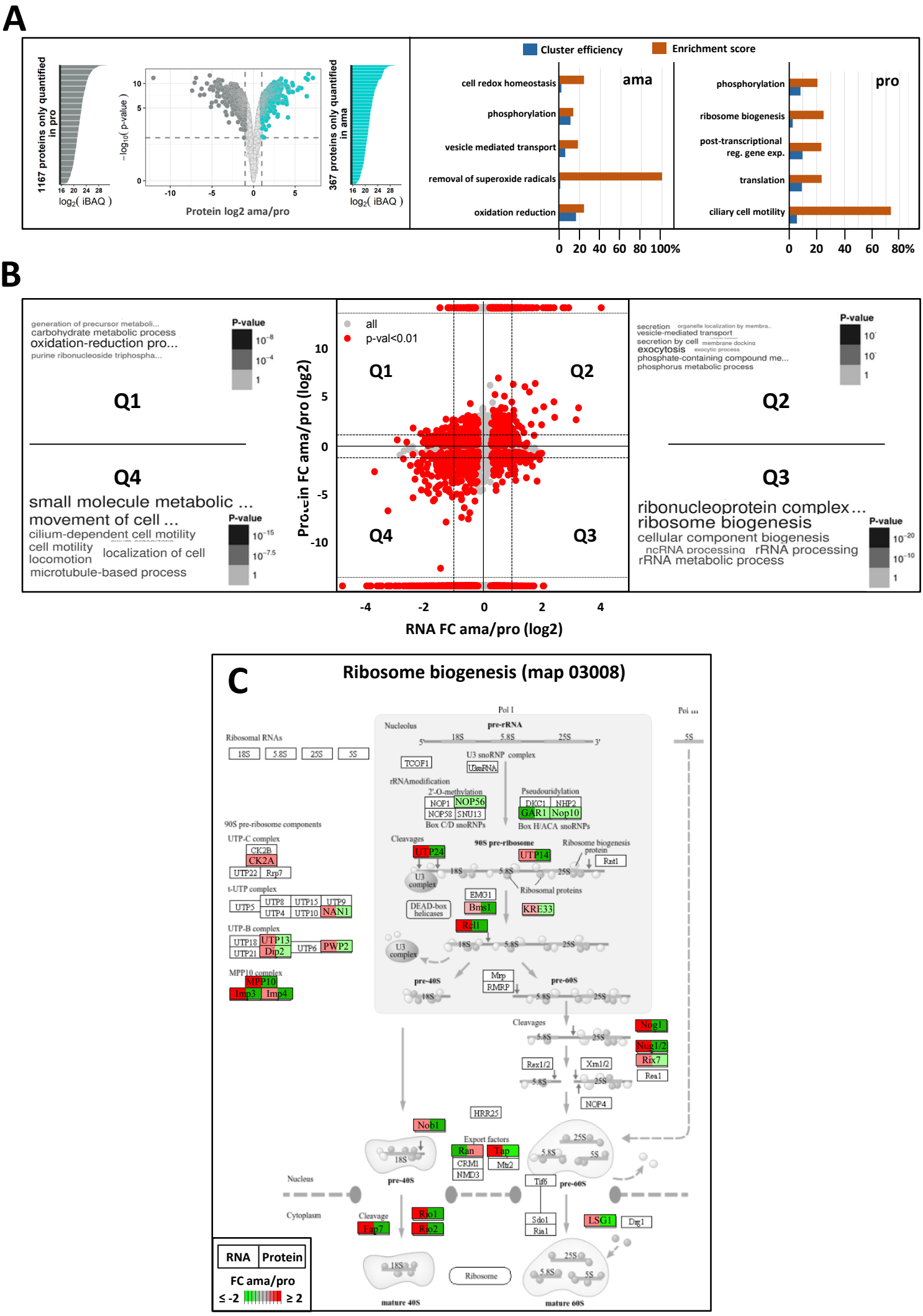
A
1167 proteins only quantified in pro
log2(iBAQ)
−log10(p-value)
Protein log2 ama/pro
367 proteins only quantified in ama
Cluster efficiency
Enrichment score
ama
cell redox homeostasis
phosphorylation
vesicle mediated transport
removal of superoxide radicals
oxidation reduction
pro
phosphorylation
ribosome biogenesis
post-transcriptional reg. gene exp.
translation
ciliary cell motility
B
P-value
Q1
Q2
Q3
Q4
all
p-val<0.01
Protein FC ama/pro (log2)
RNA FC ama/pro (log2)
small molecule metabolic ...
movement of cell ...
cilium-dependent cell motility
cell motility
localization of cell
locomotion
microtubule-based process
ribonucleoprotein complex...
ribosome biogenesis
cellular component biogenesis
ncRNA processing
rRNA processing
rRNA metabolic process
C
Ribosome biogenesis (map 03008)
Ribosomal RNAs
90S pre-ribosome components
UTP-C complex
t-UTP complex
UTP-B complex
MPP10 complex
Nucleolus
pre-rRNA
U3 snoRNP complex
rRNAmodification
Pseudouridylation
Box C/D snoRNPs
Box H/ACA snoRNPs
Cleavages
90S pre-ribosome
Ribosome biogenesis protein
Ribosomal proteins
DEAD-box helicases
pre-40S
pre-60S
Export factors
Nucleus
Cytoplasm
Cleavage
mature 40S
Ribosome
mature 60S
RNA
Protein
FC ama/pro
≤ -2
≥ 2

Figure 3

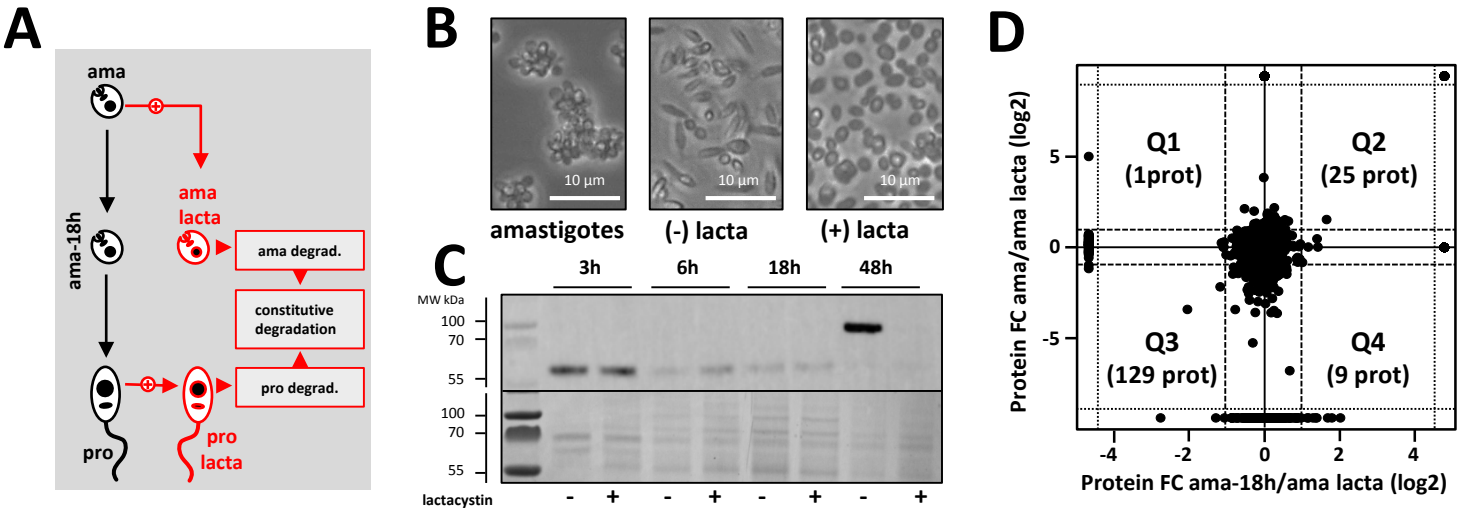

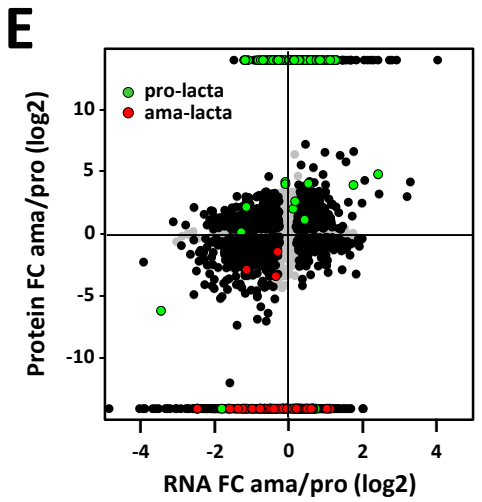

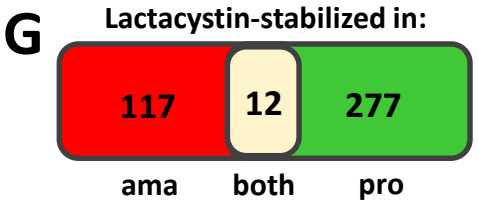

F

Gene ID	Annotation	ama vs pro	lacta rescued	
			ama	pro
Ld1S_280397500	differentiation inhibitory kinase	ama-specifc detection		X
Ld1S_320543000	protein kinase			X
Ld1S_340649100	protein kinase			X
Ld1S_350674800	casein kinase I			X
Ld1S_050815400	protein kinase	pro-specifc detection	X	
Ld1S_120047800	cell division protein kinase		X	
Ld1S_150105800	protein kinase		X	
Ld1S_320540600	repressor of differentiation kinase 1			X
Ld1S_190177600	protein kinase domain containing protein			X
Ld1S_040809500	casein kinase I	not detected		X
Ld1S_080866500	protein kinase			X
Ld1S_180153200	ser/thr kinase			X
Ld1S_210228200	protein kinase		X	
Ld1S_220237000	protein kinase		X	X

Figure 4

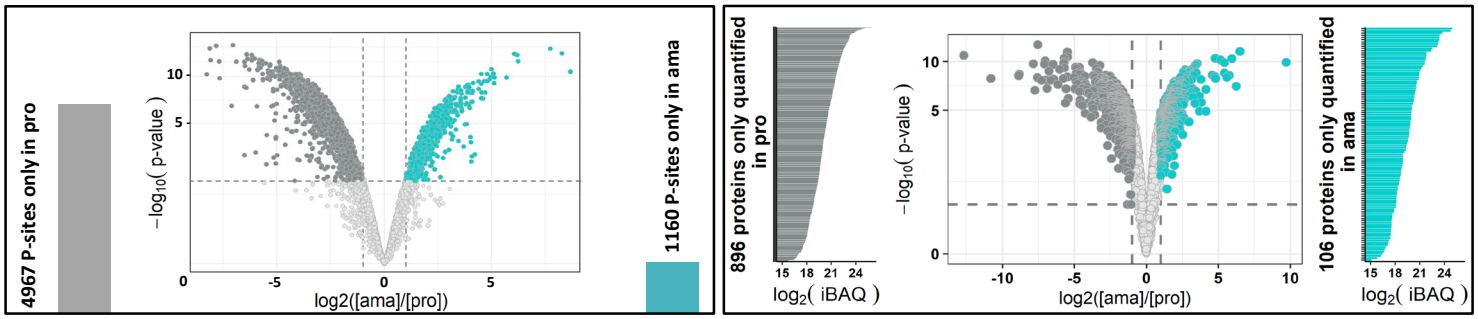
A
4967 P-sites only in pro
−log10(p-value)
log2([ama]/[pro])
1160 P-sites only in ama
896 proteins only quantified in pro
log2(iBAQ)
106 proteins only quantified in ama

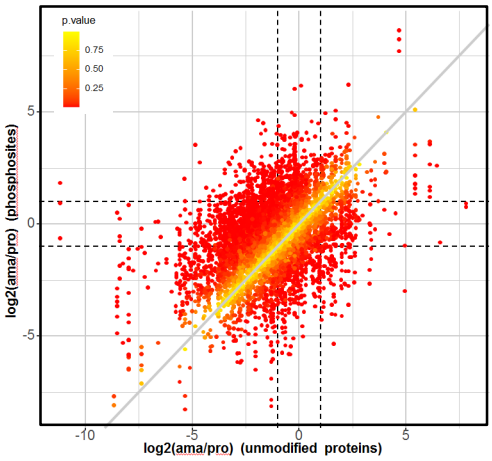
B
p.value
0.75
0.50
0.25
log2(ama/pro) (phosphosites)
log2(ama/pro) (unmodified proteins)

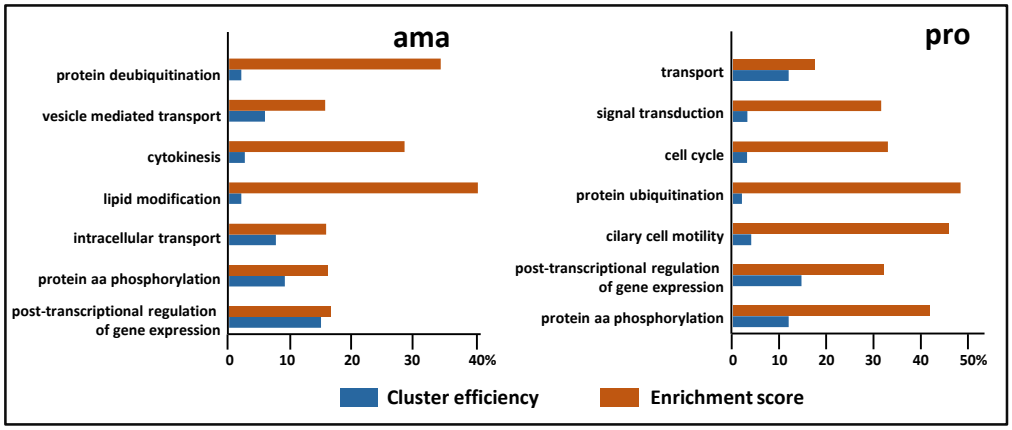
C
ama
protein deubiquitination
vesicle mediated transport
cytokinesis
lipid modification
intracellular transport
protein aa phosphorylation
post-transcriptional regulation of gene expression
pro
transport
signal transduction
cell cycle
protein ubiquitination
cilary cell motility
post-transcriptional regulation of gene expression
protein aa phosphorylation
Cluster efficiency
Enrichment score

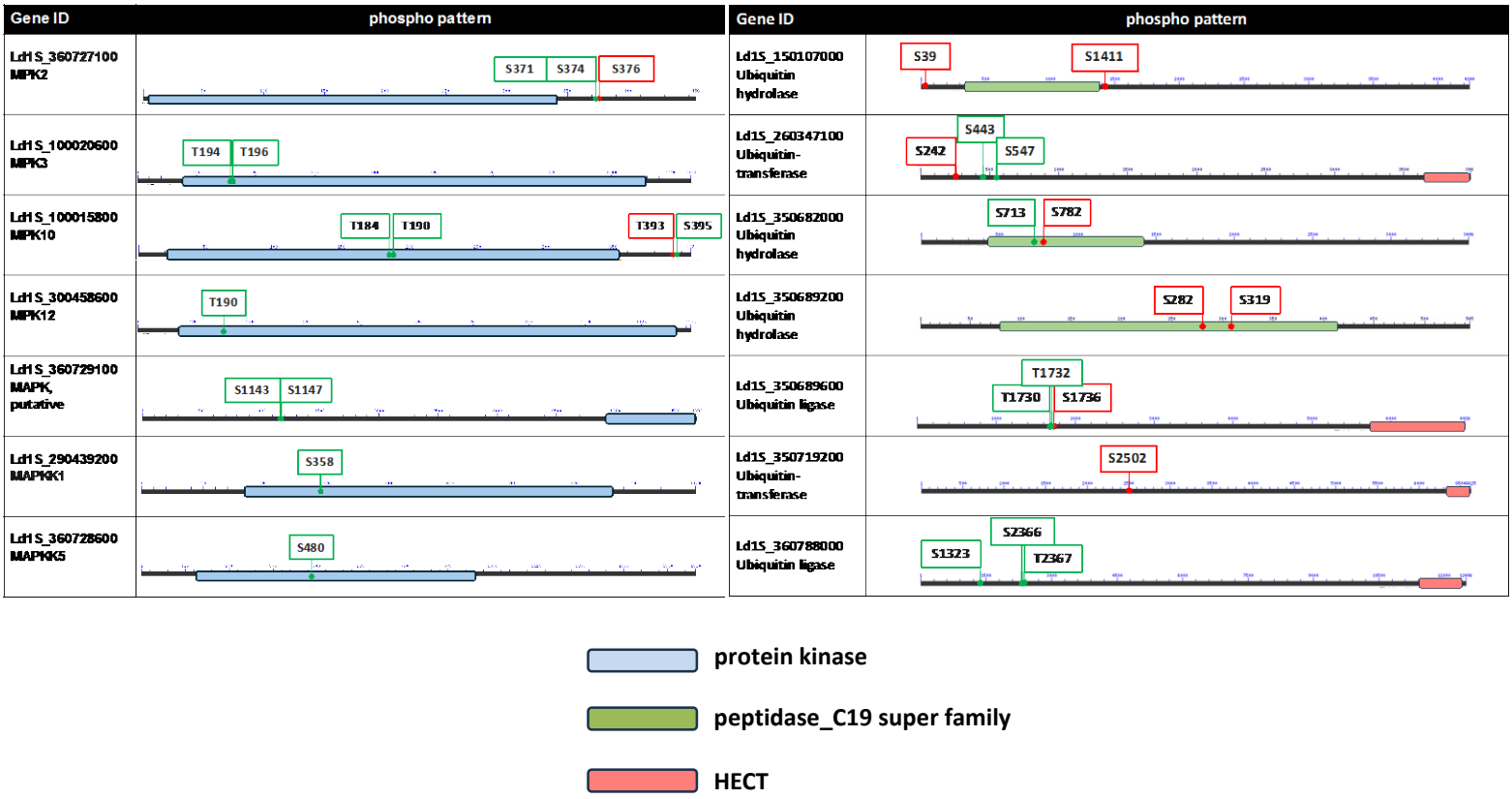
D
Gene ID
phospho pattern
Ld1S_360727100 MPK2
S371 S374 S376
Ld1S_100020600 MPK3
T194 T196
Ld1S_100015800 MPK10
T184 T190 T393 S395
Ld1S_300458600 MPK12
T190
Ld1S_360729100 MAPK, putative
S1143 S1147
Ld1S_290439200 MAPKK1
S358
Ld1S_360728600 MAPKK5
S480
Ld1S_150107000 Ubiquitin hydrolase
S39 S1411
Ld1S_260347100 Ubiquitin-transferase
S443 S242 S547
Ld1S_350682000 Ubiquitin hydrolase
S713 S782
Ld1S_350689200 Ubiquitin hydrolase
S282 S319
Ld1S_350689600 Ubiquitin ligase
T1732 T1730 S1736
Ld1S_350719200 Ubiquitin-transferase
S2502
Ld1S_360788000 Ubiquitin ligase
S2366 S1323 T2367
protein kinase
peptidase_C19 super family
HECT

Figure 5

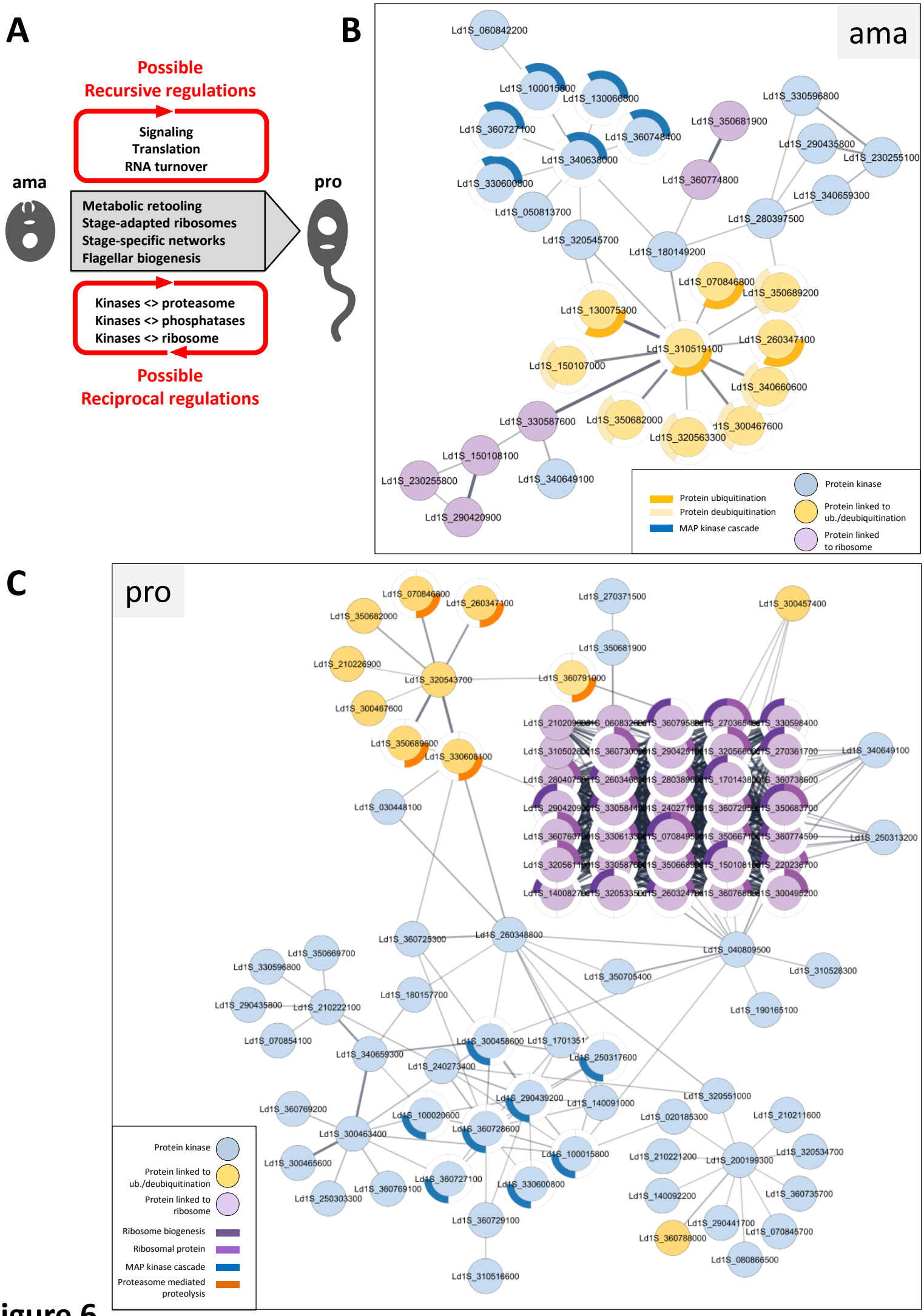
A
Possible
Recursive regulations
Signaling
Translation
RNA turnover
ama
pro
Metabolic retooling
Stage-adapted ribosomes
Stage-specific networks
Flagellar biogenesis
Kinases <> proteasome
Kinases <> phosphatases
Kinases <> ribosome
Possible
Reciprocal regulations
B
ama
Protein ubiquitination
Protein deubiquitination
MAP kinase cascade
Protein kinase
Protein linked to ub./deubiquitination
Protein linked to ribosome
C
pro
Protein kinase
Protein linked to ub./deubiquitination
Protein linked to ribosome
Ribosome biogenesis
Ribosomal protein
MAP kinase cascade
Proteasome mediated proteolysis

Figure 6

Supp Figures

Hamster	Analysis				
	DNAseq	RNAseq	Proteomic+/-lacta	Metabolomic	Proteomic/ Phosphoproteomic
H-1	ama1/pro1				
H-2	ama2/pro2				
H-4	ama3/pro3				
ERC9-1		ama4/pro4			
ERC9-2		ama5/pro5			
ERC4-2		ama6/pro6			
H313-1		ama7/pro7			
H208-2			ama8/pro8		
H211-1			ama9/pro9		
H211-2			ama10a*/pro10a** & ama10b*/pro10b**		
H131-1				ama11/pro11a** & pro11b**	
H131-2				ama 12/pro12a** & pro12b**	
H133-1				ama13	
H133-2				ama14	
H130-1					ama15
H130-2					ama16
H134-1					ama17
H134-2					pro13a** & pro13b**
H138-2					pro14
H139-2					ama18/pro15

*Foot note: * amastigote preparation from the spleen of one infected hamster was divided in 2, ** promastigote cultures derived from the same initial pool of splenic amastigotes that was split in 2 flasks for differentiation and culture until passage 2.*

Sup Figure S1

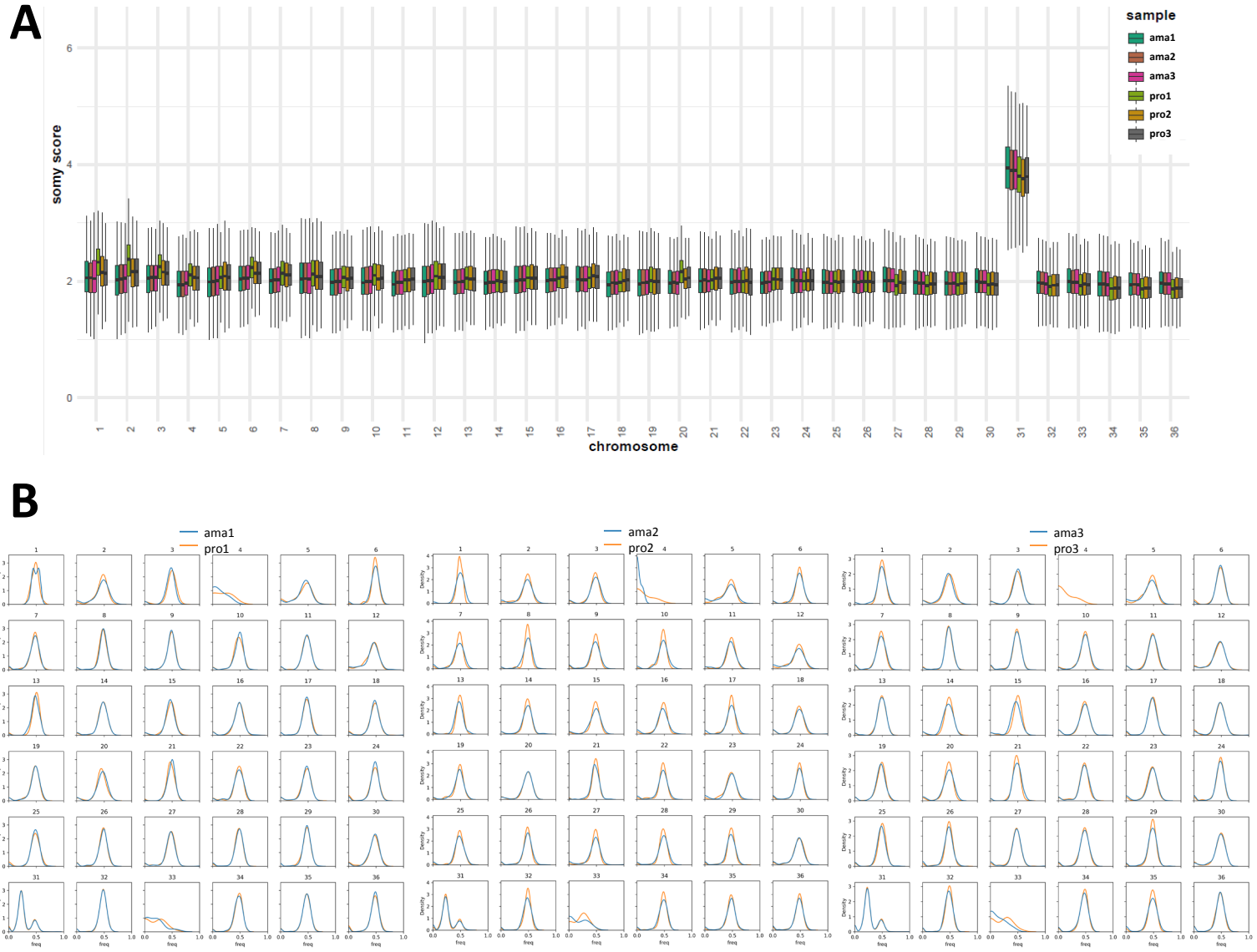

Sup Figure S2

A

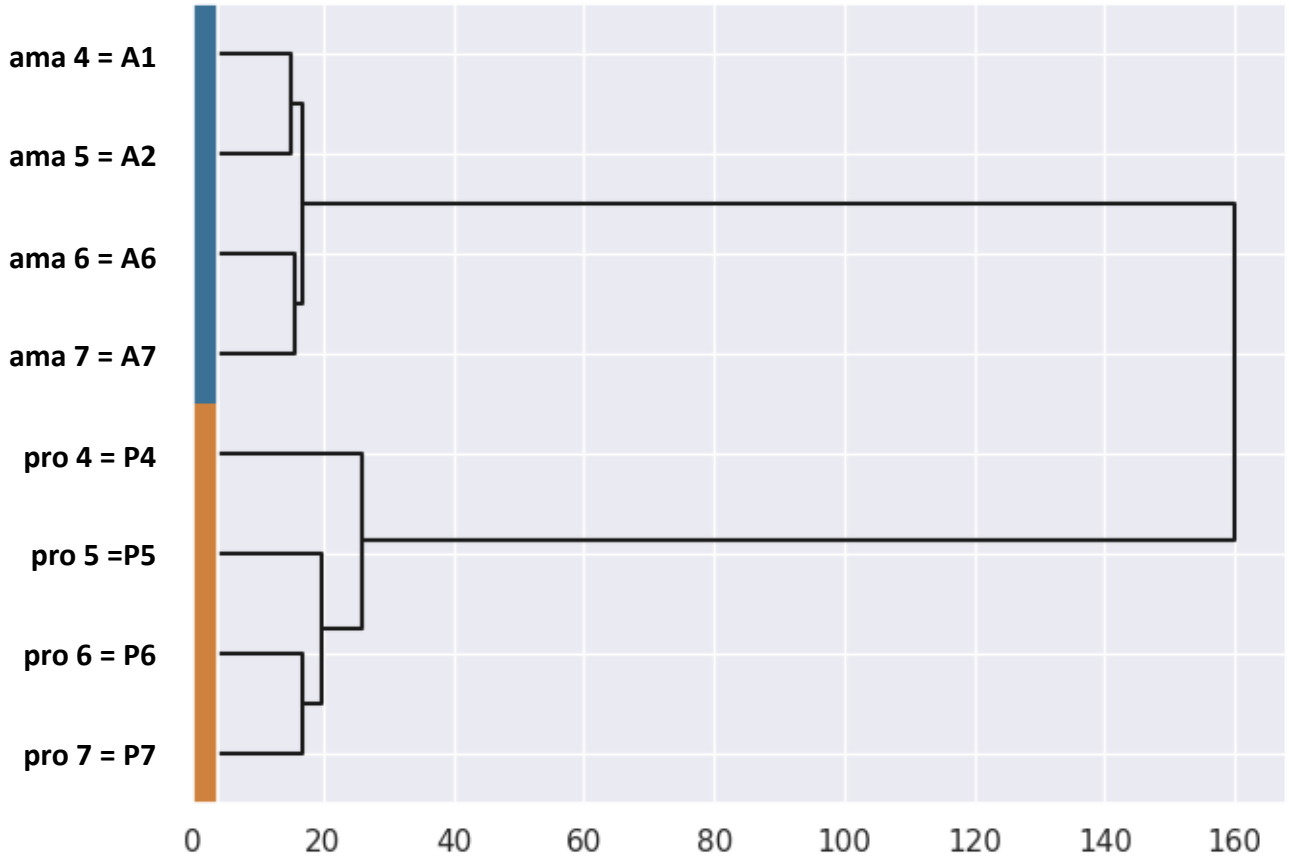

B

Sup Figure S3

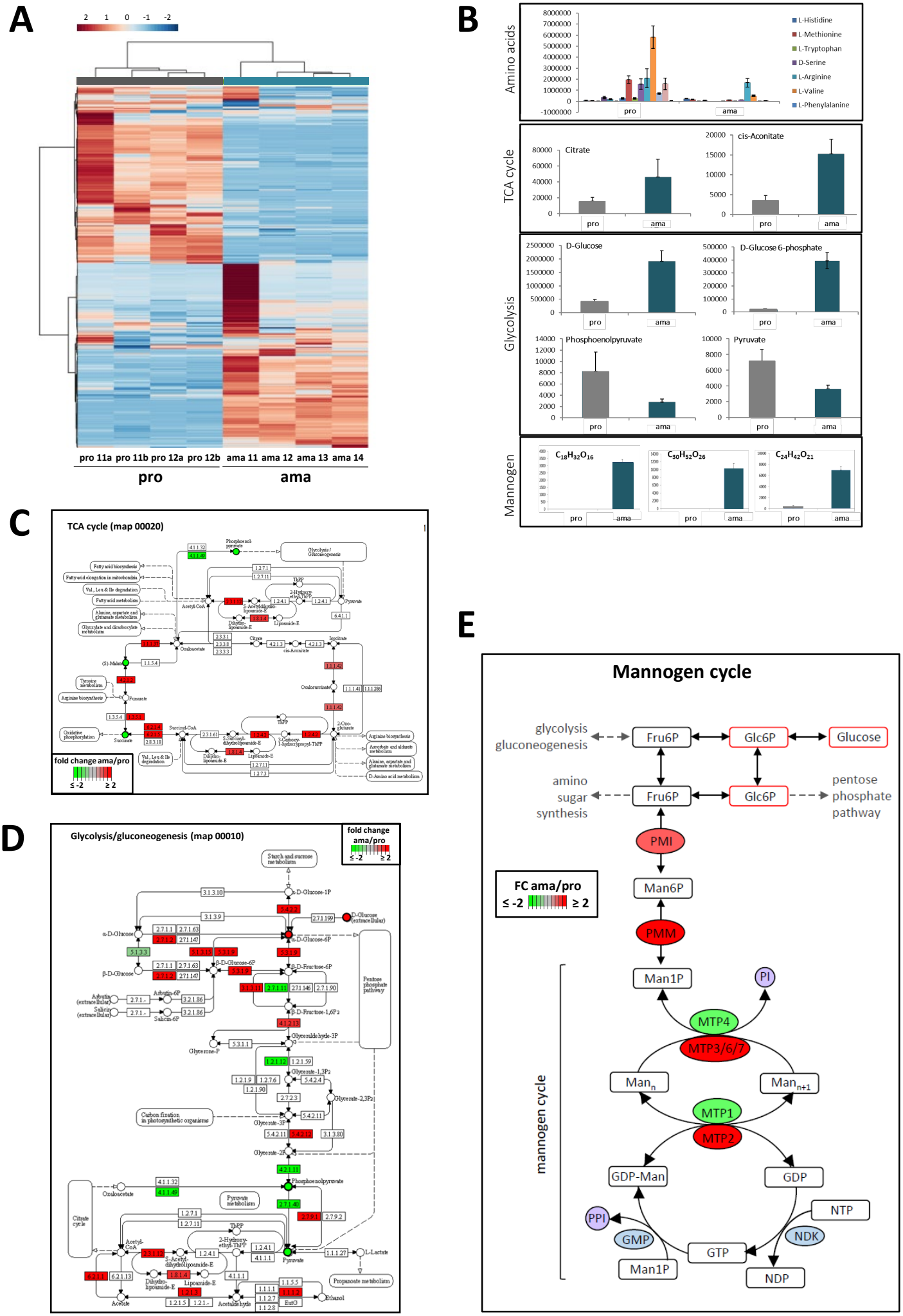

Sup Figure S4

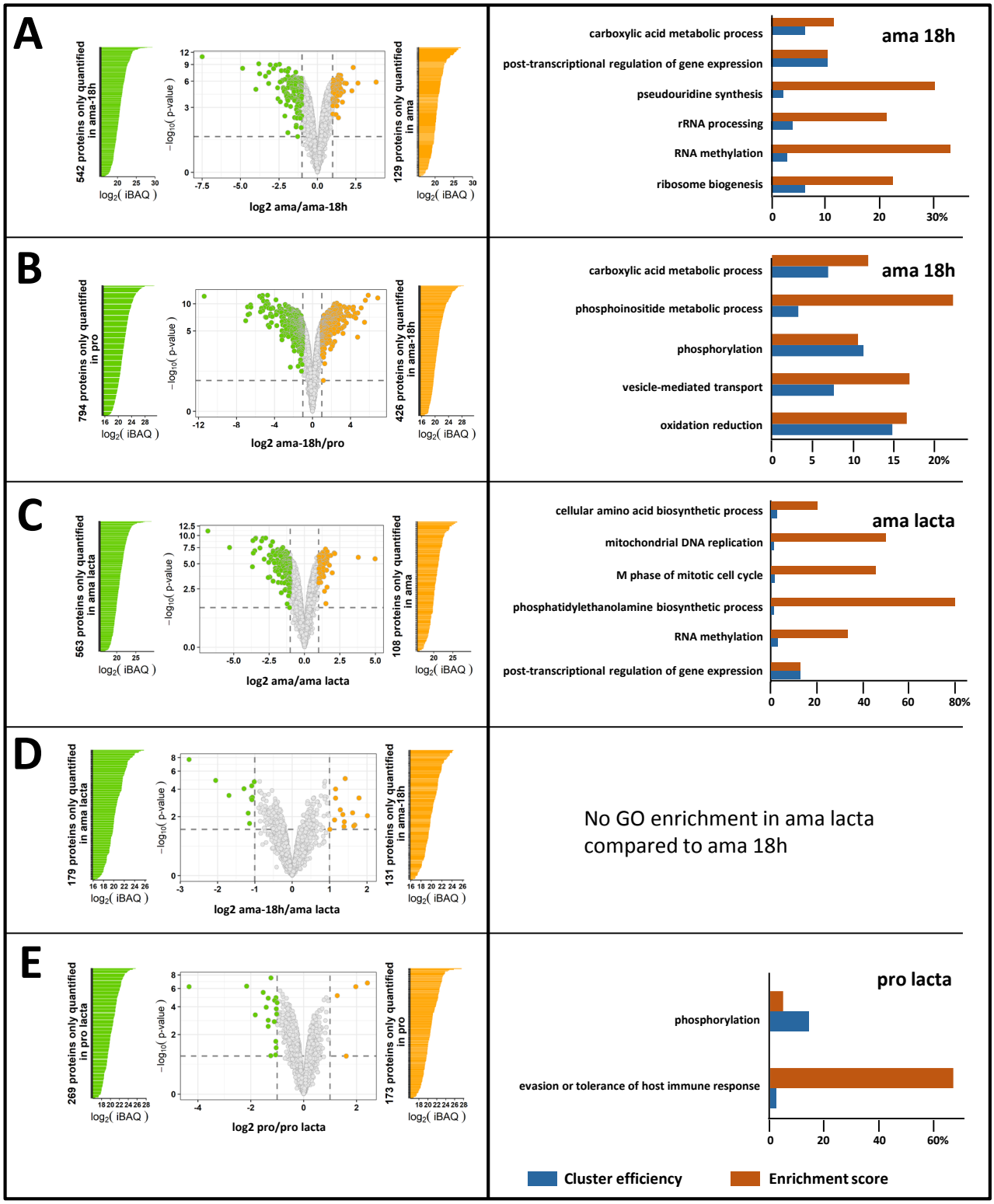

Sup Figure S5

A

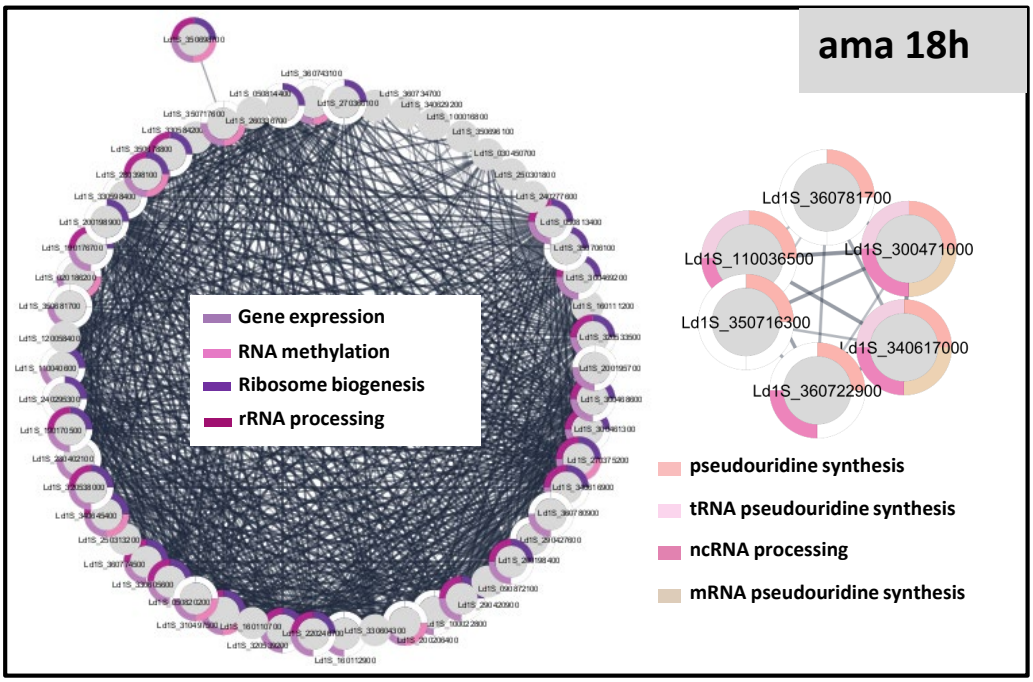

B

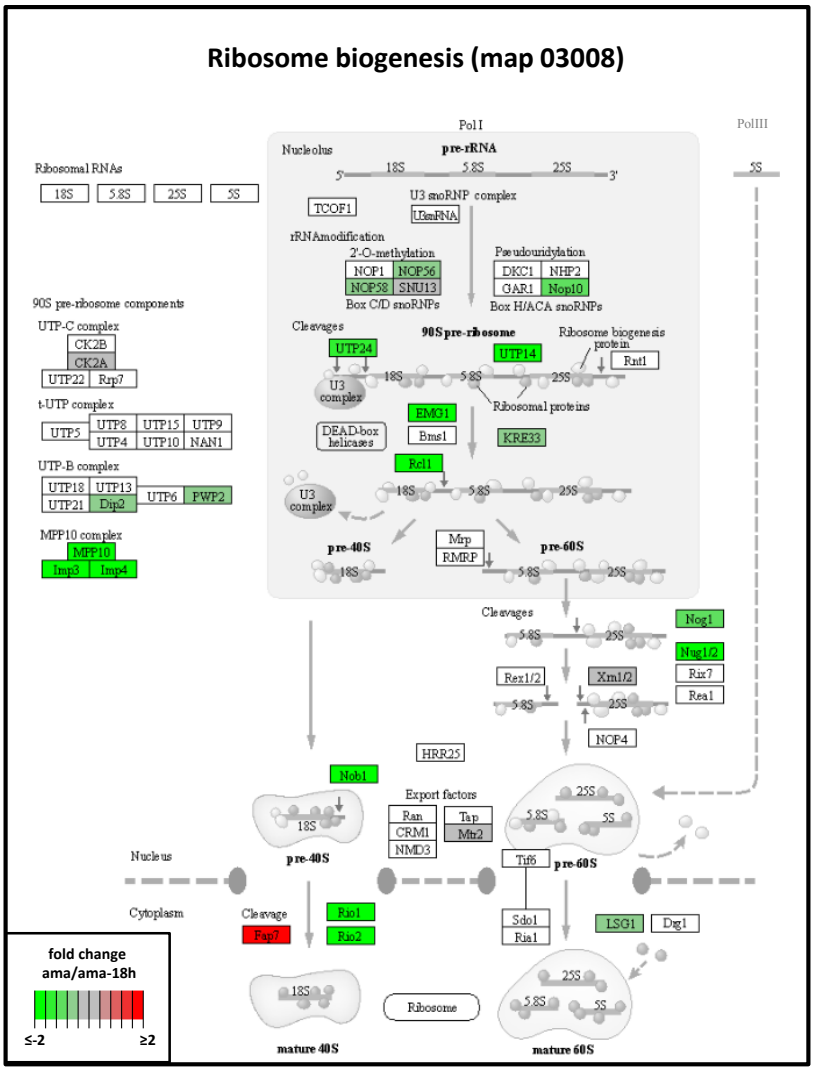

Sup Figure S6

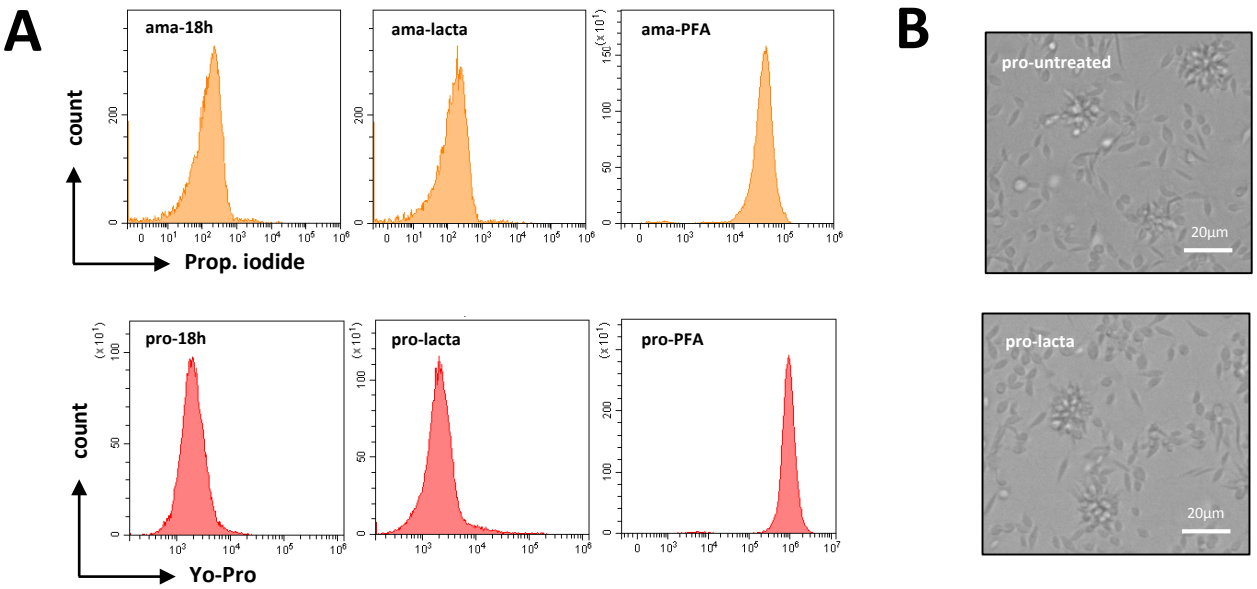

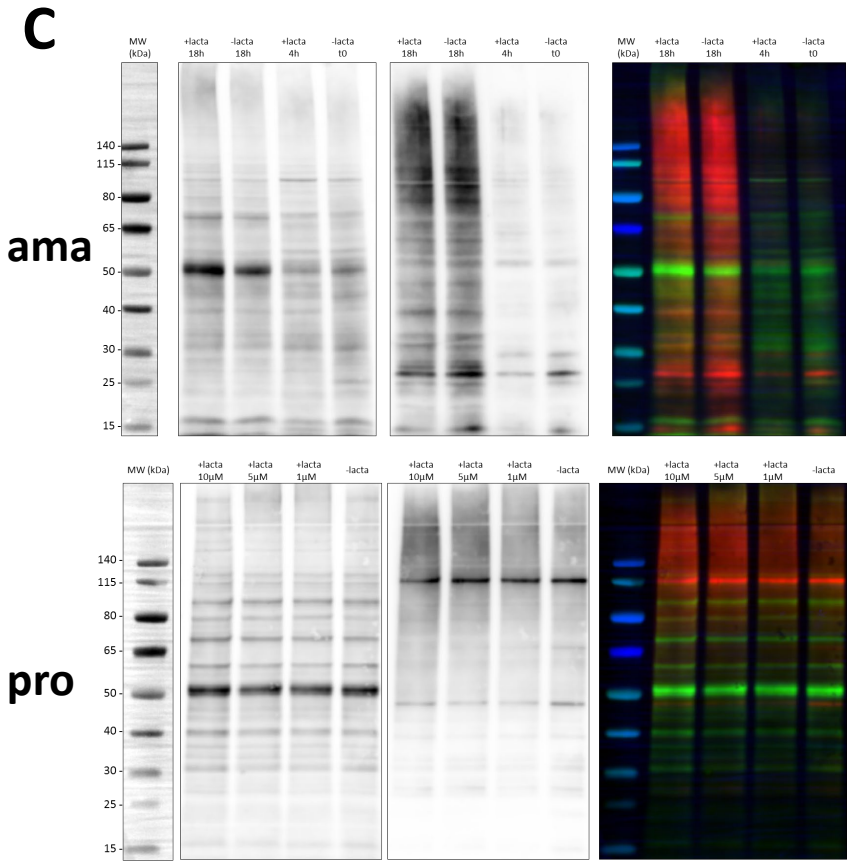

ama	
Lane	Norm. %
(-)lacta t0	100
(+)lacta 4h	60.1090572
(-)lacta 18h	250.960231
(+)lacta 18h	184.642605
pro	
Lane	Norm. %
(-)lacta	100
(+)lacta 1µM	86.199737
(+)lacta 5µM	117.443272
(+)lacta 10µM	105.37296

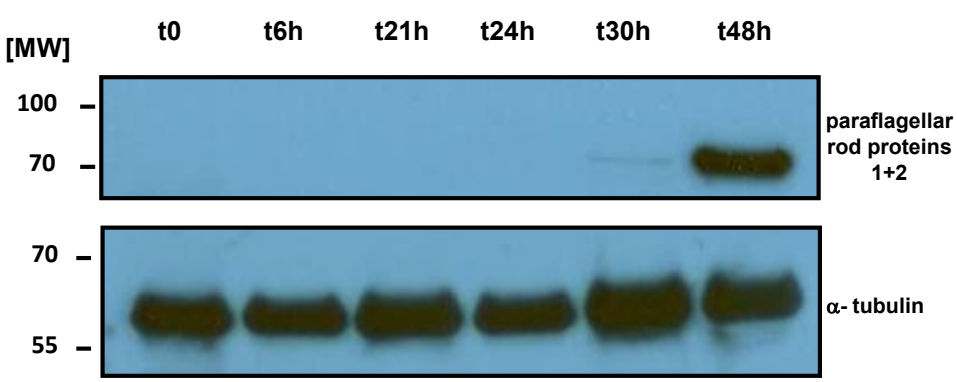

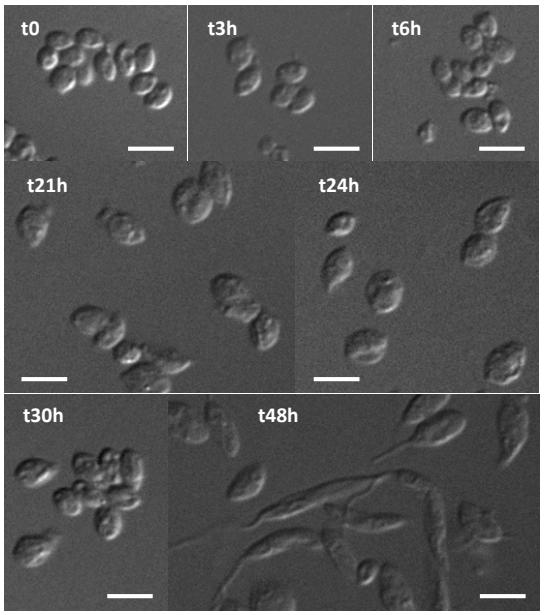

Sup Figure S7

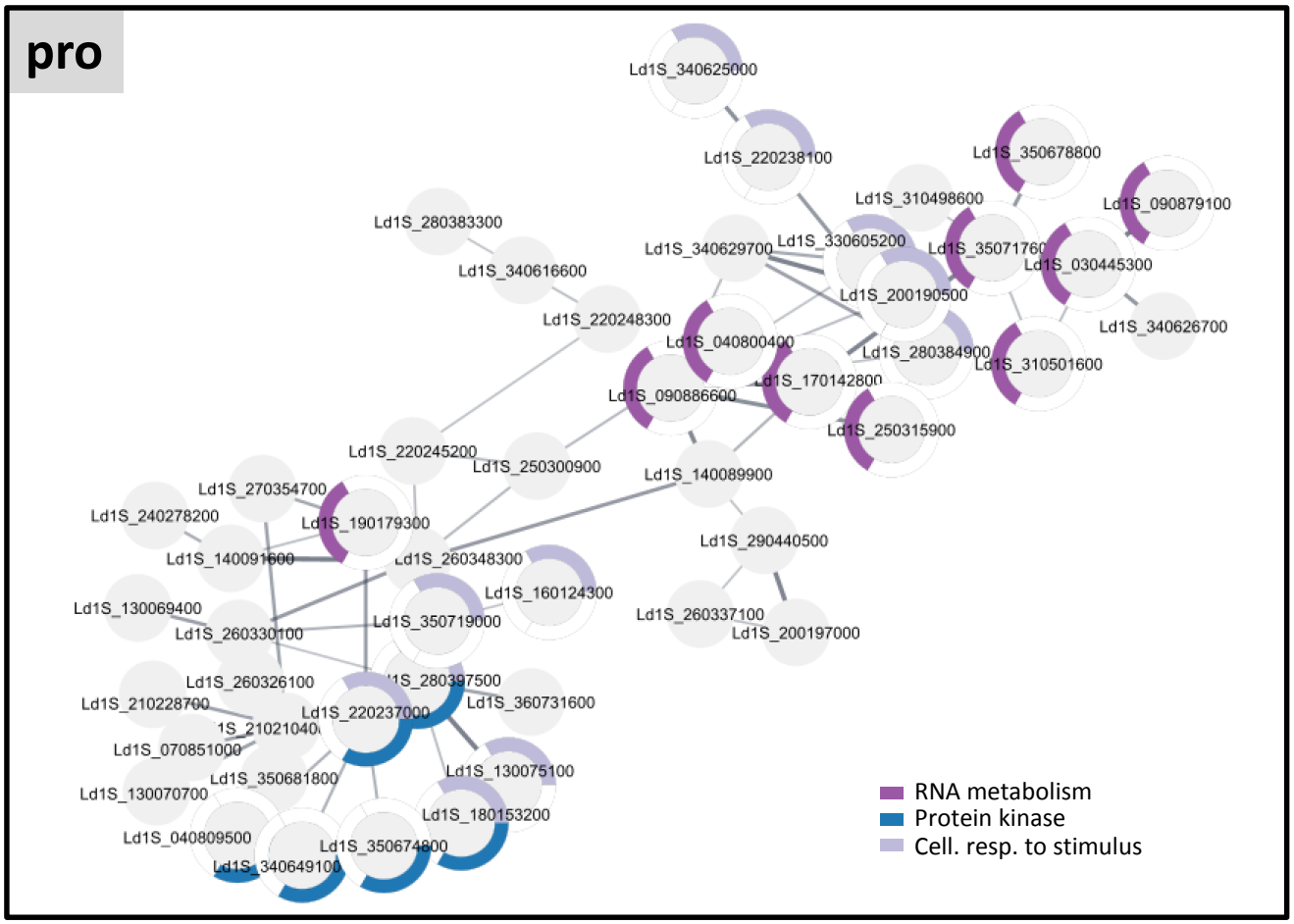

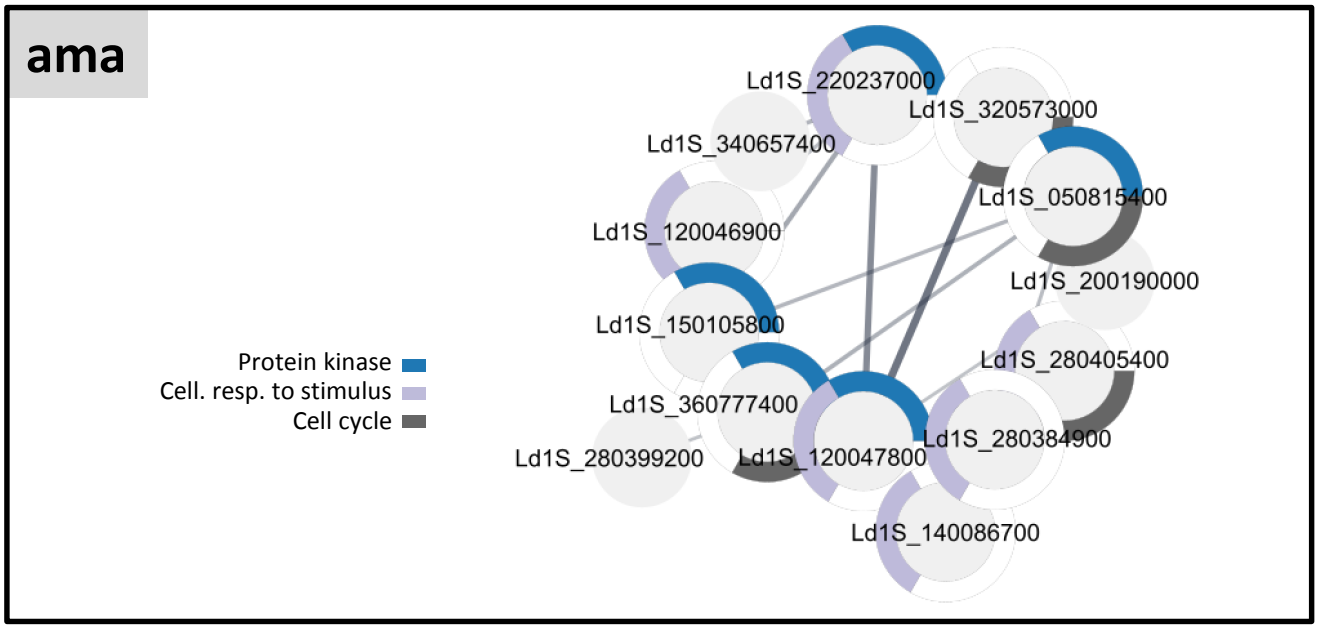

Sup Figure S8

ID Ld1S	ID LdBPK	ID LmxM	Annotation	KO phenotype*
Ld1S_320540600	LdBPK_320860.1	LmxM.31.0810.1	Repressor of differentiation kinase 1, RDK1	Loss of fitness during pro to ama differentiation Loss of fitness in animal infection
Ld1S_220244300	LdBPK_220970.1	LmxM.22.1150.1	Protein kinase domain containing protein, putative	
Ld1S_190177600	LdBPK_191290.1	LmxM.19.1300	hypothetical protein, unknown function (PP: Protein kinase domain containing protein, putative)	
Ld1S_180153200	LdBPK_180650.1	LmxM.07.0900	serine/threonine kinase-like protein, putative	
Ld1S_080866500	LdBPK_080870.1	LmxM.08.0930.1	protein kinase, putative	
Ld1S_040809500	LdBPK_041230.1	LmxM.04.1210.1	casein kinase I, putative	
Ld1S_350674800	LdBPK_351020.1	LmxM.34.1000.1	casein kinase I, putative	
Ld1S_340649100	LdBPK_342850.1	LmxM.33.3020.1	protein kinase, putative	Loss of fitness in animal infection
Ld1S_320543000	LdBPK_321080.1	LmxM.31.1020.1	protein kinase, putative	
Ld1S_280397500	LdBPK_281800.1	LmxM.28.1670.1	differentiation inhibitory kinase, putative, ZFK	Moderate loss of fitness in animal infection
Ld1S_220237000	LdBPK_220370.1	LmxM.22.0490.1	protein kinase, putative	ESSENTIAL
Ld1S_210228200	LdBPK_210330.1	LmxM.21.0270.1	protein kinase, putative	Loss of fitness in animal infection
Ld1S_150105800	LdBPK_151180.1	LmxM.15.1200	protein kinase, putative	
Ld1S_120047800	LdBPK_120130.1	LmxM.12.0130.1	Cell division protein kinase, putative	
Ld1S_050815400	LdBPK_050550.1	LmxM.05.0550.1	protein kinase, putative	

Baker et al

Sup Figure S9

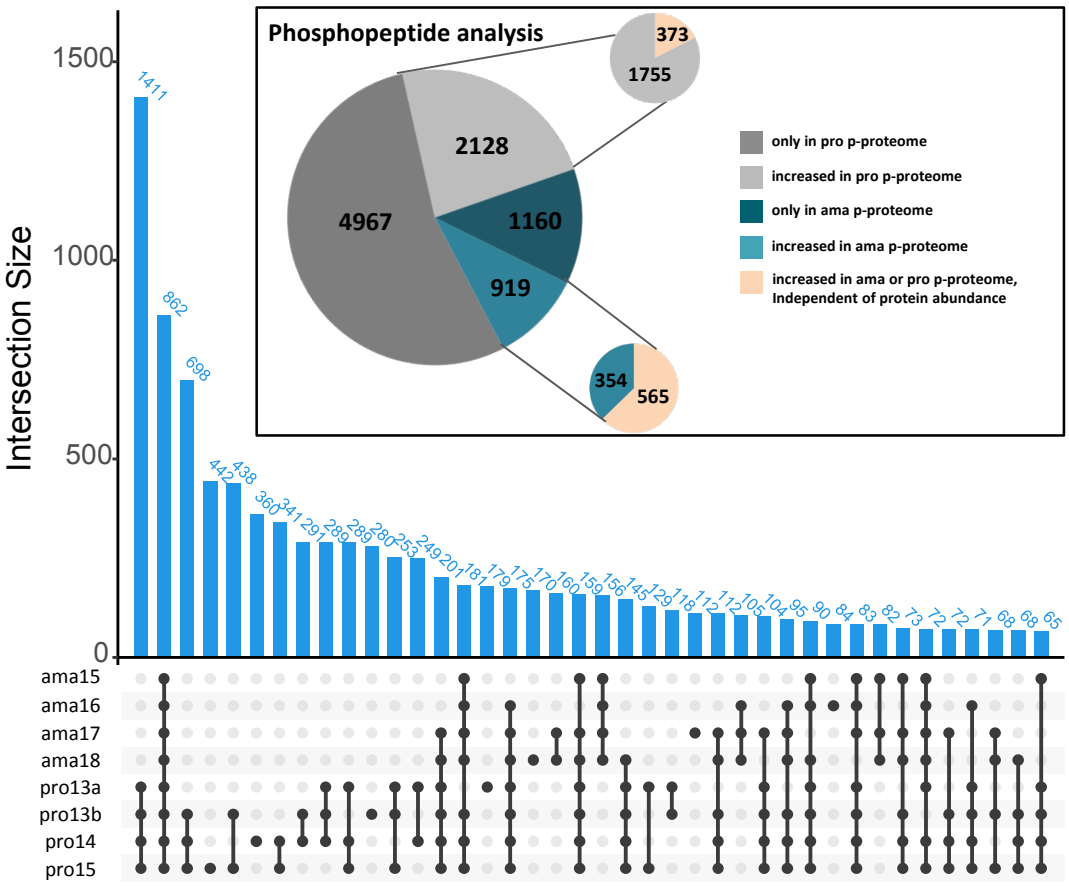

Sup Figure S10

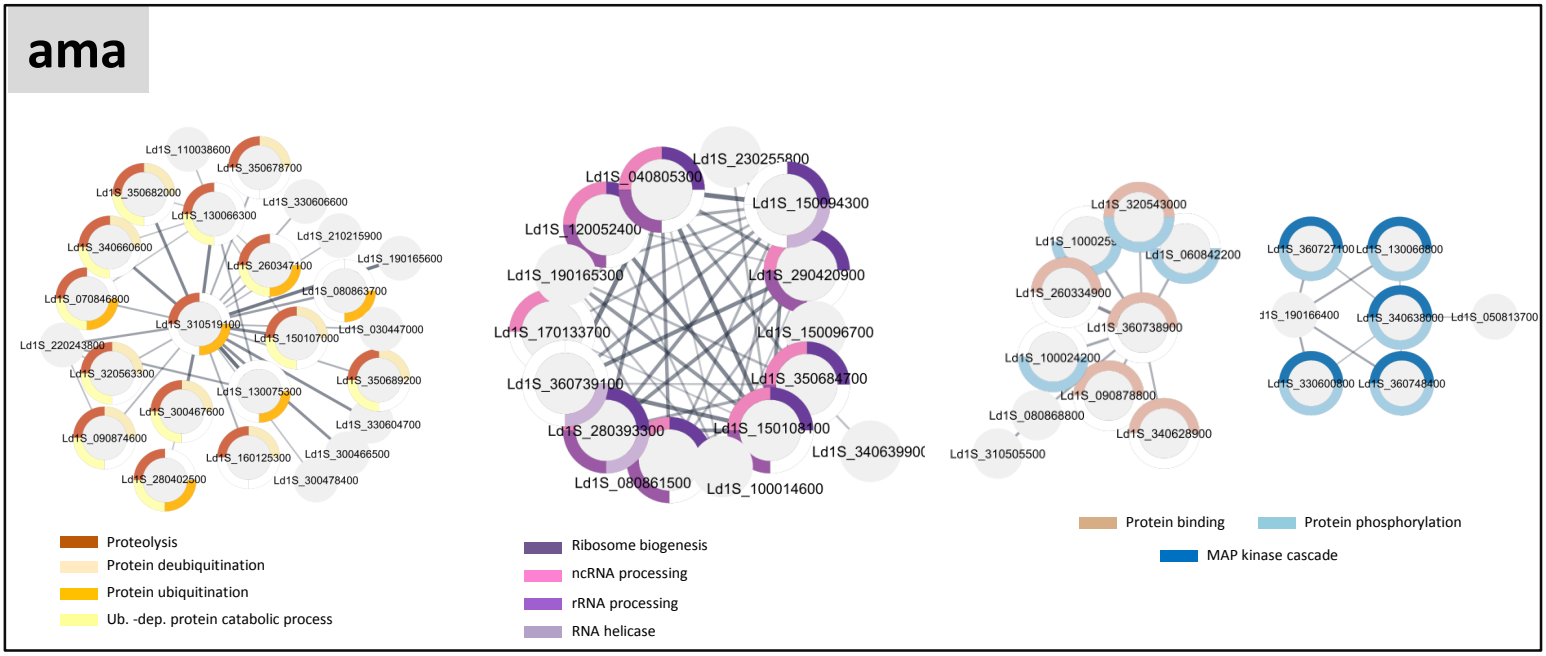

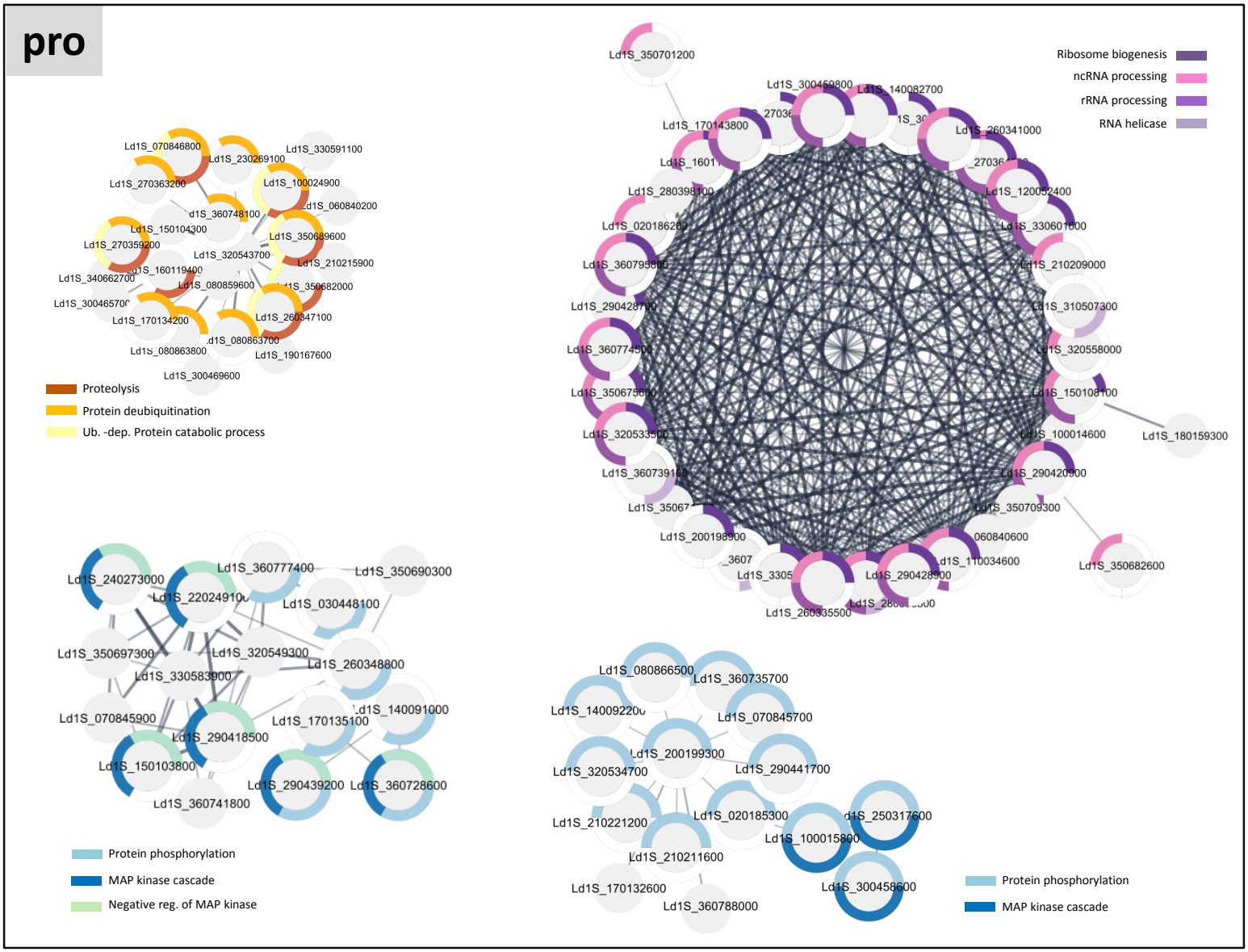

Sup Figure S11